The Pennsylvania State University

The Graduate School

Department of Food Science

ULTRASONIC CHARACTERIZATION OF CRYSTAL DISPERSIONS AND FROZEN FOODS

A Dissertation in

Food Science

by

İbrahim Gülseren

Submitted in Partial Fulfillment
of the Requirements
for the Degree of

Doctor of Philosophy

May 2008

The dissertation of İbrahim Gülseren was reviewed and approved* by the following:

John N. Coupland
Associate Professor of Food Science
Thesis Advisor
Chair of Committee

Gregory R. Ziegler
Professor of Food Science

Ramaswamy C. Anantheswaran
Professor of Food Science

Bernhard R. Tittmann
Professor of Engineering Mechanics

John D. Floros
Professor of Food Science
Head of the Department of Food Science

*Signatures are on file in the Graduate School.

Abstract

Ultrasonic wave propagation is sensitive to the physical properties and structure of materials and so ultrasonic sensors are used in the non-destructive evaluation of materials. Since ultrasonics is a non-invasive, relatively inexpensive technology that can be adapted to hygienic requirements and processing conditions that occur in the food industry, it is possible to use ultrasonic sensors in the analysis of foods, in particular online during production. The relationships between the ultrasonic properties of foods and many physical and structural parameters have been well-established (Coupland, 2004) and the motivation of this work is to establish similar relationships for frozen foods. Phase transitions (*i.e.*, freezing) are characterized by rapid changes in physical properties of materials, including ultrasonic properties so it should be possible to relating the changes in ultrasonic properties of food systems to other physical properties such as ice content. In order to do that, however, the influence of food composition and microstructure on the ultrasonic properties must be well understood.

The first objective of this study was to investigate the effect of ice content on the ultrasonic properties of model frozen solutions. The speed of sound was measured in sucrose, glycerol and orange juice solutions as a function of temperature (10°C- -10°C). Ultrasonic velocity rapidly increased starting at the onset of freezing as the samples were frozen. For samples below -8°C (*i.e.*, closer to thermal equilibrium), the ice content in the samples was approximately a linear function of the change in ultrasonic velocity. The ultrasonic attenuation in the frozen model systems was unexpectedly high.

The ice-solution system is difficult to precisely characterize experimentally so to investigate the mechanisms for the large ultrasonic losses seen a simpler model system was

considered. The ultrasonic attenuation from solid or liquid emulsion can be well-described by scattering theory, except at their melting point when there are large excess losses (McClements *et al*. 1993). The solid-liquid equilibrium in emulsion droplets is similar to the ice-solution equilibrium in frozen samples and has the advantage of being readily controlled and described. The second objective was to investigate the excess attenuation for melting lipids in emulsion droplets and suggest a mechanism for the losses that may be responsible for the very high attenuation. Large losses were seen at the melting point but these could be described by an extended version of scattering theory that incorporated effective values of the physical properties of the droplets accounting for the rapid changes in solids content at melting point (*i.e*., the effective specific heat and thermal expansion coefficient were much larger over the melting range). The influence of oil and emulsifier type and particle size on the excess losses on melting was investigated in detail to show the validity of extended theory.

The final objective was to measure the attenuation in model frozen foods and interpreting relevance of the losses in terms of the mechanism developed for the emulsion droplet model. Ultrasonic velocity and attenuation was measured as a function of temperature in partially frozen sucrose solutions that had been prepared either with or without prior degassing. Ultrasonic velocity increased approximately linearly with ice content in all samples; however the rate of change in velocity was dependent on initial sugar concentration and to a lesser extent on degassing. Attenuation increased rapidly on freezing but the final value was more a function of the degassing step and hence the presence of air bubbles than on the final ice content. This finding suggests that contrary to my initial hypothesis, air bubbles rather than ice crystals are most significant in determining the ultrasonic attenuation of partially frozen model foods.

References

1. Coupland, J.N. 2004. Low-intensity ultrasound. *Food Research International*, 37(6), 537-543.
2. McClements, D.J., Povey, M.J.W. & Dickinson, E. 1993. Absorption and velocity dispersion due to crystallization and melting of emulsion droplets. *Ultrasonics*, 31(6), 433-437.

TABLE OF CONTENTS

LIST OF FIGURES……..viii

LIST OF TABLES…….....xiii

ACKNOWLEDGEMENTS……..xiv

Chapter 1 Statement of the Problem……1

Chapter 2 Literature Review……5

2.1. Ultrasound: New tools for product improvement…….……5
2.1.1 Introduction…….5
2.1.2 Measurement Methods……8
2.1.3 Applications…….....14
2.1.4 Conclusions……...24
2.1.5 References…….26

2.2 Physical Properties of Ice…….33
2.2.1 Thermodynamics of Freezing…….....33
2.2.2 Kinetics of Freezing…….....36
2.2.3 References…….....42

2.3 Ultrasonic Propagation in Ice…….....44
2.3.1 Experimental Data……44
2.3.2 Ultrasonic Formulations for Propagation in Ice……48
2.3.3 References…….57

Chapter 3 Ultrasonic Measurements in Frozen Model Food Solutions……..61

3.1 Ultrasonic Velocity Measurements in Frozen Model Food Solutions…….61
3.1.1 Introduction…….……62
3.1.2 Materials and Methods…….……63
3.1.3 Results and Discussion…..…….....65
3.1.4 Conclusions..…….....77
3.1.5 References…….....78

3.2 Ultrasonic Attenuation Measurements in Frozen Model Food Solutions……...82
3.2.1 Introduction…….82
3.2.2 Materials and Methods……82
3.2.3 Results……82
3.2.4 Conclusions..83

3.3 Conclusions……84

Chapter 4 Excess Attenuation in Melting Emulsion Droplets…….85

4.1 Excess Ultrasonic Attenuation due to Solid-Solid and Solid-Liquid Transitions in Emulsified Octadecane…….85
4.1.1 Introduction…….86
4.1.2 Materials and Methods…..87
4.1.3 Results ……..90
4.1.4 Discussion…..96
4.1.5 Conclusions……107
4.1.6 References..……..109

4.2 The Effect of Emulsifier Type and Droplet Size on Phase Transitions in Emulsified Even Numbered *n*-Alkanes……...112
4.2.1 Introduction..113
4.2.2 Materials and Methods…..114
4.2.3 Results and Discussion.117
4.2.4 Conclusions..134
4.2.5 References…..136

4.3 Conclusions……..138

Chapter 5 Ultrasonic Properties of Partially Frozen Sucrose Solutions…...……..140

5.1 Introduction…….141
5.2 Materials and Methods…….142
5.3 Results…….144
5.4 Conclusions……151
5.5 References……..152

Chapter 6 Conclusions…….154

Appendix Ultrasonic Properties of Partially Frozen Sucrose Solutions as Affected by Sample Preparation Methods……...……...……..160

A.1 Introduction…….…….....161
A.2 Materials and Methods…..…..……162
A.3 Results……. …….....164
A.4 Conclusions……...175
A.5 References……...……..177

LIST OF FIGURES

Figure 2.1.1. Diagram showing the displacement of volume elements from (a) their equilibrium position due to the propagation of (b) L-waves and (c) T-waves. Propagation is left to right in both cases…….7

Figure 2.1.2. Diagram showing the alignment of transducers and ultrasonic path for (a) pulse-echo, (b) through transmission, (c) resonator, (d) reflectance, (e) guided wave, and (f) ultrasonic Doppler velocimetry measurement systems…….....11

Figure 2.1.3. The speed of longitudinal sound waves as influenced by sucrose concentration (10 to 70%) in aqueous solutions (5 to -10 ºC). (●: 10% sucrose, ○: 30% sucrose, ▼: 50% sucrose, ▽: 70% sucrose)..…….....18

Figure 2.2.1. The phase diagram of ice (Source: Lobban *et al*. 1998)……..……...34

Figure 2.2.2. Sucrose-water phase diagram (Source: Young & Jones, 1949)……..36

Figure 2.2.3. Free energy (ΔG) changes associated with formation of a stable nucleus. ΔG_s, free energy of surface formation; ΔG_v, free energy of volume formation; ΔG_c, critical free energy for nuclei formation; r_c = critical size (Source: Hartel, 2001)….……38

Figure 2.2.4. The representation of grain boundaries in polycrystalline materials……..41

Figure 2.3.1. Temperature dependence of longitudinal wave velocity for the polycrystalline ice samples summarized in Table 2.3.1……..……48

Figure 2.3.2. The poroelastic model prediction for (a) ultrasonic velocity, and (b) attenuation of partially frozen sucrose solutions as a function of ice content (%)……...56

Figure 3.1.1. (a) Speed of sound in sucrose solutions (●: 5%, ○: 10%, ▼: 20%, ▽: 30%, ■: 40%, □: 50%, ♦: 60%, ◊: 70%) as a function of temperature. The formation of ice corresponded to the discontinuity seen. (b) Speed of sound in supercooled sucrose solutions (symbols as Figure 3.1a). There was no ice nucleation in these samples so no discontinuity was seen. Lines shown correspond to the best fit of linear model (see text for details). (c) Change in ultrasonic velocity due to ice formation in sucrose solutions (symbols as Figure 3.1.1a).……..66

Figure 3.1.2. (a) Speed of sound in glycerol solutions (●: 1%, ○: 5%, ▼: 10%, ▽: 20%, ■: 25%,

□: 30%) as a function of temperature. The formation of ice corresponded to the discontinuity seen. (b) Speed of sound in supercooled glycerol solutions as a function of temperature (symbols as Figure 3.1.2a). There was no ice nucleation in these samples so no discontinuity was seen. Lines shown correspond to the best fit of linear model (see text for details). (c) The difference between speed of sound in frozen and supercooled glycerol solutions as a function of temperature (symbols as Figure 3.1.2a)…….....67

Figure 3.1.3. (a) Speed of sound in orange juice solutions (●: 5% , ○: 10%, ▼: 20%, ▽: 30%, ■: 40%) as a function of temperature. The formation of ice corresponded to the discontinuity seen. (b) Speed of sound in supercooled orange juice solutions as a function of temperature (symbols as Figure 3.1.3a). There was no ice nucleation in these samples so no discontinuity was seen. Lines shown correspond to the best fit of linear model (see text for details). (c) The difference between speed of sound in frozen and supercooled orange juice solutions as a function of temperature (symbols as Figure 3.1.3a).……68

Figure 3.1.4. Melting point curves for (●) sucrose, (○) glycerol and (▼) orange juice solutions…….....71

Figure 3.1.5. (a) Ice content of sucrose solutions as calculated from melting point depression data (from top to bottom: pure water, 5%, 10%, 20%, 30%, 40%, and 50%). (b) Ice content of glycerol solutions as calculated from E melting point depression data (from top to bottom: pure water, 1%, 5%, 10%, and 20%). (c) Ice content of orange juice solutions as calculated from melting point depression data (from top to bottom: pure water, 10%, 20%, 30%, 40% solid matter)……72

Figure 3.1.6. The difference between speed of sound in frozen and supercooled solutions as a function of ice content (%) in (▼) sucrose, (▽) glycerol and (○) orange juice solutions at temperatures lower than or equal to -8 ºC. A single linear regression is shown through the glycerol and orange juice data…….....73

Figure 3.1.7. Ultrasonic velocity in a frozen 20% sucrose solutions during temperature cycling Odd numbered steps correspond to the measurements at -5 ºC (○), and the even numbered ones to those in -3 ºC (●). Solid lines connect consecutive measurements while dotted lines connect the measurements at each temperature……..75

Figure 3.2.1. Ultrasonic attenuation as a function of ice content in partially frozen sucrose solutions (10-50% wt sucrose) prepared as described in Chapter 3.1. The attenuation measurements were taken at temperatures ≤ -8°C…….83

Figure 4.1.1. Crystallization of 3% C_{18} emulsion (d_{32}=0.45 μm) stabilized by 1% Tween 20 as monitored by (a) differential scanning calorimetry, (b) ultrasonic velocity and (c) ultrasonic attenuation measurements. Ultrasonic measurements are made using a 2.25 MHz center frequency transducer. Lines show predictions of ultrasonic properties calculated from scattering theory…….91

Figure 4.1.2. Melting of 3% C_{18} emulsion (d_{32}=0.45 μm) stabilized by 1% Tween 20 as monitored by (a) differential scanning calorimetry, (b) ultrasonic velocity (c) ultrasonic attenuation measurements. Ultrasonic measurements are made using a 2.25 MHz center frequency transducer. Lines show predictions of ultrasonic properties from calculated scattering theory……..……..…….94

Figure 4.1.3. (a) Heat capacity of *n*-octadecane as a function of temperature calculated from the DSC melting curve for 3% *n*-octadecane-in-water emulsion stabilized by 1% Tween 20 (d_{32} = 0.45 μm). (b) Solid fat content (% SFC) of *n*-octadecane as a function of temperature calculated from the DSC melting curve for 3% *n*-octadecane-in-water emulsion stabilized by 1% Tween 20 (d_{32} = 0.45 μm). (c) Density of *n*-octadecane as a function of temperature calculated from the solid fat content data (Figure 4.1.3b). Dotted lines are the extrapolation of tabulated properties of the pure solid and pure liquid phases. (d) Thermal expansion coefficient of *n*-octadecane as a function of temperature calculated from the density data (Figure 4.1.3c)…… 99

Figure 4.1.4. Detail of the major attenuation peak seen during the heating of a 3% *n*-octadecane-in-water emulsion stabilized by 1% Tween 20 (d_{32} = 0.45 μm) (replotted from Figure 4.1.2c). The line shown is the prediction from scattering theory using effective temperature dependent values for heat capacity, density, and thermal expansion coefficients from Figure 4.1.3……...101

Figure 4.1.5. Effect of particle size on ultrasonic attenuation of 3% C_{18} emulsion stabilized by 1% Tween 20 at the major attenuation peak temperatures (26 and 27 °C), for pure solid samples (5 °C) and for pure liquid samples (30 °C) during the melting scan. Ultrasonic measurements are made using a 2.25 MHz center frequency transducer. Lines show predictions of ultrasonic attenuation from scattering theory (ST) for the tabulated properties purely solid (5°C) and liquid (30°C) droplets as well as the semi-crystalline droplets (26 and 27°C) using data from Figure 4.1.4…….....102

Figure 4.1.6. Scattering theory prediction of attenuation as heat capacity (C_P), density (ρ) and cubical expansion coefficient (β) vary as a function of % SFC. When one parameter was varied, the other two were held constant at their 20°C value (100% SFC)…….105

Figure 4.2.1. Heating thermograms for 0.25% emulsions of (a) C_{16}, (b) C_{18}, (c) C_{20} stabilized by 1% Tween 20 recorded at a scanning rate of 10 °C/hr. The figures to the right are higher resolution zooms of the boxed area of the main, data sets shown on the left……..118

Figure 4.2.2. Heating thermograms for 0.25% emulsions of (a) C_{16}, (b) C_{18}, (c) C_{20} stabilized by 0.5% sodium caseinate recorded at a scanning rate of 10 °C/hr. The figures to the right are higher resolution zooms of the boxed area of the main, data sets shown on the left..……120

Figure 4.2.3. Heating thermograms for 5% emulsions of C_{18}, C_{20} stabilized by 1% Tween 20 (d_{32} = 0.52 μm) recorded at a scanning rate of 10 °C/hr. Data are similar to Figure 4.2.1, but the more concentrated emulsion reveals detail of the crystal-rotator transition 122

Figure 4.2.4. Cooling thermograms for 0.25% emulsions of (a) C_{18}, (b) C_{20} stabilized by 1% Tween 20 recorded at a scanning rate of 10 °C/hr. The figures to the right are higher resolution zooms of the boxed area of the main, data sets shown on the left……...124

Figure 4.2.5. Cooling thermograms for 0.25% emulsions of (a) C_{18}, (b) C_{20} stabilized by 0.5% sodium caseinate recorded at 10 °C /hr. The figures to the right are higher resolution zooms of the boxed area of the main, data sets shown on the left……...125

Figure 4.2.6. Thermograms of a 0.25% C_{18} emulsion of by 1% Tween 20 (d_{32} = 0.2 μm). Samples were (a) cooled to 10°C at 10 °C/hr then (b) reheated to 35°C at the same rate.....128

Figure 4.2.7. Ultrasonic attenuation as a function of temperature during heating (6 °C/hr) of 3% emulsions (○: 0.15 μm, ●: 0.45 μm) of (a) C_{16}, (b) C_{18}, (c) C_{20} stabilized by 1% Tween 20. Lines represent predictions from scattering theory (see text for details). Broken lines are used for 0.15 μm samples, solid lines are used for 0.45 μm samples……129

Figure 4.2.8. Ultrasonic attenuation as a function of temperature during heating (6 °C/hr) of 3% emulsions (○: 0.15 μm, ●: 0.45 μm) of (a) C_{16}, (b) $C_{18,}$ (c) C_{20} stabilized by 0.5% sodium caseinate. Lines represent predictions from scattering theory (see text for details). Broken lines are used for 0.15 μm samples, solid lines are used for 0.45 μm samples……131

Figure 5.1. Sucrose water phase diagram (calculated from data provided in Young & Jones (1949)). Points show the temperature of the discontinuity in the ultrasonic velocity (□) or attenuation (▲) temperature curves at the melting point (from Figure 5.2 and 5.4). ……145

Figure 5.2. Ultrasonic velocity in partially frozen sucrose solutions (■) 30%, (○) 40%, (▲) 50% prepared with (a) or without (b) degassing…….……146

Figure 5.3. Change in ultrasonic velocity on freezing as a function of ice content in partially frozen sucrose solutions (x: 25%, ■: 30%, ♦: 35%, ●: 40%, ▲: 50% sucrose) prepared with (a) or without (b) degassing……...148

Figure 5.4. Ultrasonic attenuation in partially frozen sucrose solutions (■) 30%, (○) 40%, (▲) 50%) prepared with (a) or without (b) degassing……149

Figure 5.5. Ultrasonic attenuation as a function of ice content in partially frozen sucrose solutions (■:30%, ▲: 40%, ●: 50%) prepared with (open points) or without (filled points) degassing……..150

Figure A.1. Cooling thermograms of 0.25% *n*-eicosane emulsions stabilized by (a) Tween emulsifiers (1%), (b) non-Tween emulsifiers (1%) recorded at a scanning rate of 10°C.h^{-1}. The mean particle size (d_{32}) for all samples is 0.52 μm…….....165

Figure A.2. Cooling thermograms of 0.25% *n*-octadecane emulsions stabilized by (a) Tween

emulsifiers (1%), (b) non-Tween emulsifiers (1%) recorded at a scanning rate of 10°C.h^{-1}. The mean particle size (d_{32}) for all samples is 0.52 μm…….....167

Figure A.3. Heating thermograms of 0.25% *n*-eicosane emulsions stabilized by (a) Tween emulsifiers (1%), (b) non-Tween emulsifiers (1%) recorded at a scanning rate of 10°C.h^{-1}. The figures to the *right* are the higher resolution zooms (5% emulsion) of the main data sets shown on the *left*. The mean particle size (d_{32}) for all samples is 0.52 μm……169

Figure A.4. Heating thermograms of 0.25% *n*-octadecane emulsions stabilized by (a) Tween emulsifiers (1%), (b) non-Tween emulsifiers (1%) recorded at a scanning rate of 10°C.h^{-1}. The figures to the *right* are the higher resolution zooms (5% emulsion) of the main data sets shown on the *left*. The mean particle size (d_{32}) for all samples is 0.52 μm……170

Figure A.5. (a) Heating thermograms of 0.25% *n*-octadecane emulsions stabilized by Tween 40 (1%) as affected by the particle size (0.19 μm to 5.58 μm). (b). The demonstration of the separation of surface melting and droplet core melting processes. (c). A simple physical model of a droplet (diameter D) with a pure lipid core (diameter d). (d). The surface melting (%) characteristics of 0.25% *n*-octadecane emulsions stabilized by Tween 40 (1%) as affected by the particle size (0.19 μm to 5.58 μm)……...173

LIST OF TABLES

Table 1.1. Schematic outline of the thesis……...3

Table 2.2.1. Physical properties of ice (Source: Petrenko & Whitworth, 1999)……...35

Table 2.3.1. Summary of ultrasonic measurements in polycrystalline ice samples from the literature…….45

Table 2.3.2. Variables in ice structure that might affect ultrasonic propagation……..49

Table 3.1.1. Constants for the linear multivariate model (Equation 1: $c(x,T) = c_w + k_T T + k_x x$) to predict the ultrasonic velocity of unfrozen solutions as a function of temperature (x, °C) and composition (x, wt%) The limits for the model are described in the text. Values for the confidence are expressed as a best fit in the 95% confidence interval……..69

Table 4.1.1. Physical properties of water and n-octadecane (C_{18}) used in the scattering theory……...……...…97

Acknowledgments

The first time I started dreaming about working at a university lab as a doctoral candidate, I believe I was a fifth grader and probably it was early 1990. Finishing up my Ph.D. studies at Penn State Food Science will be my biggest dream coming true. The person who gave me the opportunity to make this dream happen is my major advisor Dr. John N. Coupland. The first time I read his post-doc paper on the ultrasonic scattering theory on a Saturday afternoon in June 2003, I was an M.S. student at Knoxville, TN and preparing samples in the lab. I said to myself: "This is the type of work I have always wanted to do.' I think I am very fortunate to have the opportunity. I always admired the way how he combined being a research mentor and an educator, his patience and positive attitude. Not only he taught or made me learn most of what I know about food physical chemistry now, he also changed my views about lab research. I am proud to have been his student.

I would like to thank my Ph.D. committee members, Dr. Gregory R. Ziegler, Dr. Ramaswamy C. Anantheswaran and Dr. Bernhard R. Tittmann for their time and help. Special thanks are due to Dr. Anantheswaran for all I learnt from FD SC 430 as a TA.

I would like to thank all previous and current members of Food Colloids Lab for always being there when I needed help with my labwork. Special thanks are due to the great company of Emre-the Turkish roommate, Rajesh-the lunchmate, Justine, Ying, Fatih, and Umut in the chronological order of acquaintance. The presence of Özlem-the Turkish Cypriot in my life during the last year of my Ph.D. made it my favorite year. Finally, I want to thank my parents and sister living in İstanbul, Turkey for their love and support. I have been an international graduate student in US more than 5 years by now and hearing their voices over the phone every Saturday morning was my main motivation to do all I did.

Chapter 1

Statement of the Problem

Low-intensity ultrasound is used as a non-destructive evaluation (NDE) technology in the analysis of foods. The physical and thus the ultrasonic properties of foods change rapidly during phase transitions (*e.g.*, freezing) so it should be possible to relate ultrasonic measurements to the properties of frozen foods as a part of a process control tool. However, the relationship between frozen sample structure and ultrasonic properties is not well understood. Therefore, my thesis concentrates on i) measuring the ultrasonic properties of frozen foods and related semi-crystalline systems, and ii) relating ultrasonic properties to structural attributes.

Goal, Objectives, and Thesis Layout

The overall goal of my thesis is to relate the ultrasonic properties of frozen foods and related crystalline systems to their composition and structure. In order to accomplish this goal the specific objectives of my research were to:

1) Investigate the effect of ice content on the ultrasonic properties of model frozen solutions,
2) Investigate the excess attenuation[1] documented by McClements *et al.* (1993) for melting lipids in emulsion droplets and suggest a mechanism for the losses that may be responsible for the very high attenuation in frozen samples.
3) Measure the attenuation in model frozen foods and interpret the relevance of the losses in terms of the mechanism hypothesized in Objective 2.

[1] Here, I am referring to high ultrasonic attenuation that cannot be explained using scattering theory.

The structure of my thesis is outlined in Table 1.1. Chapter 3.1 is concerned with ultrasonic velocity measurements in partially frozen model foods (*i.e.*, Objective 1). Ultrasonic velocity in partially frozen sucrose, glycerol, and orange juice solutions is measured and empirically modeled in terms of ice content. Since partially frozen solutions are complex and highly attenuating it is hard to relate structure to the ultrasonic properties (Chapter 3.2). As a model system I selected melting alkane emulsion droplets whose structure could be carefully controlled and which have previously been shown to be anomalously highly attenuating (McClements *et al*. 1993).

In Chapter 4, the excess ultrasonic attenuation in melting droplets was investigated (*i.e*., Objective 2) and modeled with an extended version of scattering theory (Chapter 4.1). In Chapter 4.2, I investigated the applicability of the extended theory to a variety of alkane emulsions. In order to test the relevance of my theory to the attenuation in frozen foods, Chapter 5 returns to the measurement of attenuation in partially frozen sucrose solutions (*i.e.*, Objective 3). Chapter 6 is the conclusions from my studies.

Chapters 3.1, 4.1, 4.2 & 5.3 of this thesis are presented in the form of manuscripts co-authored with my major advisor each with a separate introduction, materials and methods, results and discussion, conclusion and references. Chapter 2.1 is a book chapter with my major advisor in which I describe the current state of knowledge on ultrasonic sensors used in foods. In addition, the investigations on the thermal and ultrasonic properties of alkane emulsions during phase transitions showed that the crystallization and melting characteristics of emulsion droplets could be affected due to oil-surfactant interactions. This is a novel conclusion although not central to my thesis and is detailed in the Appendix.

Table 1.1. Schematic outline of the thesis.

Chapter	Paper	Objective Covered
1	Statement of the problem	
2	Literature review	
2.1	Gülseren, İ. & Coupland, J.N. 2008. Ultrasound: New tools for product improvement. *In* Non-destructive Testing of Foods. J. Irudayaraj & C. Reh (ed.s). IFT Series (Blackwell Publishing), USA.	
2.2	Physical properties of ice	
2.3	Ultrasonic propagation in ice	
3.1	Gülseren, İ. & Coupland, J.N. 2007. Ultrasonic velocity measurements in frozen model food solutions. *Journal of Food Engineering*, 79(3), 1071-78.	1
3.2	Ultrasonic attenuation measurements in frozen model food solutions	1
3.3	Conclusions	1
4.1	Gülseren, İ. & Coupland, J.N. 2007. Excess ultrasonic attenuation due to solid-solid and solid-liquid transitions in emulsified octadecane. *Crystal Growth and Design*, 7 (5), 912-918.	2
4.2	Gülseren, İ. & Coupland, J.N. 2007. The effect of emulsifier type and droplet size on phase transitions in emulsified even numbered *n*-alkanes. *Journal of American Oil Chemists` Society*, 84 (7), 621-629.	2
4.3	Conclusions	2
5	Gülseren, İ. & Coupland, J.N. 2008. Ultrasonic properties of partially frozen sucrose solutions. Submitted to *Journal of Food Engineering*.	3
6	Conclusions	
Appendix	Gülseren, İ. & Coupland, J.N. 2007. Surface melting in alkane emulsion droplets as affected by surfactant type. *Journal of American Oil Chemists` Society*, 85 (5), 413-419.	

Reference

1. McClements, D.J., Povey, M.J.W. & Dickinson, E. 1993. Absorption and velocity dispersion due to crystallization and melting of emulsion droplets. *Ultrasonics*, 31(6), 433-437.

Chapter 2

Literature Review

2.1 Ultrasound: New tools for product improvement

2.1.1 Introduction

Low-intensity ultrasound is used as a non-destructive evaluation (NDE) technology in fields as diverse as oceanography, geological studies, medicine, material science, and also in foods (Blitz, 1963; Hill *et al*. 2004; Rose, 2004; Coupland, 2004). The term ultrasound here refers to inaudible, high frequency (*i.e*., > 20 kHz), low energy sound waves that propagate as deformations in the media of interest. Due to their low energy content, ultrasonic propagation for sensing applications does not influence the physical properties of the materials, but is itself influenced by them. In general, ultrasonic sensors are appropriate for online use as they are relatively cheap and robust compared to most other sensing technologies and are applicable for many food applications. In recent years, a number of reviews were published regarding ultrasound and foods (Coupland, 2004; Coupland & Saggin, 2003; Povey, 1998; McClements, 1995) and this work focuses mostly on recently published work.

The two most common types of ultrasonic waves employed in ultrasonic studies are bulk longitudinal (L) and shear/transverse (T) waves. L-waves propagate in the same direction as the direction of oscillation of material elements (Figure 2.1.1), whereas for T-waves propagation is perpendicular to the motion of the direction of oscillation (Figure 2.1.1). Liquids and gases do

not support T-wave propagation over useful distances. Shear waves travel more slowly than longitudinal waves.

Wave propagation is described in terms of the ultrasonic velocity (c, *i.e.*, distance traveled per unit time) and attenuation coefficient (α, *i.e.*, logarithmic loss of wave-energy per unit distance). These terms can be expressed concisely as a complex wavenumber, (k) (Coupland & Saggin, 2003):

$$k = \frac{\omega}{c} + i\alpha \qquad [2.1]$$

where ω (= 2πf) is the angular frequency.

Ultrasonic parameters are only useful for sensing as they can be measured and related to the physicochemical properties of the food:

$$\left(\frac{k}{\omega}\right) = \frac{\rho}{E} \qquad [2.2]$$

where E is the appropriate modulus and ρ the density. Ultrasonic propagation is an adiabatic process rather than an isothermal one and so the moduli may be different than those made in traditional measurements where heat has time to dissipate. Equation 2 is often written for L-wave propagation in low attenuation fluids as:

$$c = \sqrt{\frac{1}{\rho\kappa}} \qquad [2.3]$$

where κ is the adiabatic compressibility (*i.e.*, reciprocal bulk modulus).

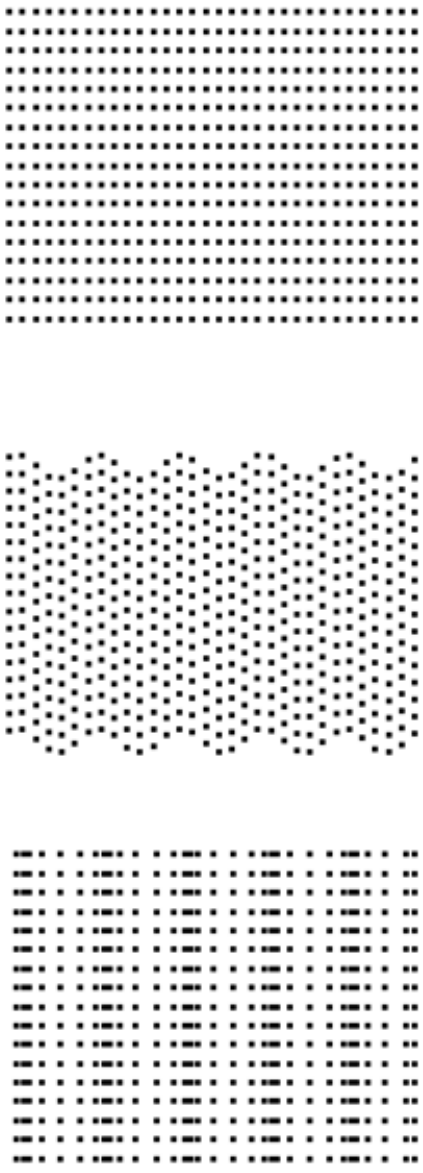

Figure 2.1.1. Diagram showing the displacement of volume elements from (a) their equilibrium position due to the propagation of (b) L-waves and (c) T-waves. Propagation is left to right in both cases.

2.1.2 Measurement Methods

The most commonly used ultrasonic measurement techniques, *i.e*., pulsed and resonance methods, have all been reviewed in detail elsewhere (*e.g*., Coupland, 2004; Buckin & Smyth, 1999; Sheen *et al*. 1995, 1996). Briefly, pulsed methods measure the time taken and energy lost for a pulse of ultrasound to travel through a fixed distance in the sample. Pulsed methods can either be implemented with a single transducer acting as a transmitter and receiver in pulse-echo mode (Figure 2.1.2a) or with separate transmitter and receiver transducers in through transmission mode (Figure 2.1.2b). Resonance methods measure the frequencies at which a fixed pathlength of sample resonates under a continuous single frequency of ultrasound (Figure 2.1.2c). While resonance methods tend to be the most precise in a lab setting, it may not be possible to achieve their advantages in an on-line setting. Pulsed measurements are often more rapid.

Precise ultrasonic measurements require a fixed and well-defined pathlength for the sound to propagate across. The pathlength must be sufficient to cause measurable changes in the ultrasonic signal, yet not too great so that diffraction of the wave and attenuation by the food will completely absorb the sound energy. This can also be a limitation for on-line applications where it is often challenging to find a suitable path for an ultrasonic signal in process equipment. Finally ultrasonic properties are highly dependent on temperature and temperature control can often limit the precision of both on-line and laboratory ultrasonic measurements.

Solid foods which cannot be contained in a pipe or sample cuvette are particularly difficult to analyze, as it is hard to couple the ultrasonic transducer to the sample (even a thin layer of air will attenuate ultrasound completely), hard to control the temperature adequately, and because the transducers must be held against the food and manually supported a fixed distance apart (usually on a pair of calipers or a via stepper-motor) it is not possible to adequately precisely calibrate the pathlength.

Two recent developments in measurement technology have increased the range of options available for ultrasonic measurements, particularly on-line.

i. Non-Contact Measurements. Unlike most ultrasonic sensors that must be in direct contact with the food (either directly or more likely via a delay line), non-contact ultrasonic sensors transmit ultrasonic waves through ambient air which makes them more practical in the monitoring of on-line processes. However, the acoustic signal will be affected by instability in the air coupling the transducer to the food and some compensation is required (Cho & Irudayaraj, 2003a). Furthermore, any non-parallelism between the food surface and transducer will massively increase the signal losses and limit the value of the readings.

ii. Reflectance Measurements. In a reflectance measurement the properties of the food are calculated from the proportion of an ultrasonic pulse reflected at the sample surface. The main ultrasonic parameter that influences the reflection/transmission of ultrasound from one material to another is the acoustic impedance (Z):

$$Z = \rho c \qquad [2.4]$$

If an ultrasonic waves passes across a boundary between two materials with different impedances (*e.g.*, between a food and the container wall) it will be partially reflected and partially transmitted (Figure 2.1.2d). The amplitude (a) of the signal reflected at the interface between material 1 and 2 can be formulated as follows:

$$R_a = \frac{a_r}{a_i} = \left| \frac{Z_2 - Z_1}{Z_1 + Z_2} \right| \qquad [2.5]$$

where subscripts r and i represent the reflected and incident echoes, respectively. The reflectance coefficient can be readily measured and related to the impedance and hence physical properties of the material under investigation.

A reflectance measurement is particularly useful when the material is too attenuating to allow a measurement of transmitted sound (*i.e.*, shear waves in fluids or highly otherwise attenuating foods). Some recent applications of reflectance methods include the determination of solution viscosity by shear wave reflectance (Saggin & Coupland, 2001c), the estimation of foam bubble size by longitudinal wave reflectance (Kulmyrzaev *et al*. 2000). In all of these cases the wave would be too highly attenuated by the food to allow transmission measurements.

In other cases, reflectance measurements may be preferred over transmission measurements as the instrumental setup is frequently simpler and easier to implement on-line, particularly as a stable pathlength is no longer required. For example, reflectance measurements have been used to estimate the concentration of simple solutions (Saggin & Coupland, 2001c), the crystallization of lipids (Saggin & Coupland, 2002a), and the dissolution of powders (Saggin & Coupland, 2002b). Reflectance measurements may be limited as they are only sensitive to the surface of the food and as the transducers may vary in output, must be regularly calibrated.

It is possible to generate combinations of shear and longitudinal waves as a guided wave that can travel long distances along a pipe (or other solid) by frequent reflections with the pipe wall (Figure 2.1.2e). Each reflection at the wall-food interface will affect the wave properties and so the guided wave signal will depend on the food material properties in a manner similar to reflectance measurements. Guided waves are particularly useful for the analysis of equipment surfaces (*e.g.*, commercial steel pipes) for example to detect fouling (Hay & Rose, 2003).

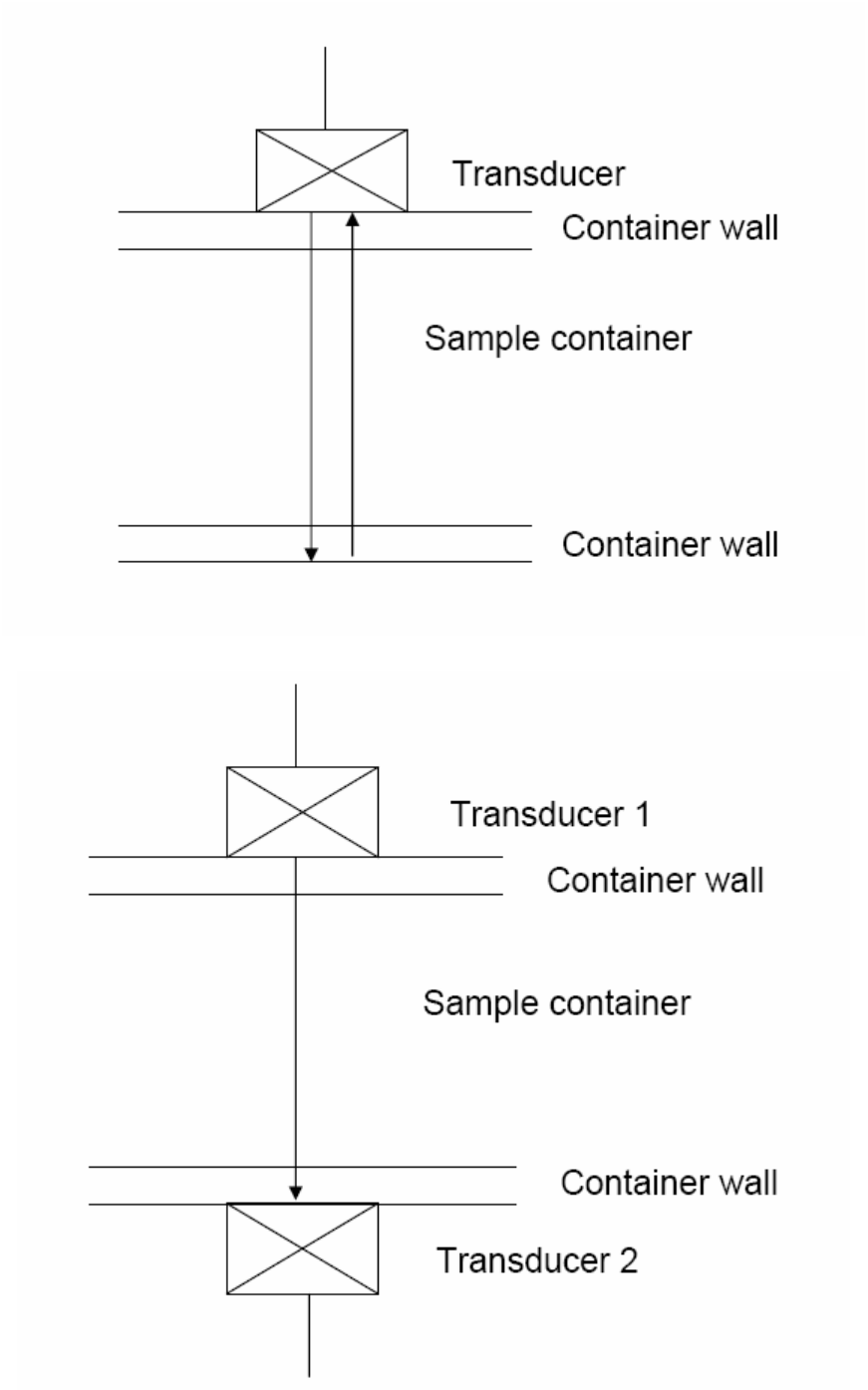

Figure 2.1.2. Diagram showing the alignment of transducers and ultrasonic path for (a) pulse-echo, (b) through transmission, (c) resonator, (d) reflectance, (e) guided wave, and (f) ultrasonic Doppler velocimetry measurement systems.

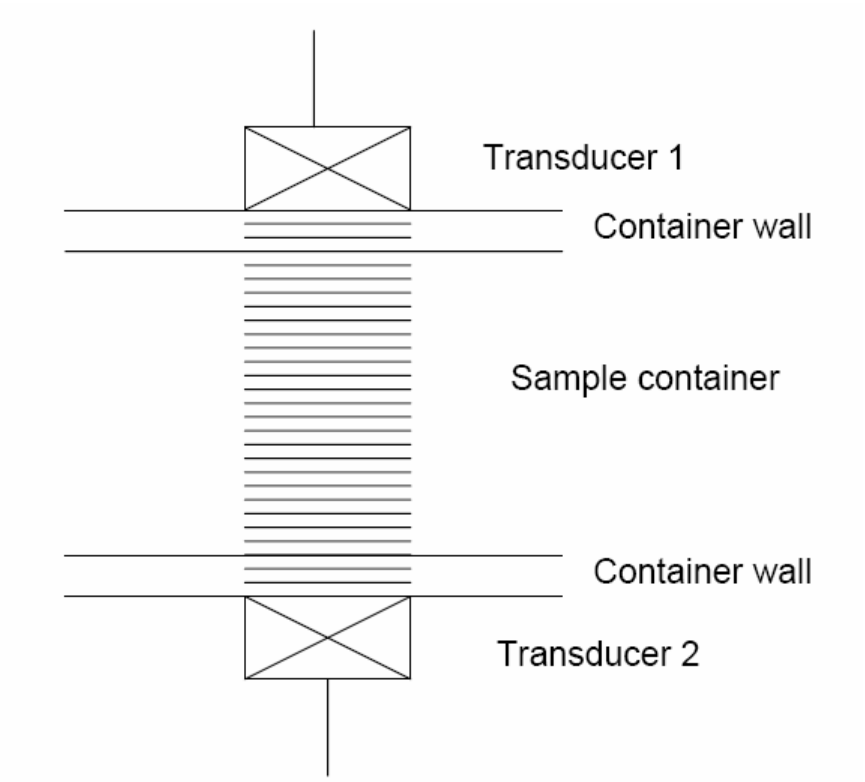

c

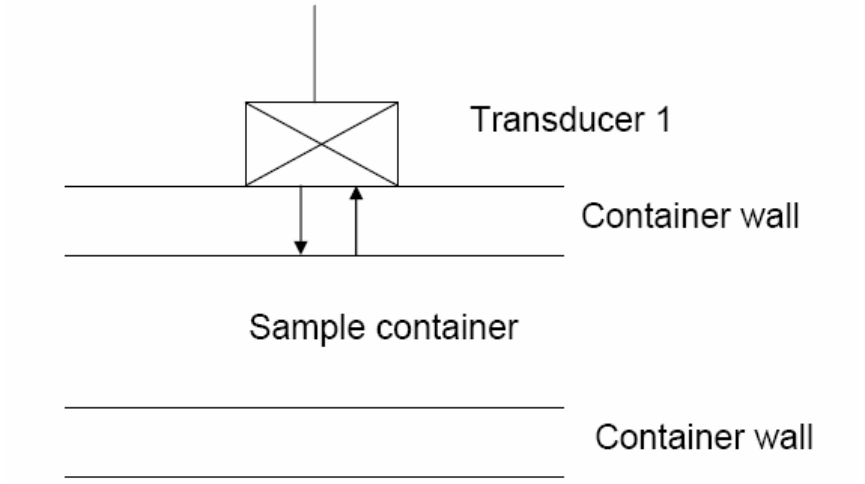

d

Figure 2.1.2 (continued)

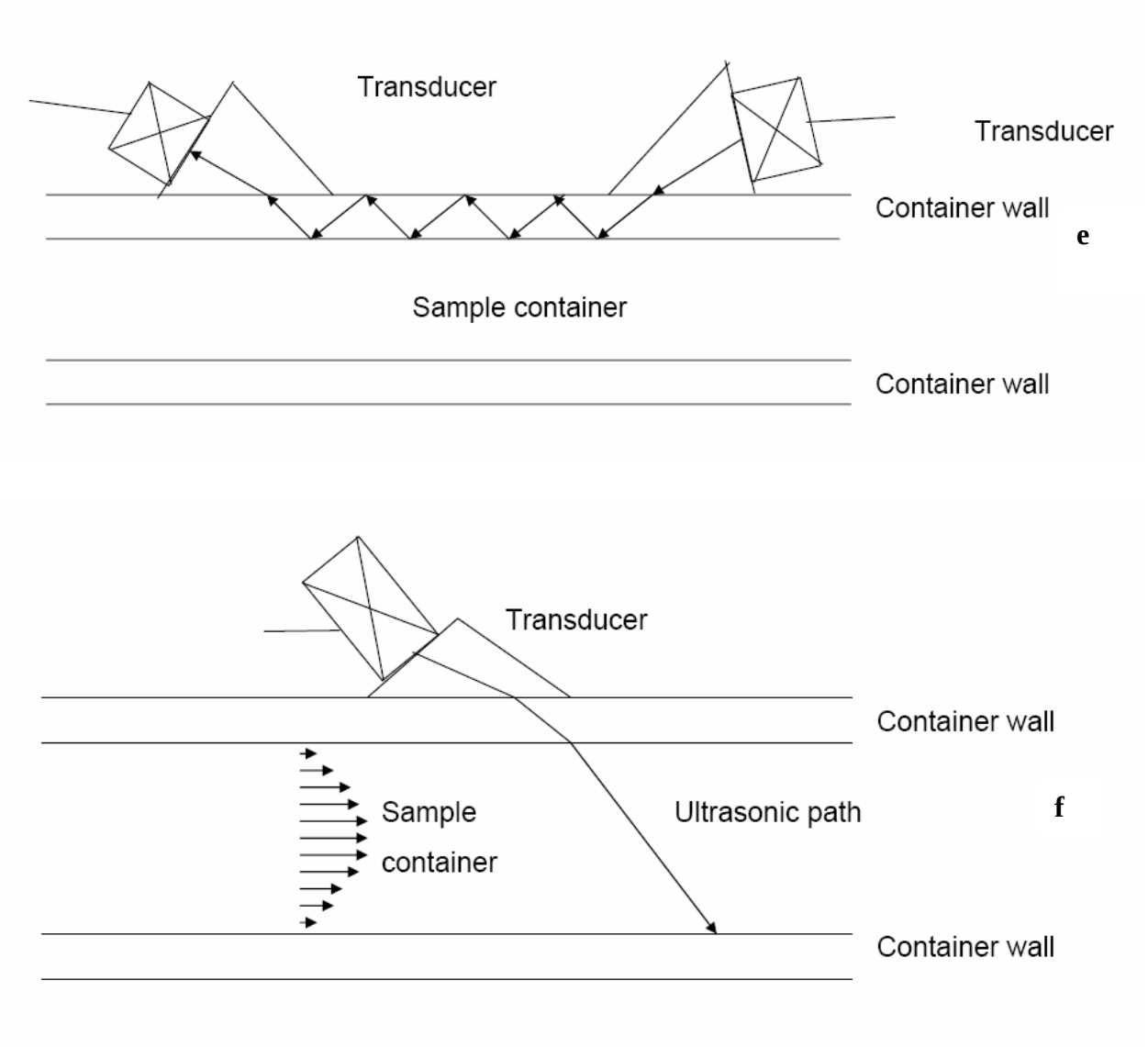

Figure 2.1.2 (continued)

2.1.3 Applications

An important paradigm in the study of food quality is that composition (ingredients) is modified by processing to produce structures that are responsible for the functional properties of foods, particularly texture. Ultrasound has been used to measure composition, structure, and texture of foods and in this section I will review some of the major recent developments in these fields.

a. Ultrasonic Measurement of Food Composition

The measurement of the composition of simple binary mixtures by ultrasonic velocity measurements is the simplest and often most successful group of applications [*e.g.*, solid fat in liquid oil (McClements & Povey, 1987 & 1988a), sugar solutions and fruit juices (Contreras *et al*. 1992), and changes in emulsion composition (Dickinson *et al*. 1994). Bamberger and Greenwood (2004) used this approach to measure the density of a liquid flowing in a pipe.

For simple liquids, attenuation is typically low and relatively hard to measure whilst velocity gives large and measurable differences. Measured velocity can be related to composition either via empirical calibration curve or by using theoretical approaches. For example, in the analysis of a two-component system, Equation 2.3 can be rewritten as:

$$c^2 = \frac{1}{[(1-\phi)\rho_1 + \phi\rho_2)]} \cdot \left(\frac{1-\phi}{\rho_1 c_1^2} + \frac{\phi}{\rho_2 c_2^2} \right) \qquad [2.6]$$

where ϕ is the volume fraction. For a two component system with known volume fraction and component velocities, a convenient definition of mixture velocity becomes:

$$c = c_1\phi + c_2(1-\phi) \qquad [2.7]$$

It is important to recognize that any changes in structure may overwhelm differences due to changes in composition. One good example is the apparent variation of ultrasonic velocity in salmon muscle due to the alignment of myosepta. It is necessary to account for this effect to allow the estimation of fat content in salmon muscle by ultrasonic velocity measurement (Shannon *et al*. 2004).

Although ultrasonic velocimetry is useful to characterize simple binary mixtures, most foods contain many more ingredients and their ultrasonic quantification is more complex. The ultrasonic properties of food vary with frequency, but the rarely enough for spectral resolution of multiple components (as is often used in IR methods). Therefore to measure multiple components it is usually necessary to combine ultrasonic with another technique (*e.g*., ultrasonic velocity and density measurements for ethanol determination in wine (Resa *et al*. 2004) or to make measurements at different temperatures to exploit the different temperature dependency of the ultrasonic properties of different food components. For example the speed of sound in the aqueous portion of chicken increases with temperature and solids content while the speed of sound in the in the fatty portion decreases with temperature. Using the method of mixtures, Chanamai and McClements (1999) were able to make measurements at two temperatures and calculate the fat, water and solids content of a chicken sample. Similarly the oil content in wastewater from an olive oil extraction process was measured (Benedito *et al*. 2004) and the composition of processed foods (Simal *et al*. 2003).

In some cases reflectance (impedance) measurements are preferable to velocity measurements. For example, foams scatter ultrasound strongly and traditionally through transmission measurements cannot usually be made. However, Fox *et al*. (2004) were able to use ultrasonic reflectance measurements to measure overrun in cake batter (This work is particularly interesting as they also considered bubble size distribution in their theoretical analysis). Elmehdi *et al*. (2003a, 2003b, 2004) were able to reach similar conclusions based on attenuation measurements made in through transmission on only by using thin (1-5 cm) bread samples that were freeze-dried and using bread dough.

Phase transitions in lipids, sugars, salts and water are important in food quality and can typically be readily detected and monitored by ultrasound, as the physical properties of the solid and liquid phases are very different. In some cases this can be considered as a simple change in composition and approached using similar methods as described above [*e.g.*, (McClements & Povey, 1987; McClements & Povey, 1988a)]. Martini and others (2005 a,b,c) simultaneously measured the temperature dependence and ultrasonic properties of six fat blends. The ultrasonic attenuation and velocity increased with increasing SFC values, velocity values being more sensitive to crystallization (Martini *et al*. 2005a). Furthermore, SFC data obtained from ultrasonics agreed well with the SFC data from low-resolution pulsed NMR (Martini *et al*. 2005b).

Ultrasound is typically more sensitive to small changes in solids than the more commonly used NMR methods, and this is particularly important in the study of droplet crystallization in emulsions. For example, the extent of supercooling in emulsified lipids (Kloek *et al*. 2000) and the effects of additives on droplet nucleation rate (Awad, 2004) were measured ultrasonically.

More recent work has examined cases where the structures formed can influence the ultrasonic properties and must also be considered. Lipid crystallization is complex because the solid can exist in a variety of different polymorphic forms and microstructures. Recently, several workers have considered whether the ultrasonic properties of a partially crystalline fat system depend simply on the solid fat content (SFC) or also on other microstructural properties. Singh *et al*. (2002, 2004) showed that for cocoa butter and anhydrous milk fat ultrasonic velocity was not a simple function of SFC and argued that more stable (i.e., more dense) polymorphic forms had higher ultrasonic velocities. Martini and co-workers (2005c) showed that ultrasonic attenuation depends on crystal size and lipid microstructure. In another study by Hindle *et al*. (2002) ultrasound was suggested to be sensitive to polymorphic changes in a cocoa butter in an oil-in-water emulsion.

Beyond approximately 10% solids, many semicrystalline lipids become highly attenuating and difficult to make ultrasonic measurements. In their recent work on highly

crystalline fats Martini and co-workers (2005a, b, c) used a novel chirp-wave signal generator and special transducers which together had exceptional penetrating power and they were able to make measurements across a substantial (~8 cm) thickness of various fats with up to ~20% solids. An alternative approach was taken by Saggin and Coupland (2002a) who measured the impedance of a sample of semi-crystalline fats by a reflectance technique and were able to measure the solid fat content.

Ultrasound has been applied less often to the study of phase transitions in water in foods (*i.e.*, freezing) but some recent work shows the technique has some possibilities. Measurement of freezing should be a relatively straightforward application, particularly as ice has (under most conditions) none of the issues around polymorphism that are controversial in the lipids work. However most frozen foods have a very large volume fraction of ice and the assumptions in the simple formulations often used to relate solids content to ultrasonic velocity (*e.g.*, Equations 2.6 and 2.7) break down. Furthermore air bubbles are usually formed during freezing which scatter sound strongly and can dominate the signal.

Lee *et al*. (2004) measured the ultrasonic velocity and ice content (by NMR) in frozen orange juice samples (0 to -50°C). Although an increase in ice content corresponded to an increase in ultrasonic velocity, they were unable to provide a simple relationship between these variables akin to those shown in Equation 2.7. Recently I made similar measurements in sucrose solutions (Figure 2.1.3) and showed (i) the onset of freezing corresponded to an increase in ultrasonic velocity, (ii) the temperature at which the increase initiated decreased with increased sugar content, and (iii) the ultimate speed of sound decreased with increased sugar content (presumably because of the reduced ice content). Taking an alternative approach, Sigfusson *et al.* (2004) measured the ultrasonic properties of a block of food parallel to the direction of heat flux. They were able to reflect part of an ultrasonic pulse from the moving ice front and thereby position it and calculate the proportion of the food frozen.

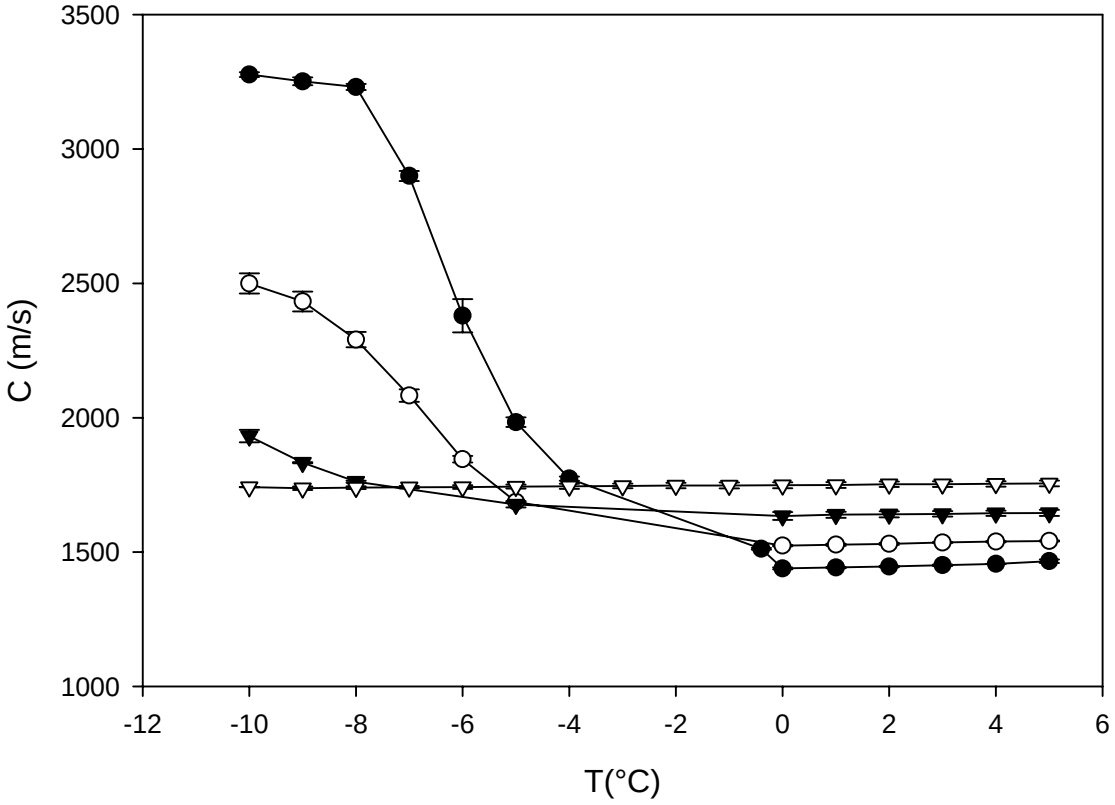

Figure 2.1.3. The speed of longitudinal sound waves as influenced by sucrose concentration (10 to 70%) in aqueous solutions (5 to -10 ºC). (●: 10% sucrose, ○: 30% sucrose, ▼: 50% sucrose, ▽: 70% sucrose).

c. Ultrasonic Measurement of Food Structure

Ultrasound can be used to characterize various scales of structure in food.

i. Macro-scale structure. Ultrasound can be used to measure millimeter scale structures in foods using the techniques of imaging. The time of flight of an ultrasonic pulse reflecting from a food surface can measure its position and hence shape by scanning the position of the transducer across a 2-dimensional grid. Similarly reflectance from internal structures can visualize internal defects. Most imaging is done with L-wave sound.

In most imaging operations both the sample and transducers are immersed in a tank of water to allow good acoustic coupling as the transducers move. This is obviously impractical with most non-packaged foods however the recent development of air-coupled ultrasound has opened up a range of new applications. For example, Saggin and Coupland (2001b) and Cho and Irudayaraj (2003b) used non-contact ultrasound to measure the thickness of a variety of sliced meat and cheese products.

One useful application of 1-D imaging is to position the surface of a liquid during a filling operation. Griffin *et al*. (2001) described how ultrasonic techniques (time of flight and Doppler shift measurements) could be used to monitor and control a bottle-filling operation. Jeffries *et al*. (2002) implemented ultrasonic sensors as part of a control system for liquid level measurements, while other workers used non-contact ultrasonic sensors to measure liquid level in containers (Gan *et al*. 2002).

Foreign bodies (*e.g*., fragments of glass, wood, metal or plastic) typically have impedances significantly different from that of the food so can be ultrasonically imaged as part of a quality control process. This approach was used to detect foreign bodies in bottled beverages, fruit juices and pie filling (Zhao *et al*. 2003, 2004). Internal defects in foods can also be imaged acoustically if there is an impedance mismatch. Benedito *et al*. (2001) were able to detect defects and air cells in cheese. Some of the difficulties that must be overcome include non-parallelism (*i.e*., oblique incidence) and the location of the foreign body and variation in the acoustic properties of the food (Hæggström & Luukkala, 2001).

ii. Micro-scale structure

Ultrasonic imaging is limited in resolution by the wavelength of the sound (~mm) and the finite size of the acoustic beam. However smaller structures can be characterized if they scatter sound (*i.e*., are acoustically dissimilar to the material in which they are imbedded). Many colloidal scale objects scatter sound in a frequency-dependant manner and the spectra can be readily measured. If a theoretical prediction of the ultrasonic properties can be made as a function of structural properties of interest (*e.g*., particle size and concentration) it is possible to calculate details of the structure. This technology has been widely implemented in the commercial development of ultrasonic particle sizers capable of measuring a wider range of size (from 0.01 up to 1000 μm) and concentration (up to 20-30%) than other devices (McClements & Coupland, 1996). The principles of scattering theory (McClements & Coupland, 1996) and ultrasonic particle sizing (Coupland & McClements, 2001) have been described in detail elsewhere. Important recent developments include the extension of scattering theory to higher volume fractions and to include flocculated systems (McClements, 1991; Dukhin & Goetz, 1996). These theoretical developments have allowed characterization of complex instability mechanisms in food emulsions. For example the flocculation of an emulsion leads to a reduction of the scattering efficiency of the individual droplets which can be detected as changes in attenuation coefficient (Herrmann *et al*. 2001; Chanamai *et al*. 2000).

Biopolymer structure can also be characterized ultrasonically. Some workers have used ultrasonic scattering to measure the apparent size of protein aggregates (Griffin & Griffin, 1990), but it is important to remember that proteins can also absorb ultrasonic energy through chemical resonance of protonation-deprotonation reactions as well as scattering from aggregates and changes in molecular hydration (Bryant & McClements, 1999). Ultrasonic attenuation and velocity were used to detect thermal denaturation in concentrated bovine serum albumin solutions (Apenten *et al*. 2000). However, Corredig *et al*. (2004) showed that the ultrasonic measurements (for whey protein) were not identical to those from differential scanning calorimetry, suggesting that the ultrasonic method is responding to distinct molecular processes.

d. Measurement of Food Texture

Rheology involves the study of the deformation of matter in response to applied forces. As ultrasonic propagation involves small deformations of the material in response to the sound wave and their elastic recovery, it is reasonable to consider an ultrasonic measurement a micro-rheological technique and for the readings to relate to macro-rheological properties. However ultrasound operates at higher frequencies (~ 10^3 to 10^6 times) than those commonly seen in most real-world material deformations and used in small deformation rheological measurements. Furthermore, ultrasonic measurements do not depend purely on the elastic modulus but also on density differences and scattering from homogeneities. Despite these difficulties there have been considerable successes in using ultrasound to measure the rheological and flow properties of foods.

The various approaches to this problem can be categorized as (i) the use of T-waves to directly probe (or infer) shear modulus, and (ii) the measurement of flow rate (or flow profile) under known conditions and back calculation of viscosity, (iii) measurement of L-wave properties and correlation with texture.

i. Shear Wave Methods. Because we are typically more concerned with the shear modulus than the bulk modulus of foods, shear ultrasonic waves (T-waves) provide a more direct method to access the appropriate modulus. However, as noted above, shear waves do not propagate well in fluids. One way around this measurement difficulty is to use reflectance (impedance) measurements at the interface between the food and a solid delay line of known properties. The proportion of ultrasonic energy reflected from the interface of two materials depends on the impedance mismatch (Equation 2.5).

The normalized shear reflectance for food and hydrocarbon oils were shown to be proportional to the viscosity of oils (Saggin & Coupland, 2001a) and diluted honey (Kulmyrzaev & McClements, 2000). However, mechanical relaxations that occur in the fluid between the high-frequency ultrasonic measurements and the low-frequency conventional measurements mean the relationship is complex (Kulmyrzaev & McClements, 2000, Saggin & Coupland,

2004a). For example, concentrated sugar syrups have a glass transition frequency below the ultrasonic measurement frequency used (*i.e.*, 10 MHz) and therefore had a very low ultrasonically measured viscosity while their conventionally measured viscosity remained high (Kulmyrzaev & McClements, 2000, Saggin & Coupland, 2004a). The presence of a biopolymer reduced the glass transition frequency by binding water (Saggin & Coupland, 2004a).

Other workers studied the mechanical properties of a casein gel using a shear resonance method and conventional low-oscillatory rheological techniques (Buckin & Kudryashov, 2001). Again time-scale and wavelength differences prevented extrapolation of physical properties such as viscosity, storage modulus, and loss tangent in between the two techniques, but shear resonance was able to reveal complementary information about submicron structure.

In other cases, a more empirical approach has been taken to the shear-wave characterization of food texture. For example, a number of studies focused on the ultrasonic evaluation of structural and rheological properties of dough and bakery products (Lee et al. 2004; Elmehdi *et al*. 2003, 2004; Ross *et al*. 2004). Fermentation of the dough was characterized by pronounced velocity dispersion at low frequencies (*i.e.*, < 6 MHz). In addition, ultrasonic measurements were shown to be more sensitive to changes in rheology compared to extensional viscometry, but problems can arise due to the high attenuation of the dough (Lee *et al*. 2004). In this last case, L-waves were employed.

ii. Flow Curve Determination. While shear waves provide a direct way to probe material bulk modulus, other workers have taken a more indirect, but frequently more practical route to rheological measurements by using ultrasonic techniques to measure the flow rate or flow profile of a fluid under known conditions and back-calculating the viscosity.

Fluid flow rate can be measured by ultrasonic Doppler velocimetry (UDV) which depends on the phase shift caused by propagation in a flowing fluid. The ultrasonic transducer is located at a fixed location on the pipe, while the wave propagates through the flowing medium (Figure 2.1.2f). The change in frequency between the transmitted wave and its corresponding

echo after propagation can be related to the flow velocity profile. Based on a rheological model for the flowing liquid, it is possible to construct a flow profile (Dogan *et al*. 2003). Recently this technique has been applied to more realistic food processing situations (*i.e*., on-line viscosity determination of a power-law fluid with a temperature gradient) (Wang *et al*. 2004).

An enhancement of the Doppler technique is to generate an entire flow profile directly by tomographic analysis. In this technique, multiple ultrasonic pulses are sent through the fluid and the position of the entrained scatterers measured by the time of flight of returning echoes while their velocity is measured from the frequency shift in the sound. Combining several of these signals it is possible to map the velocity of the entrained scattering particles (and hence the flowing fluid itself) as a function of position across the pipe. The flow profile obtained can be used to calculate the rheological properties of the fluid. Recently this approach was compared to off-line rheological measurements and on-line magnetic resonance imaging (MRI) of fluid flow for tomato juice and high-fructose corn syrup samples (Choi *et al*. 2002). While the values from all three methods agreed, UDV has the advantages of being online, non-invasive, and relatively cheap (compared to MRI). Both UDV and MRI suffer a reduction in the sensitivity of flow velocity measurements around the pipe walls (Choi *et al*. 2002).

iii. Correlation with L-wave measurements. While there is only a limited theoretical basis to expect longitudinal wave properties to depend on shear modulus there are often useful empirical correlations. For example Benedito *et al*. (2002) investigated the changes in composition of food oils during frying and were able to show a useful empirical relationship between viscosity and L-wave velocity.

However, as with any correlation-based method, uncertainty as to the exact factor to which the sensor is responding can lead to confusion. For example Dalgleish *et al*. (2004) used an ultrasonic resonator to detect the onset of formation of a casein gel. However, they were able to show that the ultrasonic measurements were more sensitive to associated changes in casein micelle microstructure compared to the changes in bulk properties.

A popular empirical texture measurement method using L-wave ultrasound is to monitor the ripening and softening of fruits. For example, a reduction of firmness in plums was associated with a parabolic reduction in attenuation (Mizrach, 2004) and maturity related parameters were correlated qualitatively and/or quantitatively to ultrasonic properties in avocado and mango (Mizrach, 2000). Similarly, measurements of resonance frequency and apparent attenuation were related to chilling injury in tomatoes (Verlinden *et al*. 2004). However, as with all measurement systems where there is no reliable theoretical basis to relate sensor response with the property of interest, it is difficult to decide *a priori* if an application will be successful. For example, while mealy apples have some physical properties distinct from non-mealy fruit, these could not be detected ultrasonically (Mizrach *et al*. 2003). Similar changes in texture, structure and composition occur during the ripening of cheeses and ultrasound has also been used to empirically characterize the changes (Benedito *et al*. 2000).

A novel approach to ultrasonic viscosity determination was taken by Herrmann and McClements (1999) who measured the ultrasonic spectra of fine (190 nm) monodisperse silica particles (5% by volume) suspended in different fluids. Rather than solving the scattering problem to measure particle size (see above), they solved for continuous phase viscosity.

2.1.4 Conclusions

Using ultrasonics, we can characterize the food composition, monitor some unit operations (*e.g*. fermentation, heating, cooling), or elucidate molecular processes that may not be otherwise measurable (*e.g*., high frequency rheology, particle sizing in concentrated systems, some on-line applications). However, the complex structure and composition of foods makes it difficult to uniquely characterize foods using ultrasound alone. The development of ultrasonic sensors will depend on their two major strengths: (i) making measurements in places where other measurement methods are not appropriate, and (ii) measuring events not detectable by other devices.

One of the major advantages of ultrasound is its flexibility in an on-line environment. I expect more measurement devices to be integrated into production equipment in novel ways. These will allow greater process control but also better understanding of changes in product structure in process conditions. This will be particularly important in crystallization operations (*e.g.*, freezing, confectionary manufacture), baking and dough preparation technologies, and homogenization of fluids. In particular the combination of ultrasonic and other sensing devices will be used to develop sensor suites capable of a more holistic description of product/process.

Acknowledgement. The project was supported by the National Research Initiative of the USDA Cooperative State Research, Education and Extension Service, grant number 2003-35503-13852.

2.1.5 References

1. Apenten, R.K.O., Buttner, B. & Mignot, B., Pascal, D. & Povey, M.J.W. 2000. Determination of the adiabatic compressibility of bovine serum albumen in concentrated solution by a new ultrasonic method. *Food Hydrocolloids*, 14(1), 83-91.
2. Awad, T.S. Ultrasonic studies of the crystallization behavior of two palm fats O/W emulsions and its modification. 2004. *Food Research International*, 37(6), 579-586.
3. Bamberger, J.A. & Greenwood, M.S. 2004. Non-invasive characterization of fluid foodstuffs based on ultrasonic measurements. *Food Research International*, 37(6), 621-625.
4. Benedito, J., Carcel, J., Gisbert, M. & Mulet, A. 2001.Quality control of cheese maturation and defects using ultrasonics. *Journal of Food Science*, 66(1), 100-104.
5. Benedito, J., Carcel, J.A., Sanjuan, N. & Mulet, A. 2000. Use of ultrasound to assess Cheddar cheese characteristics. *Ultrasonics*, 38(1-8), 727-730.
6. Benedito, J., Mulet, A., Clements, G., & Garcia-Perez, J.V. 2004. Use of ultrasonics for the composition assessment of olive mill wastewater (alpechin). *Food Research International*, 37(6), 595-601.
7. Benedito, J., Mulet, A., Velasco, J. & Dobarganes, M.C. 2002. Ultrasonic assessment of oil quality during frying. *Journal of Agricultural and Food Chemistry*, 50(16), 4531-36.
8. Blitz, J. 1963. Fundamentals of ultrasonics. Butterworths, London.
9. Bryant, C.M. & McClements, D.J. 1999. Ultrasonic spectroscopy study of relaxation and scattering in whey protein solutions. *Journal of the Science of Food and Agriculture*, 79(12), 1754-1760.
10. Buckin, V. & Kudryashov, E.2001. Ultrasonic shear wave rheology of weak particle gels. *Advances in Colloid and Interface Science*, 89(Sp. Iss), 401-422.
11. Buckin, V. & Smyth, C. 1999. High-resolution ultrasonic resonator measurements for

analysis of liquids. *Seminars in Food Analysis*, 4(2), 113-130.

12. Chanamai, R., Herrmann, N. & McClements, D.J. 2000. Probing floc structure by ultrasonic spectroscopy, viscometry, and creaming measurements. *Langmuir*, 16(14), 5884-91.
13. Chanamai, R. & McClements, D.J. 1999. Ultrasonic determination of chicken composition. *Journal of Agricultural and Food Chemistry*, 47(11), 4686-92.
14. Choi, Y.I., McCarthy, K.L. & McCarthy, M.J. 2002. Tomographic techniques for measuring fluid flow properties. *Journal of Food Science*, 67(7), 2718-24.
15. Cho, B. & Irudayaraj, J.M.K. 2003a. Design and application of a non-contact ultrasound velocity measurement system with air instability compensation. *Transactions of the ASAE*, 46(3), 901-909.
16. Cho, B.K. & Irudayaraj, J.M.K. 2003b. A noncontact ultrasound approach for mechanical property determination of cheeses. *Journal of Food Science*, 68(7), 2243-47.
17. Contreras, N.I., Fairley, P., McClements, D.J., & Povey, M.J.W. 1992. Analysis of the sugar content of fruit juices and drinks using ultrasonic velocity measurements. *International Journal of Food Science and Technology*, 27(5), 515-529.
18. Corredig, M., Verespej, E. & Dalgleish, D.G. 2004. Heat-induced changes in the ultrasonic properties of whey proteins. *Journal of Agricultural and Food Chemistry*, 52(14), 4465-71.
19. Coupland, J.N. 2004. Low-intensity ultrasound. *Food Research International*, 37 (6), *537-543*.
20. Coupland, J.N. & McClements, D.J. 2001. Droplet size determination in food emulsions: comparison of ultrasonic and light scattering methods. *Journal of Food Engineering* 50(2), 117-120.
21. Coupland, J.N. & Saggin, R. 2003. Ultrasonic sensors for the food industry. 45, 101-166.
22. Dalgleish, D., Alexander, M. & Corredig, M. 2004. Studies of the acid gelation of milk using ultrasonic spectroscopy and diffusing wave spectroscopy. *Food Hydrocolloids,* 18(5), 747-755.
23. Dickinson, E., Jianguo, M. & Povey, M. J. W. 1994. Creaming of concentrated oil-in-water emulsions containing xanthan. *Food-Hydrocolloids,* 8(5), 481-497.
24. Dogan, N., McCarthy, M.J. & Powell, R.L. 2003. Comparison of in-line consistency

measurement of tomato concentrates using ultrasonics and capillary methods. *Journal of Process Engineering*, 25 (6), 571-587.

25. Dukhin, A.S., Goetz, P.J. & Hamlet, C.W., Jr. 1996. Acoustic spectroscopy for concentrated polydisperse colloids with low density contrast. *Langmuir*, 12(21), 4998-5003.
26. Elmehdi, H.M., Page J.H. & Scanlon, M.G. 2003a. Using ultrasound to investigate the cellular structure of bread crumb. *Journal of Cereal Science*, 38(1), 33-42.
27. Elmehdi, H.M., Page, J.H. & Scanlon, M.G. 2003b. Monitoring dough fermentation using acoustic waves. *Food and Bioproducts Processing*, 81(C3), 217-223.
28. Elmehdi, H.M., Page, J.H. & Scanlon, M.G. 2004. Ultrasonic investigation of the effect of mixing under reduced pressure on the mechanical properties of bread dough. *Cereal Chemistry*, 81(4), 504-510.
29. Fox, P., Probert Smith, P. & Sahi, S. 2004. Ultrasound measurements to monitor the specific gravity of cake batters. *Journal of Food Engineering*, 65(3), 317-324.
30. Gan, T.H., Hutchins, D.A. & Billson, D.R. 2002. Preliminary studies of a novel air-coupled ultrasonic inspection system for food containers. *Journal of Food Engineering*, 53(4), 315-323.
31. Griffin, S.J., Hull, J.B. & Lai, E. 2001. Development of a novel ultrasound monitoring system for container filling operations. *Journal of Materials Processing Technology*, 109(1-2), 72-77.
32. Griffin, W.G. & Griffin, M.C.A. 1990. The attenuation of ultrasound in aqueous suspensions of casein micelles from bovine milk. *Journal of the Acoustical Society of America*, 87(6), 2541-50.
33. Hæggström, E. & Luukkala, M. 2001. Ultrasound detection and identification of foreign bodies in food products. *Food Control*, 12(1), 37-45.
34. Hay, T.R. & Rose, J.L. 2003. Fouling detection in the food industry using ultrasonic guided waves. *Food Control*, 14(7), 481-488.
35. Herrmann N., Hemar Y., Lemaréchal P. & McClements D.J. 2001. Probing particle-particle interactions in flocculated oil-in-water emulsions using ultrasonic attenuation spectrometry. *European Physical Journal E*, 5(2), 183-188.
36. Herrmann, N. &McClements D. J. 1999. Influence of visco-inertial effects on the

ultrasonic properties of monodisperse silica suspensions. *Journal of the Acoustical Society of America*, 106(2), 1178-1181.

37. Hill, C.R., Bamber, J.C. & ter Haar, G.R. 2004. Physical principles of medical ultrasonics. 2nd ed. John Wiley & Sons, Ltd. West Sussex, England.
38. Hindle, S.A., Povey, M.J.W. & Smith, K.W. 2002. Characterizing cocoa-butter seed crystals by the oil-in-water emulsion crystallization method. *Journal of the American Oil Chemists` Society*, 79(10), 993-1002.
39. Jeffries, M., Lai, E. & Hull, J.B. 2002. Fuzzy flow estimation for ultrasound-based liquid level measurement. *Engineering Applications of Artificial Intelligence*, 15(1), 31-40.
40. Kloek, W., Walstra, P. & van Vliet, T. 2000. Nucleation kinetics of emulsified triglyceride mixtures. *Journal of the American Oil Chemists' Society*. 77(6), 643-652.
41. Kulmyrzaev, A., Cancelliere, C. & McClements, D.J. 2000. Characterization of aerated foods using ultrasonic reflectance spectroscopy. *Journal of Food Engineering*, 46(4), 235-241.
42. Kulmyrzaev, A. & McClements, D.J. 2000. High frequency dynamic shear rheology of honey. *Journal of Food Engineering*, 45(4), 219-224.
43. Lee, S., Pyrak-Nolte, L.J., Cornillon, P. & Campanella, O. 2004. Characterisation of frozen orange juice by ultrasound and wavelet analysis. *Journal of the Science of Food and Agriculture*, 84(5), 405-410.
44. Lee, S., Pyrak-Nolte, L.J. & Campanella, O. 2004. Determination of ultrasonic-based rheological properties of dough during fermentation. *Journal of the Texture Studies*, 85, 33-51.
45. Martini, S., Bertoli, C., Herrera, M.L., Neeson, I. & Marangoni, A. 2005a. *In situ* monitoring of solid fat content by means of pulsed nuclear magnetic resonance spectrometry and ultrasonics. *Journal of the American Oil Chemists' Society*, 82(5), 305-312.
46. Martini, S., Herrera, M.L. & Marangoni, A. 2005b. New technologies to determine solid fat content online. *Journal of the American Oil Chemists' Society*, 82(5), 313-317.
47. Martini, S., Bertoli, C., Herrera, M.L., Neeson, I. & Marangoni, A. 2005c. Attenuation of ultrasonic waves: influence of microstructure and solid fat content. *Journal of the American Oil Chemists' Society*, 82(5), 319-328.
48. McClements, D.J., & Povey, M.J.W. 1987. Solid fat content determination using ultrasonic

velocity measurements. *International Journal of Food Science and Technology*, 22(5), 491-499.

49. McClements, D.J., & Povey, M.J.W. 1988a. Comparison of pulsed NMR and ultrasonic velocity techniques for determining solid fat contents. *International Journal of Food Science and Technology*, 23(2), 159-170.
50. McClements, D.J. 1991. Ultrasonic characterisation of emulsions and suspensions. *Advances in Colloid and Interface Science*, 37(1-2), 33-72.
51. McClements, D.J. 1995. Advances in the application of ultrasound in food analysis and processing. *Trends in Food Science and Technology*, 6, 293-299.
52. McClements, D. J. & Coupland, J. N. 1996. Theory of droplet size distribution measurements in emulsions using ultrasonic spectroscopy. *Colloids and Surfaces A: Physicochemical and Engineering Aspects*, 117(1-2), 161-170.
53. Mizrach, A. 2000. Determination of avocado and mango fruit properties by ultrasonic method. *Food Research International*, 38(1-8), 717-722.
54. Mizrach, A. 2004. Assessing plum fruit quality attributes with an ultrasonic method. *Food Research International*, 37(6), 627-631.
55. Mizrach, A., Bechar, A., Grinshpon, Y., Hofman, A., Egozi, H. & Rosenfeld, L. 2003. Ultrasonic classification of mealiness in apples. *Transactions of the ASAE*, 46(2), 397-400.
56. Povey, M.J.W. 1998. Ultrasonics of food. *Contemporary Physics*, 39(6), 467-478.
57. Resa, P., Elvira, L. & Mondero de Espinosa, F.M. 2004. Concentration control in alcoholic fermentation processes from ultrasonic velocity measurements. *Food Research International*, 37(6), 587-594.
58. Rose, J.L. 2004. Ultrasonic waves in solid media. Cambridge University Press, Cambridge, UK.
59. Ross, K. A., Pyrak-Nolte, L. J. & Campanella, O. H. 2004. The use of ultrasound and shear oscillatory tests to characterize the effect of mixing time on the rheological properties of dough. *Food Research International*, 37(6), 567-577.
60. Saggin, R. & Coupland, J.N. 2001a. Oil viscosity measurement by ultrasonic reflectance. *Journal of the American Oil Chemists Society*, 78(5), 509-511.

61. Saggin, R. & Coupland, J.N. 2001b. Non-contact ultrasonic measurements in food materials. *Food Research International*, 34(10), 865-870.

62. Saggin, R. & Coupland, J.N. 2001c. Concentration measurement by acoustic reflectance. *Journal of Food Science*, 66(5), 681-685.

63. Saggin, R. & Coupland, J.N. 2002a. Measurement of solid fat content by ultrasonic reflectance in model systems and chocolate. *Food Research International*, 35(10), 999-1005.

64. Saggin, R. & Coupland, J.N. 2002b. Ultrasonic monitoring of powder dissolution. *Journal of Food Science*, 67(4), 1473-1477.

65. Saggin, R. & Coupland, J.N. 2004a. Rheology of xanthan/sucrose mixtures at ultrasonic frequencies. *Journal of Food Engineering*, 65 (1), 49-53.

66. Shannon, R. A., Probert-Smith, P. J., Lines, J. & Mayia, F. 2004. Ultrasound velocity measurement to determine lipid content in salmon muscle; the effects of myosepta. *Food Research International*, 37(6), 611-620.

67. Sheen, S., Chien, H. & Raptis, A. 1995. An in-line ultrasonic viscometer. *Review of Progress in Nondestructive Evaluation*, 14A, 1151-58.

68. Sheen, S., Chien, H. & Raptis, A. 1996. Measurement of shear impedances of viscoelastic fluids. *IEEE Ultrasonics Symposium Proceedings*, 453-457.

69. Sigfusson, H., Ziegler, G.R. & Coupland, J.N. 2004. Ultrasonic monitoring of food freezing. 62(3), 263-269.

70. Singh, A.P., McClements, D.J.& Marangoni, A.G. 2002. Comparison of ultrasonic and pulsed NMR techniques for determination of solid fat content. *Journal of the American Oil Chemists' Society*, 79(5), 431-437.

71. Simal, S., Benedito, J., Clemente, G., Femenia, A. & Rosselló, C. 2003. Ultrasonic determination of the composition of a meat-based product. *Journal of Food Engineering*, 58(3), 253-257.

72. Verlinden, B.E., De Smedt, V. & Nicolaï, B.M. 2004. Evaluation of ultrasonic wave propagation to measure chilling injury in tomatoes. *Postharvest Biology and Technology*, 32(1), 109-113.

73. Wang, L., McCarthy, K.L. & McCarthy, M.J. 2004. Effect of temperature gradient on

ultrasonic Doppler velocimetry measurement during pipe flow. *Food Research International*, 37(6), 633-642.

74. Zhao, B., Basir. O.A. & Mittal, G.S. 2003. Detection of metal, glass and plastic pieces in bottled beverages using ultrasound. *Food Research International,* 36(5), 513-521.

75. Zhao B., Jiang Y., Basir O.A. & Mittal, G.S. 2004. Foreign body detection in foods using the ultrasound pulse/echo method. *Journal of Food Quality*, 27 (4), 274-288.

2.2 Physical Properties of Ice

2.2.1 Thermodynamics of Freezing

According to the current ice phase diagram, there are at least 12 different known ice phases that can be formed under different temperature and pressure combinations (Figure 2.2.1) (Lobban *et al*. 1998). What is generally referred to as "ice" is the crystalline form of pure water at atmospheric pressure and temperatures above -120°C. Under these conditions, ice crystals naturally occur in the phase "Ice Ih" (I for phase 1 and h for the "hexagonal" geometry of the ice crystals). This phase was named after the discovery of various other crystal structures formed at high pressure or by direct condensation of water vapor around -100 °C. A brief collection of the physical properties of ice (Ih) are summarized on Table 2.2.1. Ice Ih is characterized by volume expansion on formation (about 9% at 0°C) while most of the variants are formed under high pressures and their densities are higher than that of water (Li & Sun, 2002). Due to the uncertainties in the metastable phases and the presence of contaminating phases identified under unexpected conditions, the phase diagram of ice is far from being complete (Petrenko & Whitworth, 1999).

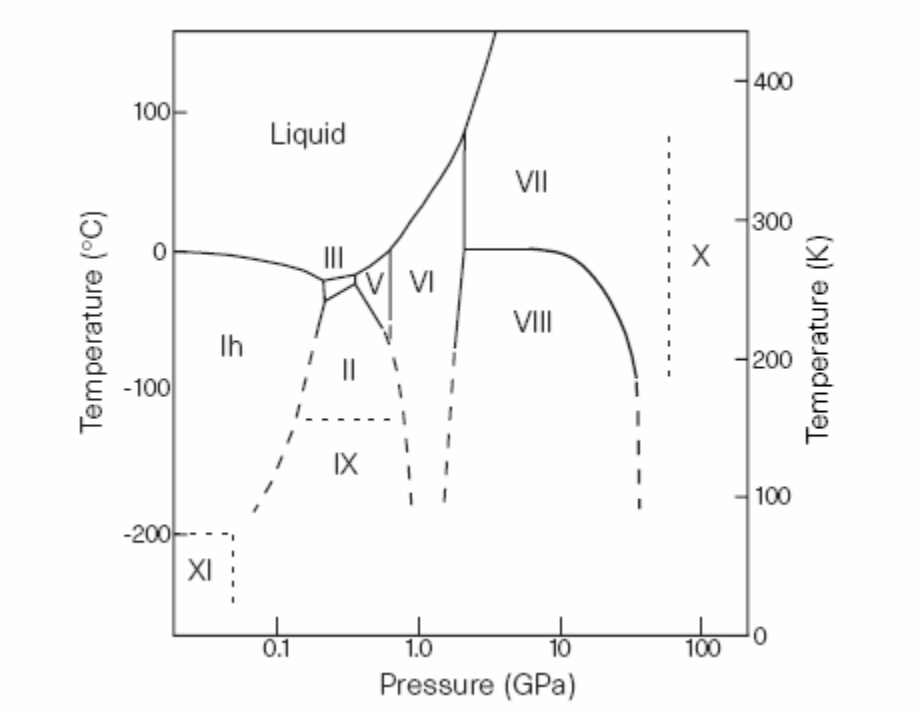

Figure 2.2.1. The phase diagram of ice (Source: Lobban *et al*. 1998).

Table 2.2.1. Physical properties of ice (Source: Petrenko & Whitworth, 1999).

Physical Property	**Value**
STRUCTURAL PROPERTIES (-20 °C)	
Lattice parameter (a)	4.519 Å
Lattice parameter (c)	7.357 Å
Molecules per unit volume	3.074×10^{28} m^{-3}
Volume per molecule	32.53 $Å^3$
Density	917.3 kg m^{-3}
ELASTIC MODULI (-16 °C)	
Bulk modulus	8.9 GPa
Young's modulus	9.33 GPa
Shear modulus	35.2 GPa
Poisson`s ratio	0.325
THERMAL PROPERTIES (-20 °C)	
Latent heat of fusion (0 °C)	333.5 kJ kg^{-1}
Specific heat capacity	1.962 kJ K^{-1} kg^{-1}
Coefficient of linear expansion	5.3×10^{-5} K^{-1}
Thermal conductivity	2.4 W m^{-1} K^{-1}

Since frozen foods contain solutes in addition to water, a solution phase diagram is more relevant than the phase diagram of pure water. As an example, part of the sucrose/water phase diagram is shown as Figure 2.2.2 (Young & Jones, 1949). The equilibrium freezing temperature of pure water at atmospheric pressure is 0°C while the freezing point of water in a solution is depressed by the presence of the solute. The extent of depression is generally proportional to the concentration of solutes in the solution. Since at any given temperature, the equilibrium solute concentration is known, the ice content in sucrose solutions can be calculated as a function of temperature. For example, a 50% sucrose solution is at equilibrium with ice at -7°C so when a

20% solution is cooled to -7°C, 60% of the water will freeze so the remaining solution is 50% sucrose.

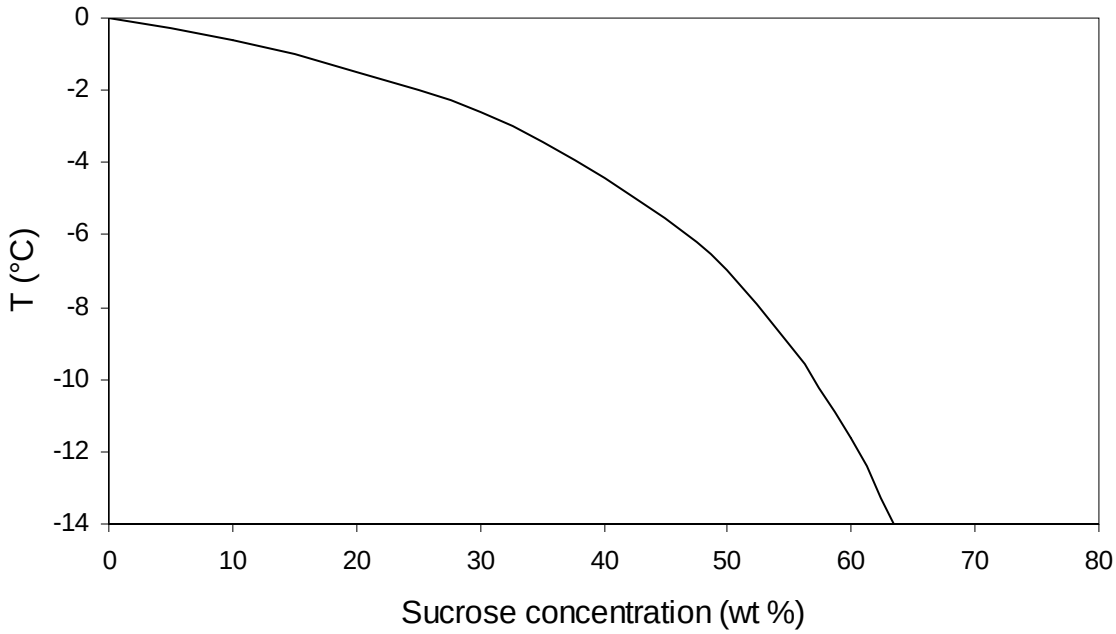

Figure 2.2.2. Sucrose-water phase diagram (Source: Young & Jones, 1949).

2.2.2 Kinetics of Freezing

The freezing of foods requires the formation of ice crystal nuclei that will grow into ice crystals and eventually into a partially frozen matrix as the temperature is lowered. Nucleation and growth processes are kinetically limited processes (*i.e.*, mostly heat and mass transfer) and the attainment of equilibrium requires time.

2.2.2.1 Ice Nucleation

Nucleation is the first step in crystallization. In this step, tiny crystal embryos called nuclei are formed which later grow into crystals. The fate of an individual nucleus depends on the change

in free energy as a result of its growth or shrinkage. Surface free energy increases with the square of crystal size as there is an interfacial tension between the two phases while the free energy of crystallization decreases with the cube of size. The change in overall energy of crystal formation as a function of crystal nucleus size can be calculated as:

$$\Delta G = \frac{4}{3}\pi r^3 \Delta G_p + 4\pi r^2 \sigma \qquad [2.8]$$

where ΔG is the change in free energy due to the formation of a spherical particle, r is the radius of the spherical particle, ΔG_p is the difference in free energy between solid and liquid phases, σ is the interfacial tension between the two phases (Fennema *et al*. 1973). Below a critical radius the surface term dominates and small crystals will tend to melt while above that size the volume term favors crystal growth (Figure 2.2.3). The critical nucleus size (r_c) is defined as:

$$r_c = \frac{2\sigma\ \upsilon T_f}{\Delta H_f (T_f - T)} \qquad [2.9]$$

where T_f is the freezing temperature in absolute scale, T is the temperature of the investigation in (K), ΔH_f is the latent heat of fusion, and υ is the molecular volume. According to Equation 2.8, there is an energy maximum preventing the formation of macroscopic crystals and overcoming that barrier determines the kinetics of nucleation. A lower energy barrier to nucleation means the time needed for nucleation (*i.e*., induction time) is lower and the nucleation rate is higher. According to Equation 2.9, cooling the system below the freezing temperature is necessary ($T < T_f$) for the stable nuclei to form and as the extent of supercooling ($T-T_f$) increases, the critical nucleus size decreases and hence the likelihood of the formation of nuclei increases.

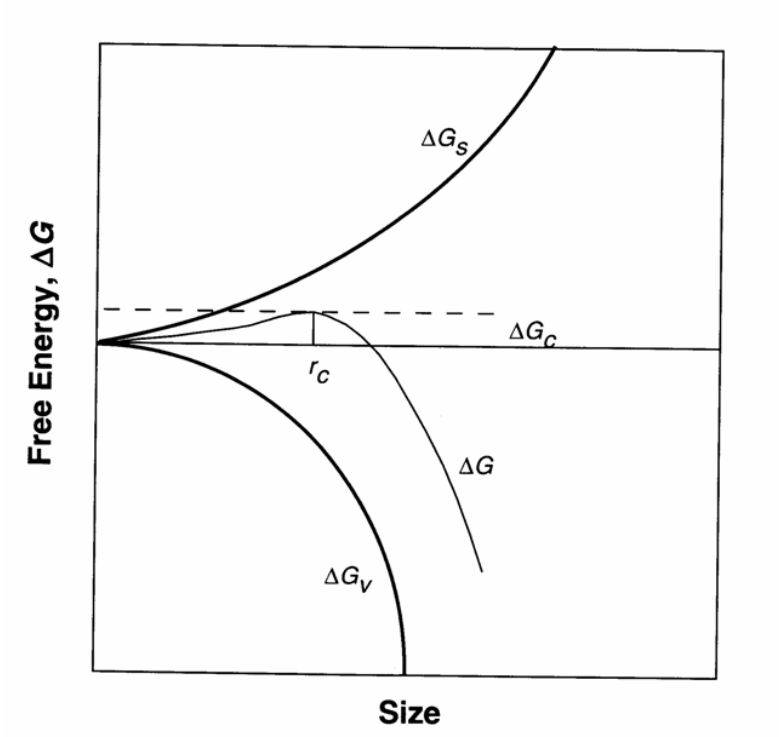

Figure 2.2.3. Free energy (ΔG) changes associated with formation of a stable nucleus. ΔG_s, free energy of surface formation; ΔG_v, free energy of volume formation; ΔG_c, critical free energy for nuclei formation; r_c = critical size (Source: Hartel, 2001).

According to this mechanism the nuclei form spontaneously from density fluctuations in the liquid phase (*i.e*., homogeneous nucleation) (Sahagian & Goff, 1996). However, in most experiments, crystallization occurs at considerably higher temperatures than the expected homogeneous nucleation temperature, due to the presence of solid impurities that form a stable surface for nuclei formation (Hartel, 2001). This type of crystallization is known as "heterogeneous nucleation" and is more commonly observed than homogeneous nucleation. The distinction between heterogeneous and homogeneous nucleation can be made using DSC techniques (Özilgen & Reid, 1993).

The capacity of impurities to induce heterogeneous nucleation depends on their structural match with the crystallizing molecules, as well as their low solubility. The probability of

heterogeneous nucleation increases with the decreasing contact angle between the crystallizing matter and the nucleation agent; at a contact angle of 0°, nucleation is spontaneous whereas at 180°, change in surface energy for heterogeneous nucleation equals that of homogeneous nucleation (Sahagian & Goff, 1996). Examples of ice nucleating materials include AgI, silicate minerals, sterols and certain proteins (Hartel, 2001; Archer *et al*. 1996; Özilgen & Reid, 1993). Some bacteria synthesize ice nucleation proteins and reduce the supercooling required to freeze water. In the presence of these bacteria, the heterogeneous nucleation temperature for water can be as high as -1°C (Lee *et al*. 1995). Freeze-dried and standardized cellular suspensions of *Pseudomonas syringae* are commercially available as biological ice nucleation agents and commonly used in ski resorts in artificial snow-making (Cazorla *et al*. 1995).

Heterogeneous and homogeneous nucleation are together defined as primary nucleation since the nuclei are formed within the system. In many food processing operations, previously formed crystals of the crystallizing matter (*i.e.*, seed crystals) are used in order to facilitate nucleation. This is called "secondary nucleation". The applications of secondary nucleation are limited by the available sizes of the seed crystals. In addition to seed crystals, the mechanically disrupted parts of seed crystals or newly formed crystals can induce secondary nucleation (Hartel, 2001).

2.2.2.2 Crystal Growth

The formation of stable nuclei (*i.e*., nucleation) is followed by their growth into crystals, although in some systems nucleation and crystal growth can occur simultaneously. During crystal growth, most of the crystalline mass is formed. In the earlier stage of crystal growth, the crystallizing species attach themselves to the growing crystals while there are available incorporation sites (Hartel, 2001). Other, non-crystallizing material must diffuse out of the way of the growing ice front or be entrapped by the crystal or incorporated into the lattice. For example, dissolved gases are excluded from the crystal phase and become concentrated in the unfrozen phase. If the rate of crystal growth is fast ($> 2.5\ \mu m.s^{-1}$) then the gasses do not have the

time to diffuse out before their concentration exceeds the saturation point and bubbles begin to form between the crystals (Bari & Hallett, 1974; Cole, 1979). Gas bubble formation can be reduced by prior degassing of the solution and by slow cooling rates to allow the dissolved gas to diffuse away from the moving crystal face. In general slower crystal growth allows the crystallizing molecules to reach their optimum alignment on the lattice while the non-crystallizing material is excluded and the resultant crystals will show greater perfection. Crystal growth will continue until limited by attainment of chemical equilibrium or by mass and heat transfer limitations.

2.2.2.3 Polycrystalline Ice

As the crystals grow larger and reach a certain volume fraction they will eventually come into contact with one another (Schulson, 1999). Two abutting crystals do not merge to form one larger one as their crystal lattices do not necessarily align with one another so there will remain a planar defect line separating them even after the material is completely crystallized. This defect is known as a grain boundary. At the grain boundaries, the material strength decreases, whereas the concentration of impurities can increase and there is likely to be a thin layer of liquid separating the grains (Flewitt & Wild, 2001). For example, sea ice can contain large pockets of brine or other impurities (air bubbles) within the grain boundaries totaling 4-5 vol. % (Schulson, 1999).

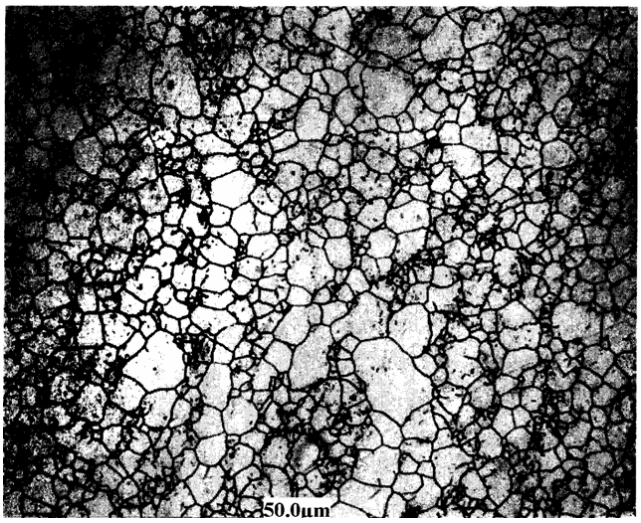

Figure 2.2.4: The representation of grain boundaries in a polished and etched metal sample (Source: Flewitt & Wild, 2001).

2.2.3 References

1. Archer, G.P., Kennedy, C.J. & Povey, M.J.W. 1996. Investigations of ice nucleation in water-in-oil emulsions using ultrasound measurements. *Cryo-Letters*, 17(6), 391-396.
2. Bari, S.A.& Hallett, J. 1974. Nucleation and growth of bubbles at an ice-water interface. *Journal of Glaciology*, 13(69), 489-520.
3. Cazorla, F.M., Olalla, L., Torés, J.A., Peréz-Garcia, A., Codina, J.C. & de Vicente, A. 1995. A method for estimation of population densities of ice nucleating active *Pseudomonas syringae* in buds and leaves of mango. *Journal of Applied Bacteriology*, 79, 341-346.
4. Cole, D.M. 1979. Preparation of polycrystalline ice samples for laboratory experiments. *Cold Regions Science and Technology*, 1, 153-179.
5. Fennema, W.D. Powrie & Marth, E.H. 1973. Low-temperature preservation of foods and living matter. Marcel Dekker, Inc., USA.
6. Flewitt, P.E. & Wild, R.K. 2001. Grain boundaries: their microstructure and chemistry. John Wiley & Sons, Ltd., England.
7. Hartel, R.W. 2001. Crystallization in foods. Aspen Publishers, USA.
8. Lee, Jr., R.E., Warren, G.J. & Lawrence, V.G. 1995. Biological ice nucleation and its applications. APS Press, St. Paul, MN.
9. Li, B. & Sun, D. 2002. Novel methods for rapid freezing and thawing of foods - a review. *Journal of Food Engineering*, 54(3), 175-182.
10. Lobban, C., Finney, J.L. & Kuhs, W.F. 1998. The structure of a new phase of ice. *Nature*, 391(6664), 268-270.
11. Özilgen, S. & Reid, D.S. 1993. The use of DSC to study the effects of solutes on

heterogeneous ice nucleation kinetics in model food emulsions. *Lebensmittel Wissenschaft und Technologie*, 26(2), 116-120.

12. Petrenko, V.F. & Whitworth, R.W. 1999. Physics of Ice. Oxford University Press, UK.
13. Sahagian, M.E. & Goff, H.D. 1996. Fundamental aspects of the freezing process. *In* Freezing Effects on Food Quality, L.E. Jeremiah (*ed*.), Marcel Dekker, Inc., USA.
14. Schulson, E.M. 1999. The structure and mechanical behavior of ice. *Journal of the Minerals, Metals and Materials*, 51(2), 21-27.
15. Young, F.E. & Jones, F.T. 1949. Sucrose hydrates. The sucrose-water phase diagram. *Journal of Physical Chemistry*, 1334-50.

2.3 Ultrasonic Propagation in Ice

2.3.1 Experimental Data

Ultrasonic propagation in ice has been widely studied, although the majority of the published data involves velocity rather than attenuation measurements (Table 2.3.1). Perhaps because of the various defects that can exist in ice structure there is a surprising degree of scatter in the data (*e.g.*, there is no clear relation between ultrasonic velocity in ice and temperature Figure 2.3.1). For example, Bogoroskii *et al*. (1976) suggested that as sea ice went through aging the volume of voids decreased, increasing the bulk ultrasonic velocity.

Table 2.3.1. Summary of ultrasonic measurements in polycrystalline ice samples from the literature.

Sample	Experimental Conditions	Results	Notes	Reference
Polycrystalline and isotropic ice	-15°C, 300 kHz	V_L = 3280 ± 20 m/s V_R = 1850 ± 50 m/s	L: Longitudinal R: Rayleigh	Northwood, 1947
Polycrystalline ice at high pressures	80 to 180 K, 5 MHz, 0 to 2 GPa.	V_L changes from 3600 to 3800 m/s in a temperature range of 80 to 180 K.		Gromnitskaya & Stal`gorova, 2001
Polycrystalline ice (Ih)	0-2 kbar T = -35.5°C	V_L increases with pressure (from approx. 3900 to 4100 m/s). V_T decreases with pressure (from approx. 2000 to 1900 m/s).	Brillouin spectroscopy was used.	Gagnon *et al*. 1990
Polycrystalline (isotropic) ice	T = -16°C	V_L = 3845 m/s V_T = 1957 m/s	Brillouin spectectroscopy used	Gagnon *et al*. 1983
Polycrystalline (Ih) ice	5 MHz sine burst	V_L = 3890 m/s, V_T = 1900 m/s (T=-25°C and 1 atm). V_L = 3990 m/s, V_T = 1870 m/s (T=-25°C and 2072.54 atm).		Shaw, 1986

Polycrystalline ice	T = -26°C	V_L = 3940 m/s		Smith & Kishoni, 1986
Polycrystalline ice	T = -16°C	V_L = 3844.94 m/s V_T = 1956.9 m/s		Gagnon *et al*. 1983
Sea ice	800 kHz -11°C to -13°C. 10 to 40 mm thick	Velocity varied as a function of thickness. V_L = 1400 to 3000 m/s	Salinity varied in between 8% and 36.6%.	Bogorodskii & Gusev, 1973
Attenuation in sea and freshwater ice	0.2 - 1.1 MHz, -5 to -20°C.	Attenuation varies between 10 to 150 dB/m.	Attenuation was defined equal to the sum of two frequency dependent terms.	Bogorodskii & Gusev, 1973
Attenuation in sea ice	10 – 500 kHz Approx. -6°C	Attenuation function: $\alpha(f) = 0.445f + 2.18 \times 10^{-10} f^4$ (f: frequency in Hz, α: attenuation in $dB.m^{-1}$)	Attenuation was defined equal to the sum of two frequency dependent terms.	Langleben, 1969

Table 2.3.1 (continued)

Attenuation in sea and freshwater ice	0.2 - 1.1 MHz, -5 to -20°C.	Attenuation varies between 10 to 150 dB.m-1.	Attenuation was defined equal to the sum of two frequency dependent terms.	Bogorodskii & Gusev, 1973

Table 2.3.1 (continued)

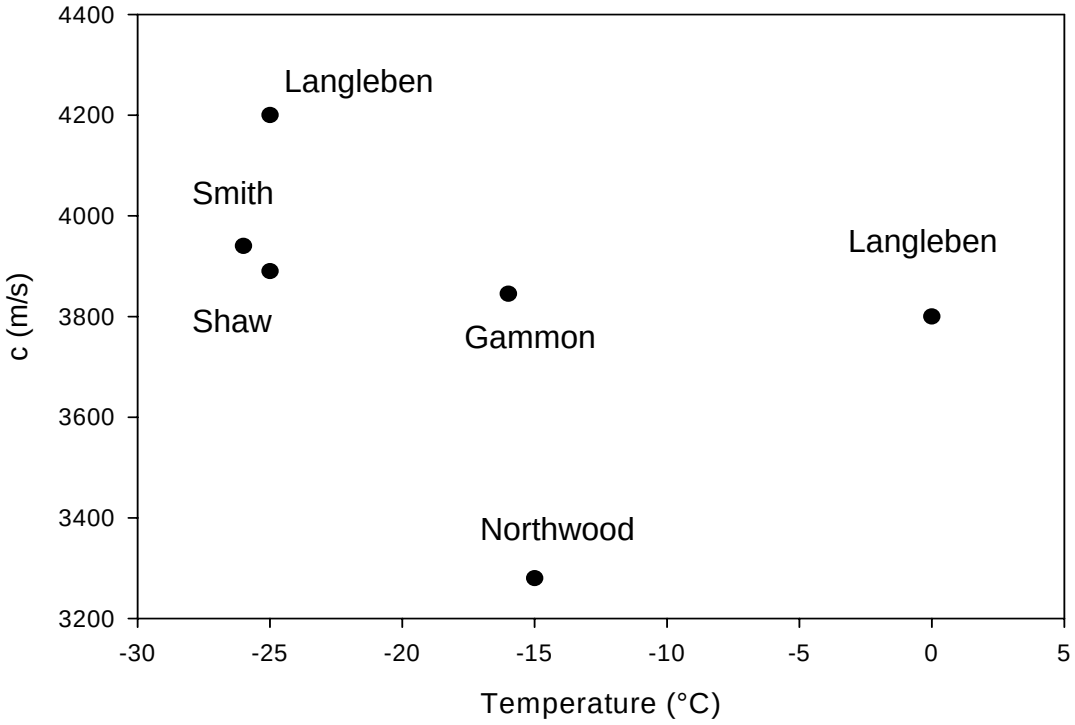

Figure 2.3.1. Temperature dependence of longitudinal wave velocity for the polycrystalline ice samples summarized in Table 2.3.1.

2.3.2 Ultrasonic Formulations for Propagation in Ice

There are a number of structural variables that could affect the propagation of ultrasound in ice (Table 2.3.2). A useful model will provide a description of ultrasonic propagation in terms of some or all of these as well as the frequency of the sound. Although no such model exists, various partial models have been proposed for this and for related systems including the Urick model (*i.e.*, additive influence of component phases), scattering theory (*i.e.*, scattering from ice crystals), grain boundaries theory (*i.e.*, absorption due to the presence of crystal grains), relaxations at the ice-water interface (*i.e.*, ultrasonic perturbation of phase equilibrium), bubbly liquids theory (*i.e.*, air bubble resonance) and poroelastic model (*i.e.*, viscous interactions between the fluid and solid).

Table 2.3.2. Variables in ice structure that might affect ultrasonic propagation.

Ice content
Solution composition
Ice crystal size distribution
Grain structure
Gas bubble size and number
Temperature
Crystal form

2.3.2.1 Urick models

According to Urick (1947, 1948), ultrasonic velocity in heterogeneous systems can be predicted using the volume weighted effective density and adiabatic compressibility of component phases. Ultrasonic velocity is defined as follows:

$$c = \sqrt{\frac{1}{\rho_{eff}\,\kappa_{eff}}} \qquad [2.10]$$

where c is ultrasonic velocity, ρ_{eff} and κ_{eff} are volume weighted effective density and effective adiabatic compressibility, respectively. For a two component system the effective parameters are defined as:

$$\begin{aligned} \rho_{eff} &= \rho_1\phi_1 + \rho_2\phi_2 \\ \kappa_{eff} &= \kappa_1\phi_1 + \kappa_2\phi_2 \end{aligned} \qquad [2.11]$$

where the indices represent component 1 and 2. Using this formulation, velocity in a two component system will be

$$c = \sqrt{\frac{1}{[\phi\rho_1 + (1-\phi)\rho_2][\frac{\phi}{\rho_1 c_1^{\ 2}} + \frac{1-\phi}{\rho_2 c_2^{\ 2}}]}} \qquad [2.12]$$

These models assume that velocity is frequency independent, scattering is negligible and particles are small compared to ultrasonic wavelength (Tebbutt & Challis, 1996). This approach was successfully used in simple model foods in the determination of the concentration of dilute suspensions of solid fat in liquid oil (McClements & Povey, 1987, 1988a, b) and composition of sugar solutions (Contreras *et al*. 1992).

The size of ice crystals in ice cream are in the order of tens of micrometers and in quiescently frozen solutions larger, perhaps approaching the millimeter scale (Hartel, 2001). Ultrasonic wavelengths are also typically in the millimeter scale so the assumption of no scattering is likely to be invalid. The density contrast between ice (0.917 g. cm^{-3}) and water (~ 1 g. cm^{-3}) is small but may be somewhat larger in the presence of solutes. Various workers have reported frequency dependence in ultrasonic velocity (McClements, 1992; McClements & Coupland, 1996). Considering these deviations from the assumptions, it seems likely that the Urick model will only be useful in a few frozen systems.

2.3.2.2 Scattering theory

According to scattering theory, the losses in ultrasonic energy are due to differences between the thermophysical properties of a continuous phase and a dispersed phase. As an ultrasonic wave passes through a heterogeneous system, it is scattered by the heterogeneities which pulsate and oscillate in the passing pressure gradient. The total ultrasonic attenuation is the sum of contributions due to the intrinsic properties of the component phases, scattering losses as the sound is directed into different paths by interaction with the heterogeneities, thermal losses due to heat flow between the pulsating heterogeneities and surrounding continuous phase and viscous

losses due to the drag the continuous phase exerts on the oscillatory motions of the droplets. The extent of scattering depends on the type, concentration, and size of dispersed phase(s) (McClements & Coupland, 1996).

The foundations of the scattering theory depend on the work of Rayleigh (Strutt, 1945). Epstein & Carhart (1953) developed a special case of the theory including contributions from thermal losses. However their work went unnoticed among researchers other than those who specialized on aerosols due to its title (Allegra & Hawley, 1972). A complete description of the scattering of ultrasound was given in Allegra & Hawley (1972).

In summary, Allegra-Hawley theory assumes Rayleigh (*i.e.*, long wavelength limit) scattering where the ultrasonic wavelength is significantly larger than the characteristic length of the scatterers, and negligible multiple scattering. The first step in scattering theory calculations is the determination of individual scattering amplitudes. In all but the most dilute systems the scattering from one particle will interfere with the scattering from another and the overall behavior of the system must be understood using multiple scattering theory (Waterman & Truell, 1962).

Scattering is a function of particle size and it is possible to calculate droplet size distributions by solving the inverse scattering problem (*e.g.*, for particle sizing in alkane emulsions 0.01 – 1000 μm, Riebel & LÖffler, 1989). McClements *et al*. (1993) were also able to use scattering theory to predict the ultrasonic velocity and attenuation in solid and liquid alkane droplets.

In the earliest stage of freezing, crystal impingement is limited and the crystals or crystal aggregates can be expected to behave as individual particles (Marshall *et al*. 2002) that could be understood in terms of scattering theory. However, as volume concentration increases, contact between crystals is unavoidable, and frozen phase becomes the continuous phase. In this case, scattering can mostly be attributed to the presence of liquid inclusions within the frozen matrix,

however the definition of size of scatterers becomes challenging. Under these circumstances, the applicability of scattering theory in frozen foods will be limited.

2.3.2.3 Relaxations at the Ice-Water Interface

When an ultrasonic wave passes through a mixture of two phases at equilibrium, the compressions and decompressions and associated temperature changes caused by the acoustic wave can be expected to shift the position of the equilibrium. If the process is inefficient, some ultrasonic energy is lost as heat and there will be an increase in attenuation and dispersion of velocity (Akulichev & Bulanov, 1981, 1983). Perhaps due to the lack of clarity in the mathematical expression of this model, it has never been quantitatively implemented by other workers. However, a qualitative discussion on the molecular basis of this theory was used by McClements *et al*. (1993) in an effort to understand the high ultrasonic attenuation seen in melting *n*-hexadecane droplets.

Frozen and unfrozen phases coexist in partially frozen foods and semi-crystalline lipid systems, therefore relaxational losses can be expected to contribute to the overall attenuation. Since relaxational losses are primarily due to the shift in phase equilibrium with a small change in temperature, the extent of this shift should determine the extent of possible relaxational losses. For example, the rate of change in ice content in a dilute aqueous solution is more rapid than that in more concentrated solutions and can be expected to cause higher relaxational attenuation.

2.3.3.4 Grain Boundaries Theory

Many investigations have been carried out on ultrasonic propagation during the solidification of granular polycrystalline metals and a number of grain boundary theories exist. Serabian & Williams (1978) defined three different regimes for ultrasonic attenuation in granular materials: a scattering zone in the long wavelength limit (Rayleigh regime), a grain boundary zone where

grains are significantly larger than the ultrasonic wavelength (diffusion regime), and a transition zone between the two regimes (phase regime). Importantly, due to the distribution of grain sizes, more than one of the loss regimes can contribute to ultrasonic losses in polycrystalline materials (Nicoletti *et al*. 1992).

i) Rayleigh regime: Ultrasonic wavelength is much longer than the grain size and the whole grain is treated as an isolated scattering unit (Huntington, 1950). Attenuation increases with the fourth power of the ultrasonic frequency and the third power of the grain size.
ii) Diffusion regime: Ultrasonic wavelength is much shorter than the grain size and losses at the grain boundary are dominant. Attenuation increases with the inverse of the grain size, because the extent of ultrasonic losses is associated with the number of grain boundaries encountered during the propagation.
iii) Phase regime: Ultrasonic wavelength is comparable to grain size. Attenuation increases with the grain size and the square of frequency.

The grain boundaries approach is well-established for metallic materials. However, a general problem with this theory is the definition of the variety of thermophysical constants needed to describe the system. Alternative approaches such as parameterization can be used to reduce the number of physical properties required (Botvina *et al*. 2000).

Due to the temperature sensitivity, complex composition of foods and the difficulties in determining the grain size distribution in frozen foods, application of grain boundaries approach to frozen foods seems to be challenging. Despite these difficulties the structural similarities between ice and polycrystalline granular metals means these theories may be useful in frozen foods.

2.3.3.5 Bubbly Liquids Theory

As ultrasound propagates through a bubbly liquid, the bubble surfaces oscillate in and out rapidly in a process known as resonance and scatter sound very effectively (Feuillade, 1995). Resonance is the tendency of a system to oscillate with maximum amplitude under even low levels of stress applied at a critical frequency. For most inclusions in an ultrasonic field, resonance frequencies are at quite high, however gas bubbles in fluids is a good example of low frequency (i.e., Rayleigh region) resonance (Feuillade, 1995) and is typically in the order of 2 MHz for 10 μm bubbles in aqueous foams (Kulmyrzaev *et al*. 2000).

The resonant (or the natural) frequency for bubbles was first defined in Minnaert (1933) but current theory for bubbly liquids also considers the collective action of bubbles and other loss mechanisms such as thermal and viscous damping (Feuillade, 1995 & 1996). An alternative theoretical approach was proposed by Guanaurd and Überall (1982) who formulated the losses in bubbly water through the definition of "effective" parameters. For example, the effective density of the bubbles is the density of equivalent monopole scatterers that would cause similar attenuation and velocity dispersion. In any case, ultrasonic losses are highly dependent on the ultrasonic frequency and bubble size distribution since the extent of losses will increase as ultrasonic frequency tends to the resonance frequency.

In the ultrasonic characterization of cake batter, Fox *et al*. (2004) employed the bubbly liquids formulation by Feuillade (1996). The investigations confirmed that air bubbles in water behaved more like an ensemble rather than as individual scatterers. Therefore, the interactions in between the bubbles and multiple-scattering effects have to be considered. The effective parameter approach (Guanaurd & Überall, 1982) was used in the characterization of aerated model foods by ultrasonic attenuation spectroscopy (Kulmyrzaev *et al*. 2000). The authors found a qualitative agreement between the theoretical and experimental determination of bubble size and concentration and although the presented results were accurate, the definitions of the scattering coefficient included typographical mistakes.

In most frozen foods, some reduction in ultrasonic energy can be expected due to air bubble resonance. Unlike the bubbles in fluids, bubbles in frozen foods cannot resonate freely since their movement is highly constrained by the ice grains which could decrease the importance of this mechanism. In any case there is no published theory for the ultrasonic resonance of highly constrained bubbles.

2.3.3.6 Poroelastic Model

The analysis of elastic wave propagation in two-phase porous solid medium is the basis of the poroelastic model (Biot 1956 & 1962). The fluid phase interconnects and saturates the pores in the solid phase and is treated as a continuum and the ultrasonic losses are due to the viscous interactions between the fluid and the solid. Poroelastic theory assumes large ultrasonic wavelength compared to the pore size, negligible scattering, and an isotropic medium.

Recently, Carcione *et al*. (2007) used a poroelastic model to calculate the ultrasonic velocity and attenuation in partly frozen samples of orange juice as a function of ice content (Figure 2.3.2). According to their predictions, velocity increased slightly non-linearly with ice content and was a reasonable fit to the experimental measurements. While not measured, their model predicted attenuation would initially increase with ice content to a peak around 40% ice then tend to zero at higher ice contents. However, the measured attenuation in ice is significant and quite large (up to 300 $Np.m^{-1}$ in partially frozen orange juice, Lee *et al*. 2004) which is clearly a deviation from poroelastic behavior. In any case even if the poroelastic model was valid, it would still be a difficult task to define the pore size distribution in frozen foods.

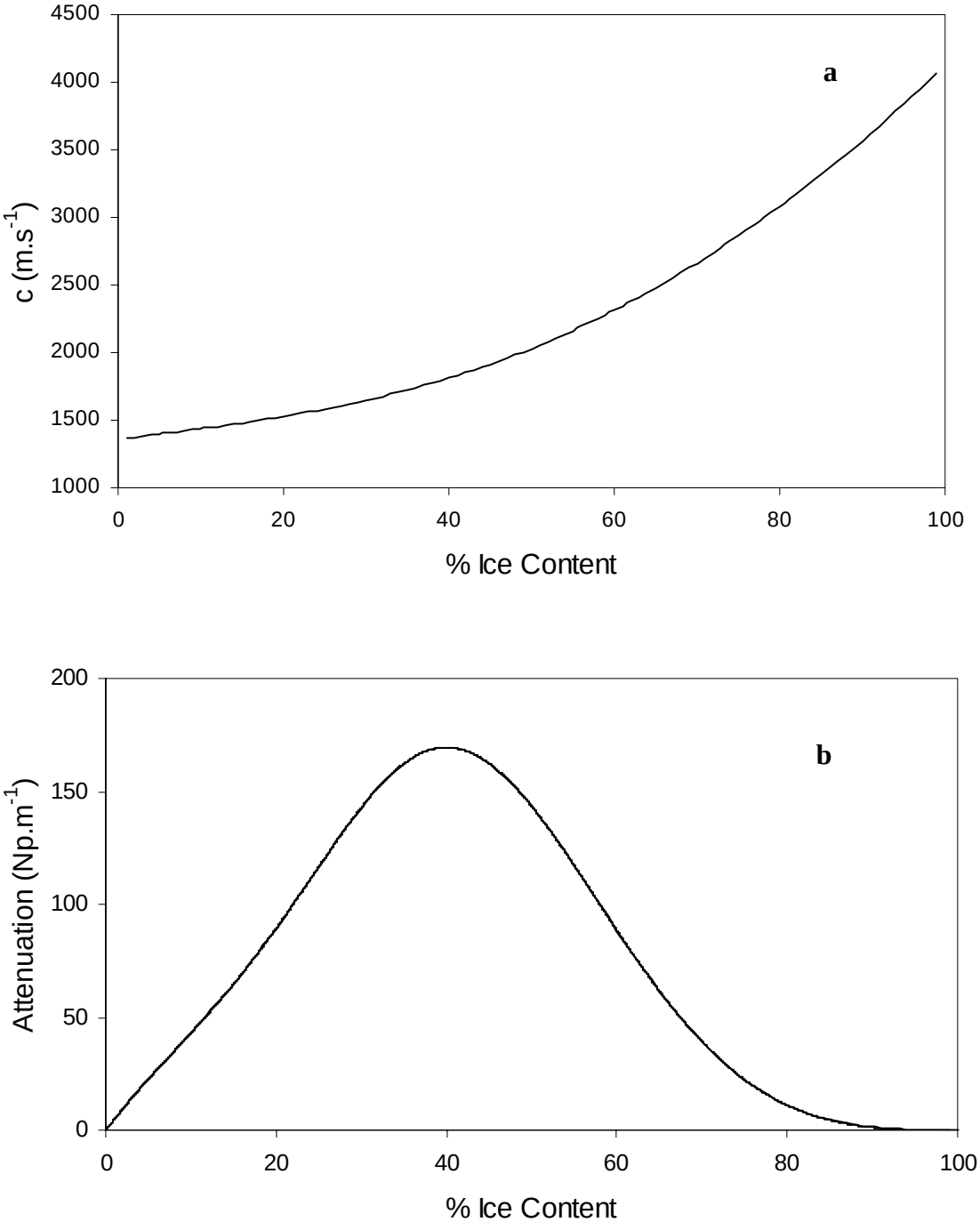

Figure 2.3.2. The poroelastic model prediction for (a) ultrasonic velocity, and (b) attenuation of partially frozen sucrose solutions as a function of ice content (%).

2.3.3 References

1. Akulichev, V.A. & Bulanov, V.N. 1981. Sound propagation in a crystallizing liquid. *Soviet Physics Acoustics*, 27(5), 377-381.
2. Akulichev, V.A. & Bulanov, V.N. 1983. Crystallizing nuclei in liquid in a sound field. *International Journal of Heat and Mass Transfer*, 26(2), 289-300.
3. Allegra, J.R. & Hawley, S.A. 1972. Attenuation of sound in suspensions and emulsions: Theory and experiments. *Journal of the Acoustical Society of America*, 51(5), 553-565.
4. Biot, M. A. 1956. Theory of propagation of elastic waves in a fluid saturated porous solid. I. Low-frequency range. *Journal of the Acoustical Society of America*, 28, 168–178.
5. Biot, M. A. 1962. Mechanics of deformation and acoustic propagation in porous media. *Journal of Applied Physics*, 33, 1482–1498.
6. Bogorodskii, V.V., Gavrillo, V.P. & Nikitin, V.A. 1976. Sound propagation in ice crystallized from salt water. *Soviet Physics*. *Acoustics*, 22(2), 158-160.
7. Bogorodskii, V.V. & Gusev, A.V. 1973. Attenuation of sound in ice in the frequency range 200-1100 kHz. *Soviet Physics*. *Acoustics*, 19(2), 97-100.
8. Botvina, L.R., Fradkin, L.J. & Bridge, B. 2000. A new method for assessing the mean grain size of polycrystalline materials using ultrasonic NDE. *Journal of Materials Science*, 35(18), 4673-83.
9. Carcione, J.M., Campanella, O.H. & Santos, J.E. 2007. A poroelastic model for wave propagation in partially frozen orange juice. *Journal of Food Engineering*, 80(1), 11-17.
10. Contreras, N.I., Fairley, P., McClements, D.J. & Povey, M.J.W. 1992. Analysis of the sugar

content of fruit juices and drinks using ultrasonic velocity measurements. *International Journal of Food Science and Technology*, 27(5), 515-529.

11. Epstein, P.S. & Carhart, R.R. 1953. The absorption of sound in suspensions and emulsions. 1. Water Fog in Air. *Journal of the Acoustical Society of America*, 25(3), 553-565.
12. Feuillade, C. 1995. Scattering from collective modes of air bubbles in water and the physical mechanism of superresonances. *Journal of the Acoustical Society of America*, 99(6), 3412-30.
13. Feuillade, C. 1996. The attenuation and dispersion of sound in water containing multiply interacting air bubbles. *Journal of the Acoustical Society of America*, 99(6), 3412-30.
14. Fox, P., Probert Smith, P. & Sahi, S. 2004. Ultrasound measurements to monitor the specific gravity of cake batters. *Journal of Food Engineering*, 65(3), 317-324.
15. Gagnon, R.E., Kiefte, H., Clouter, M.J. & Denner, W.W. 1983. Elastic constants of artificial and natural ice samples by Brillouin spectroscopy. *Journal of Glaciology*, 29(103), 433-460.
16. Gagnon, R.E., Kiefte, H., Clouter, M.J. & Whalley, E. 1990. Acoustic velocities and densities of polycrystalline ice Ih, II, III, IV, and VI by Brillouin spectroscopy. *Journal of Chemical Physics*, 92(3), 1909-14.
17. Gromnitskaya, E.L., Stal`gorova, O.V. 2001. Ultrasonic study of the nonequilibrium pressure-temperature diagram of H_2O ice. *Physical Review B*, 64, 094205.
18. Guanaurd, G.C. & Überall, H. 1982. Resonance theory of bubbly liquids. *Journal of the Acoustical Society of America*, 69(2), 362-370.
19. Hartel, R.W. 2001. Crystallization in foods. Aspen Publishers, USA.
20. Huntington, H.B. 1950. On ultrasonic scattering by polycrystals. *Journal of the Acoustical Society of America*, 91(6), 3278-84.
21. Kulmyrzaev, A., Cancelliere, C. & McClements, D.J. 2000. Characterization of aerated foods using ultrasonic reflectance spectroscopy. *Journal of Food Engineering*, 46(4), 235-241.
22. Langleben, M.P. 1969. Attenuation of sound in sea ice, 10-500 kHz. *Journal of Glaciology*, 54(8), 399-406.
23. Lee, S., Pyrak-Nolte, L.J., Cornillon, P., & Campanella, O. 2004. Characterization of frozen

orange juice by ultrasound and wavelet analysis. *Journal of the Science of Food and Agriculture*, 84(5), 405-410.

24. Marshall, T., Challis, R.E., Holmes, A.K. & Tebbutt, J.S. 2002. Modeling ultrasonic compression wave absorption during the seeded crystallization of copper (II) sulphate pentahydrate from aqueous solution. *IEEE Transactions on Ultrasonics, Ferroelectrics, and Frequency Control*, 49(11), 1583- 91.
25. McClements, D.J. 1992. Comparison of multiple scattering theories with experimental measurements in emulsions. *Journal of the Acoustical Society of America*, 91 (2), 849-853.
26. McClements, D.J. & Coupland, J.N. 1996. Theory of droplet size distribution in emulsions using ultrasonic spectroscopy. *Colloids and Surfaces A: Physicochemical and Engineering Aspects*, 117(1-2), 161-170.
27. McClements, D.J. & Povey, M.J.W. 1987. Solid fat content determination using ultrasonic velocity measurements. *International Journal of Food Science and Technology*, 22(5), 491-499.
28. McClements, D.J. & Povey, M.J.W. 1988a. Comparison of pulsed NMR and ultrasonic velocity techniques for determining solid fat contents. *International Journal of Food Science and Technology*, 23(2), 159-170.
29. McClements, D.J. & Povey, M.J.W. 1988b. Investigation of phase transitions in glyceride/paraffin oil mixtures using ultrasonic velocity measurements. *Journal of American Oil Chemists` Society*, 65(11), 1791-95.
30. McClements, D.J., Povey, M.J.W. & Dickinson, E. 1993. Absorption and velocity dispersion due to crystallization and melting of emulsion droplets. *Ultrasonics*, 31(6), 433-437.
31. Minnaert, M. 1933. On the musical air bubbles and sounds of running water. *Philosophical Magazine*, 16, 235-248.
32. Nicoletti, D., Bilgutay, N. & Onaral, B. 1992. Power-law relationships between the dependence of ultrasonic attenuation on wavelength and the grain size distribution. *Journal of the Acoustical Society of America*, 91(6), 3278-84.
33. Northwood, T.D. 1947. Sonic determination of the elastic properties of ice. *Canadian Journal of Research*, 25(A), 88-95.

34. Riebel, U. & Löffler, F. 1989. The fundamentals of particle size analysis by means of ultrasonic spectroscopy. *Particle and Particle Systems Characterization*, 6(1-4), 135-143.

35. Serabian, S. & Williams, R.S. 1978. Experimental determination of ultrasonic attenuation characteristics using the Roney generalized theory. *Materials Evaluation*, 36(8), 55-62.

36. Shaw, G.H. 1986. Elastic properties and equation of state of high pressure ice. *Journal of Chemical Physics*, 84(10), 5862-68.

37. Smith, A.C., & Kishoni, D. 1986. Measurement of speed of sound in ice. *AIAA Journal*, 24(10), 1713-15.

38. Strutt, J.W. Lord Rayleigh. 1945. *The Theory of Sound*. Dover Publications, New York (reprint).

39. Tebbutt, J.S. & Challis, R.E. 1996. Ultrasonic wave propagation in colloidal suspensions and emulsions: a comparison of four models. *Ultrasonics*, 34(2), 363-368.

40. Urick, R.J. 1947. A sound velocity method for determining the compressibility of finely divided substances. *Journal of Applied Physics*, 18(11), 983-987.

41. Urick, R.J. 1948. A sound velocity method for determining the compressibility of finely divided substances. *Journal of the Acoustical Society of America*, 20(3), 283-289.

42. Waterman, P.C. & Truell, R. 1962. Multiple scattering of waves. *Journal of Mathematical Physics*, 2(4), 512-537.

Chapter 3

Ultrasonic Measurements in Frozen Model Food Solutions

3.1 Ultrasonic Velocity Measurements in Frozen Model Food Solutions

Abstract

The speed of sound was measured in solutions of sucrose (0-70 wt/vol%), glycerol (0-30 wt/vol%) and orange juice (0-40 solids wt/vol%) as a function of temperature (10°C to -13°C). The velocity (c) in the unfrozen solutions, including the supercooled samples, could be modeled as a simple linear function of temperature (T, °C) and composition (x, wt/vol%): $c = c_w + k_x x + k_T T$ where c_w is the speed of sound in water at 0°C, and k_x and k_T are solute-dependant constants. There was a large increase in ultrasonic velocity corresponding to freezing in these samples (*e.g.*, an unfrozen 10% sucrose solution has a speed of sound of 1416 ms^{-1} at -5°C while a similar frozen solution has a velocity of 1983 ms^{-1}.) The ice content was estimated from phase diagrams of similar samples and was a linear function of the change in ultrasonic velocity upon freezing for samples <-8°C. Some details of the effects of ice microstructure and possible theoretical approaches to its effects on ultrasonic properties are also discussed.

3.1.1 Introduction

Food stabilization by freezing involves primarily a phase transition in the aqueous portion and consequent freeze-concentration of the unfrozen part. There may also be other phase transitions in the unfrozen and non-aqueous portions. Cooling is typically fast to minimize ice crystal size and damage to food structure and the heat transfer is an unsteady state process, difficult to model due to the heterogeneous nature of the partly frozen food and its changing thermal properties (Dinçer, 1997; Mittal and Zhang, 2000). Because of this, the theoretical predictions only provide a limited degree of certainty (Amarante & Lanoisellé, 2005) and process optimization requires sensitive techniques to measure the formation of ice *in-situ*.

Ultrasound is high-frequency, low energy sound that has the capability of penetrating opaque materials non-destructively. The transmission characteristics of the ultrasonic waves are affected by material properties, and can be used to evaluate composition and structure (Saggin & Coupland, 2001). Ultrasonic sensors are suitable for on-line applications and have the advantages of propagating through processing equipment walls and also being relatively cheap and suitable for automation (Saggin & Coupland, 2001). A successful application of ultrasonic characterization of food materials is the measurement of composition of a binary solution. For example, the sugar content of fruit juices (Contreras, Fairley, McClements & Povey, 1992), the solids content of fat (McClements & Povey, 1987; McClements & Povey, 1988a) and, significantly for this work, phase transitions in lipids (McClements & Povey, 1988b).

The longitudinal sound wave velocity in water (~1500 ms^{-1}, Bilaniuk & Wong, 1993) is much less than the velocity in ice (~3900 ms^{-1}, Smith & Kishoni, 1986) and this large difference suggests that ultrasonic velocity measurements in partially frozen foods might offer a way to

monitor the freezing processes (Miles & Cutting, 1974). The relationship between ultrasonic properties and ice content (as measured by NMR) of frozen orange juice was investigated over a wide temperature range by Lee *et al*. (2004). Both ultrasonic velocity and ice content increased as temperature decreased, however a direct quantitative relation between ultrasonic properties and ice fraction was not proposed. In another recent study Sigfusson *et al*. (2004) calculated the frozen fraction of samples of frozen food by ultrasonically measuring the position of the moving ice front in a 1-dimensional freezing experiment.

In the present work I report measurements of the speed of ultrasound and ice content in frozen and unfrozen aqueous solutions as a function of temperature and composition. I use a phase diagram to estimate the ice content of these samples and show empirically that it is related to measured ultrasonic velocity.

3.1.2 Materials and Methods

Chemicals and Sample Preparation. Anhydrous sucrose (Grade I) and glycerol (99%) were obtained from Sigma Chemical Company (St. Louis, MO). Frozen orange juice concentrate (Tropicana brand) was purchased from a local retailer. According to the manufacturer, the solid material content of the juice was 40.17% (~ 96.5% carbohydrates) and its solutions were prepared on a percentage solids basis. The orange juice was thawed overnight at 4°C prior to use. All solutions were prepared in purified (Nanopure Barnstead, Dubuque, IA) and rigorously degassed water to ensure the exclusion of air bubbles.

Ultrasonic Velocity Measurements. The speed of sound was measured using a modified pulse-echo technique (McClements & Fairley, 1991) as described by Saggin & Coupland (2002). An electrical spike signal (Panametrics 500 PR, Waltham, MA) was passed to a 2.25 MHz broadband ultrasonic transducer (Panametrics V606), which converted the energy to ultrasound. The pulse of sound traveled into a Plexiglas delay line, and was partially reflected at the plastic-sample interface. The reflected part returned through the delay line to the transducer (echo 1) and

the transmitted part traveled through the sample (~1 cm), was reflected from the brass plate and returned through the sample and the delay line to the transducer (echo 2). The transducer reconverted the acoustic signal to an electrical signal, which was stored for analysis with a digital oscilloscope (LeCroy 9310c, Chestnut Ridge, NY, USA). The time difference between echo 1 and echo 2 was used to measure the ultrasonic velocity in the sample in conjunction with a water calibration (McClements & Fairley, 1992). [1]

The temperature dependence of longitudinal wave velocities were measured for sucrose and glycerol solutions, and diluted orange juice concentrates in a temperature range of -10 to 10°C. The sample temperature was measured using a logging thermometer (Omega HH-2000, Stamford, CT) equipped by copper-constantan thermocouples with a precision of 0.1°C. The samples were cooled at about 0.5 °C min^{-1} above their freezing point (T_f, the point at which ice was first observed) and about 4°C $hour^{-1}$ below. The samples were allowed to come to come to thermal equilibrium at each measurement temperature prior to ultrasonic velocity determination. In some samples the liquid samples were gentle mixed at each temperature before taking a measurement to facilitate ice nucleation and minimize supercooling, while other samples were cooled without mixing and would remain liquid significantly below T_f.

Differential Scanning Calorimetry (DSC). Phase diagrams for the three samples (sucrose, glycerol and orange juice) were measured using the method of Ponsawatmanit & Miyawaki (1993). Briefly, the samples were diluted in water and aliquots (~15 mg) were cooled in a differential scanning calorimeter (DSC, Perkin-Elmer DSC-7, Norwalk, CT) to -70ºC to ensure complete freezing, and then slowly reheated (0.5°C min^{-1} to 40ºC). The melting point of the solution was calculated from the melting curve obtained from DSC analysis in conjunction with a water calibration for the instrument. To prepare higher solids orange juice samples to complete the phase diagram, some samples were concentrated by heating to 40°C overnight in temperature controlled cabinet.

[1] Although the measurement of ultrasonic attenuation (α) was not the focus of this section of my work as published, attenuation of similar samples were also carried out using the same experimental setup (Chapter 3.2).

3.1.3. Results and Discussion

Ultrasonic Measurements. The temperature dependence of speed of longitudinal sound waves in sucrose, glycerol, and orange juice solutions was measured as a function of temperature as described above and the results are reported in Figures 3.1.1a, 3.1.2a, and 3.1.3a respectively. For temperatures above the freezing point of the solutions, the speed of sound increased with increasing solute concentrations and temperature. However, once the samples began to freeze there was a sudden and dramatic increase in ultrasonic velocity in the samples. This is probably because the speed of sound in pure water at 0°C (~1402 ms^{-1}, Bilaniuk & Wong, 1993) is less than half that in ice at -26°C (3940 ms^{-1}, Smith & Kishoni, 1986). The temperature of the discontinuity in ultrasonic velocity decreases with solute concentration due to the freezing point depression.

Recently Lee, Pyrak-Nolte, Cornillon, and Campanella (2004) reported similar ultrasonic measurements in orange juice (10% solids) over a wider temperature range (30°C to -60°C). While the form of their velocity-temperature function was similar to the results seen here, the values in the frozen samples were somewhat different. In their work freezing was not seen until below -10°C at which point velocity increased at a decreasing rate to a final value of close to 4000 ms^{-1} at -60°C. The maximum seen here for a similar sample was less than 3500 ms^{-1} at -10°C.

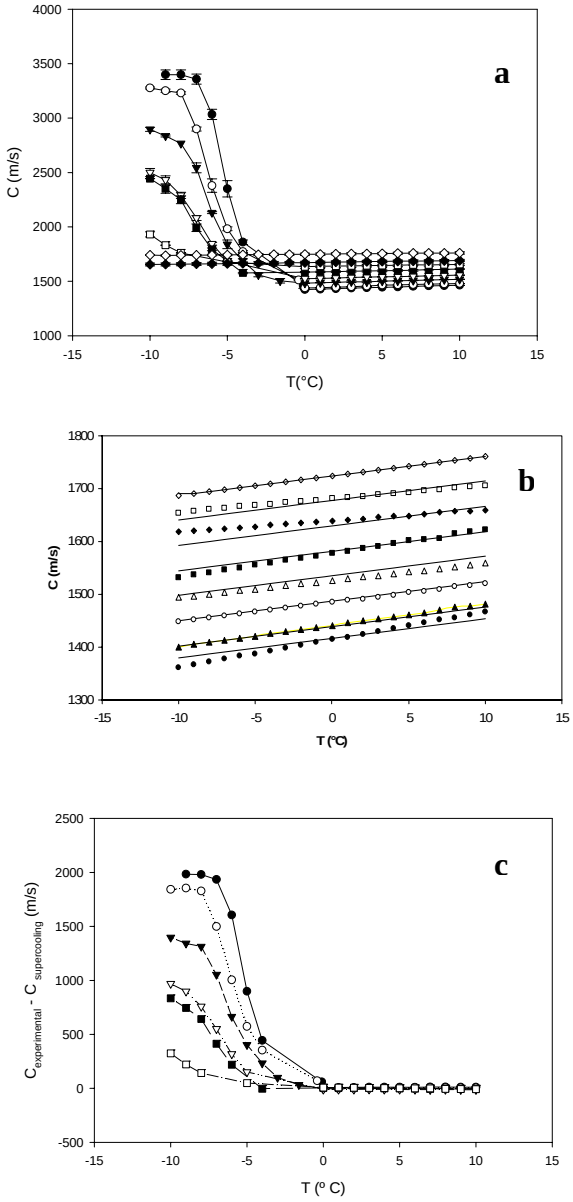

Figure 3.1.1. (a) Speed of sound in sucrose solutions (●: 5%, ○: 10%, ▼: 20%, ▽: 30%, ■: 40%, □: 50%, ♦: 60%, ◊: 70%) as a function of temperature. The formation of ice corresponded to the discontinuity seen. (b) Speed of sound in supercooled sucrose solutions (symbols as Figure 3.1a). There was no ice nucleation in these samples so no discontinuity was seen. Lines shown correspond to the best fit of linear model (see text for details). (c) Change in ultrasonic velocity due to ice formation in sucrose solutions (symbols as Figure 3.1.1a).

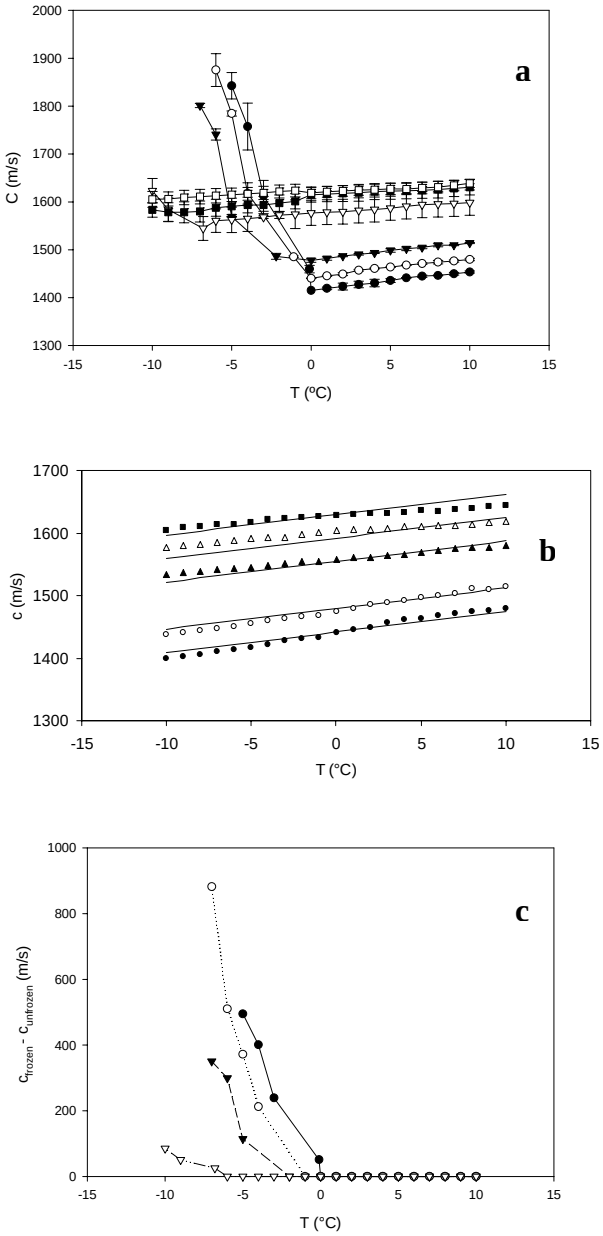

Figure 3.1.2. (a) Speed of sound in glycerol solutions (●: 1%, ○: 5%, ▼: 10%, ▽: 20%, ■: 25%, □: 30%) as a function of temperature. The formation of ice corresponded to the discontinuity seen. (b) Speed of sound in supercooled glycerol solutions as a function of temperature (symbols as Figure 3.1.2a). There was no ice nucleation in these samples so no discontinuity was seen. Lines shown correspond to the best fit of linear model (see text for details). (c) The difference between speed of sound in frozen and supercooled glycerol solutions as a function of temperature (symbols as Figure 3.1.2a).

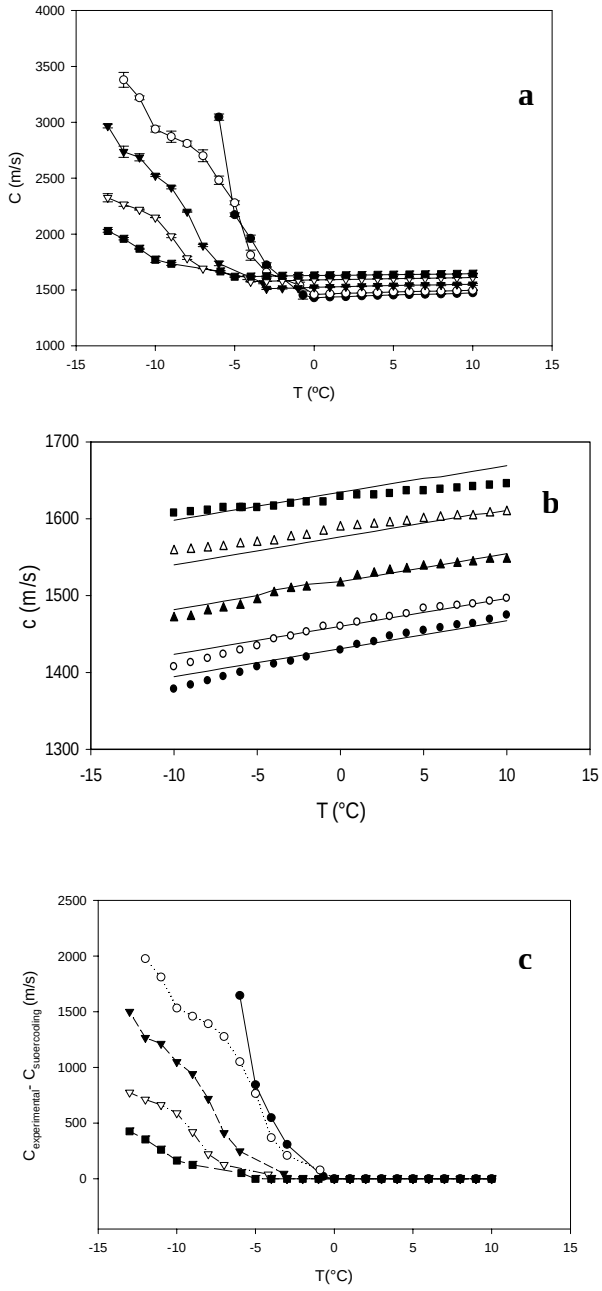

Figure 3.1.3. (a) Speed of sound in orange juice solutions (●: 5% , ○: 10%, ▼: 20%, ▽: 30%, ■: 40%) as a function of temperature. The formation of ice corresponded to the discontinuity seen. (b) Speed of sound in supercooled orange juice solutions as a function of temperature (symbols as Figure 3.1.3a). There was no ice nucleation in these samples so no discontinuity was seen. Lines shown correspond to the best fit of linear model (see text for details). (c) The difference between speed of sound in frozen and supercooled orange juice solutions as a function of temperature (symbols as Figure 3.1.3a).

In a similar series of experiments, the samples were allowed to cool without the gentle stirring which served to facilitate ice nucleation, and remained as supercooled solutions throughout the experiment (sucrose Figure 3.1.1b, glycerol Figure 3.1.2b, and orange juice Figure 3.1.3b). In these measurements, the trends in velocity with temperature persisted to lower temperatures, confirming that the discontinuity seen previously (Figures 3.1a, 3.2a, and 3.3a) was due to ice formation.

An empirical model was derived to describe the ultrasonic velocity in unfrozen (including supercooled) solutions as a function of temperature and concentration:

$$c_{unfrozen} = c_w + k_T T + k_x x \qquad [3.1]$$

The values of the constants (c_w, k_T and k_x) and the regression statistics are listed in Table 3.1.1). The parameter, c_w corresponds to the speed of sound in pure water at 0°C. The values obtained from the correlation analysis for the glycerol and orange juice samples are statistically similar to each other and to the tabulated value for pure water (=1400 ms^{-1} Bilaniuk & Wong, 1993), whereas a slightly lower value is observed for sucrose. The influence of ice formation could be separated from the effects of concentration and temperature by subtracting the regression values from Equation 1 from the experimental measurements of velocity. The results of this manipulation of the data are shown in Figure 3.1.1c (sucrose), 3.1.2c (glycerol) and 3.1.3c (orange juice).

Table 3.1.1. Constants for the linear multivariate model (Equation 3.1: $c(x,T) = c_w + k_T T + k_x x$) to predict the ultrasonic velocity of unfrozen solutions as a function of temperature (x, °C) and composition (x, wt%) The limits for the model are described in the text. Values for the confidence are expressed as a best fit in the 95% confidence interval.

Solute	c_w	k_T	k_x	r^2	RMS error
Sucrose (n=168)	1392 ± 1.45	3.70 ± 0.13	474.94 ± 3.46	0.992	0.77%
Glycerol (n=114)	1404 ± 5.60	3.29 ± 0.13	751.09 ± 6.687	0.992	0.41%
Orange juice (n=106)	1401 ± 1.76	3.61 ± 0.15	581.014 ± 7.089	0.986	0.48%

Measurement of Ice Content. The melting points of the solutions decreased with solute concentrations and the rate of decrease was inversely related to the molecular weight of the solute (glycerol > sucrose ~ orange juice; note the major carbohydrate in orange juice is sucrose) (Figure 3.1.4). From these data a phase diagram was calculated for each solute showing the equilibrium ice content as a function of temperature for the solute concentrations used in the ultrasonic studies (Figure 3.1.5).

Even though the samples used in the ultrasonic investigation were not necessarily at thermodynamic equilibrium, the forms of the functions seen in Figure 3.1.5 are similar to the change in ultrasonic velocity upon freezing (Figures 3.1.1c, 3.1.2c, and 3.1.3c). The simplest model for a relationship between the change in ultrasonic velocity on freezing (Δc_{freeze}) and ice fraction (ϕ_{ice}) is:

$$\Delta c_{freeze} = \Delta c_{water} \phi_{ice} \qquad [3.2]$$

where Δc_{water} the difference in ultrasonic velocity between ice and unfrozen water (=3940-1400=2540 ms^{-1}). However neither this, nor other functions could be found to adequately describe the relationship between the change of speed of sound on freezing and the ice content for the full set of measurements (data not shown). One reason for this could be that because the two measurements were performed on independent samples, the ice content was not the same in each. Ultrasonic velocity was measured during a cooling cycle, albeit a very slow one, and the ice content would typically be expected to be lower than the thermodynamic ice content measured from the phase diagram. This difference would be expected to be less when the change in ice content with temperature is fairly low, *i.e.*, when the system has nucleated and the actual crystal load is determined by the growth mechanisms. Consequently, I repeated my analysis for just that data gathered T<-8°C where the freezing curves had largely leveled off (Figure 3.1.6).

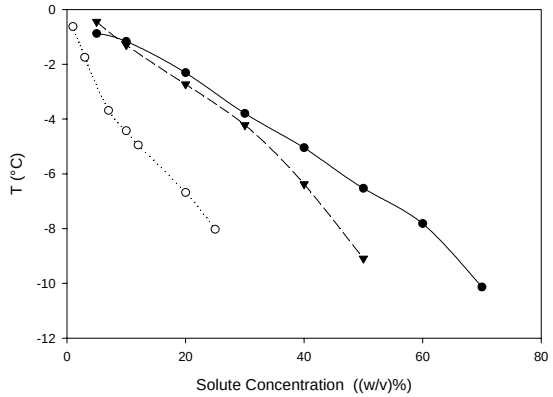

Figure 3.1.4. Melting point curves for (●) sucrose, (○) glycerol and (▼) orange juice solutions.

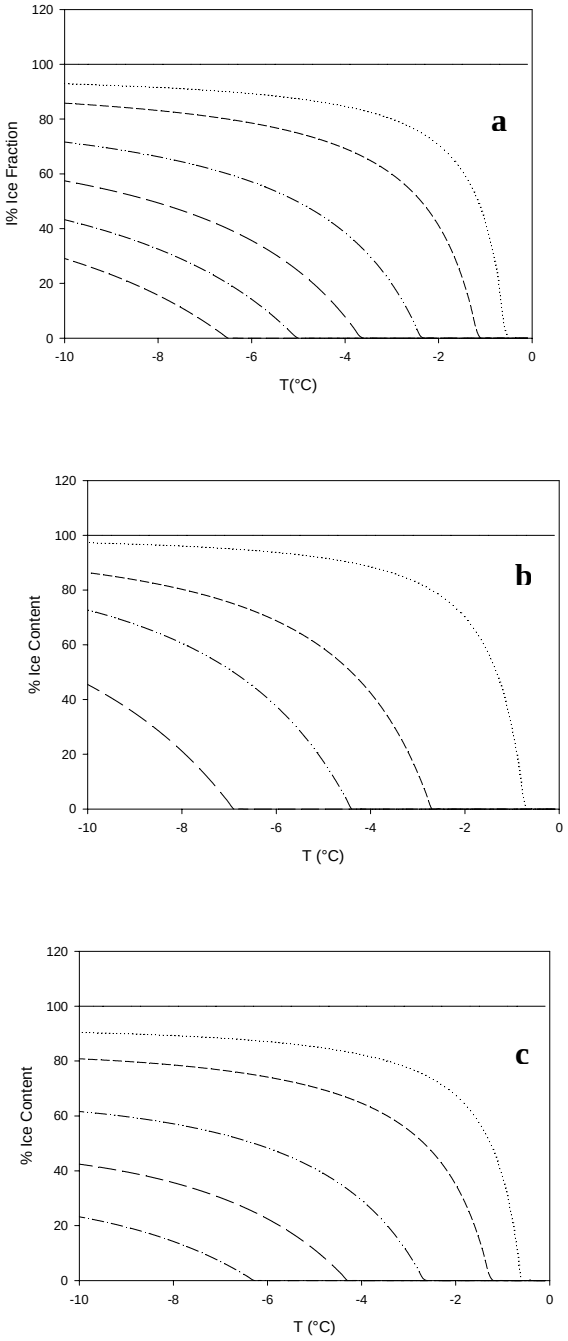

Figure 3.1.5. (a) Ice content of sucrose solutions as calculated from melting point depression data (from top to bottom: pure water, 5%, 10%, 20%, 30%, 40%, and 50%). (b) Ice content of glycerol solutions as calculated from equilibrium melting point depression data (from top to bottom: pure water, 1%, 5%, 10%, and 20%). (c) Ice content of orange juice solutions as calculated from melting point depression data (from top to bottom: pure water, 10%, 20%, 30%, 40% solid matter).

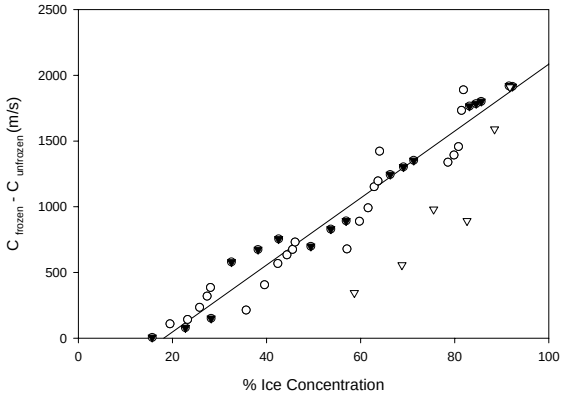

Figure 3.1.6. The difference between speed of sound in frozen and supercooled solutions as a function of ice content (%) in (▼) sucrose, (∇) glycerol and (○) orange juice solutions at temperatures lower than or equal to -8 ºC. A single linear regression is shown through the glycerol and orange juice data.

In Figure 3.1.6 there was a reasonable linear relationship between the ice content of sucrose and orange juice samples and the change in ultrasonic velocity. The slope of the linear regression shown through the data was 25.5 ± 0.956 ms^{-1} per 1% ice content which is statistically similar to the value of $\Delta c_{water}/100$ ($\approx$ 25.4 ms^{-1} per 1% ice content) suggesting that the change in ultrasonic velocity upon freezing was proportional to the amount of ice formed.

An interesting feature of the regression is the intercept with the x-axis is 18% ice, suggesting there is no change in ultrasonic velocity until approximately this much ice has formed. I do not believe this is a real phenomenon and may result from either (i) the inhomogeneous distribution of ice in the ultrasonic cell during the early stages of freezing or (ii) the difficulties in comparing a measurement of a kinetically frozen sample with a thermodynamic measure of ice content. More striking is the fact that the data for glycerol do not fit this regression pattern at all. However, this might be related to the fact that frozen glycerol solutions had a higher attenuation coefficient, only allowing the intermediate concentrations to be used in the analysis. The ultrasonic attenuation coefficient of glycerol is ten times that of pure water (Slie *et al*. 1966).

Effect of Ice Microstructure. Equation 3.3, if generally true, provides a useful practical basis for the ultrasonic determination of ice content in frozen foods. However, it seems extremely unlikely that the presence of ice will be generally explicable in such simple terms. A frozen solution is extremely complex. First the solution is supercooled, then ice nuclei form at catalytic impurities either on the container wall or suspended in the bulk solution. The initial nuclei may be as small as 0.5 nm (*i.e.*, lattice parameters of hexagonal ice are 4.5 and 7.4 Å, Petrenko & Whitworth, 1999) but they will rapidly grow to crystals several millimeters in size and to a variety of shapes (Hartel, 2001). The ice crystals will impinge on one another as they grow and will quickly form a network and eventually a densely packed matrix with small amounts of interstitial unfrozen solution trapped between the crystals. The exact position of the equilibrium will depend on both the temperature and composition of the solution; however, many systems will only slowly approach their equilibrium state. The crystal morphology may vary across the sample depending on the ways heat is removed and will change during storage due to Ostwald ripening. Furthermore, air is very soluble in water but not in ice and significant air bubbles will form during freezing. I present the results of two preliminary experiments which attempt to identify which microstructural features are likely to be most important and offer a critique of some of the available theories available to explain their effects.

Firstly, in an effort to understand the relative importance of air cells in the frozen samples, the speed of sound in a 20 wt/vol% sucrose solution at -10°C (*i.e.*, thermodynamically ~ 71% ice) that had been thoroughly degassed (5 min under a vacuum) was compared to a similar sample that had been vigorously vortexed before freezing. The speed of sound in the degassed samples was only about 20 ms^{-1} (<1%) less than that in the shaken sample suggesting either (i) air cells are either too large, too small or too few to impact the ultrasonic velocity, or (ii) the shaking/degassing processes were insufficient to cause significant differences in size or number of air bubbles formed. Ultrasonic attenuation was approximately 10% less in the degassed sample.

In a second series of experiments I attempted to vary the ice microstructure. Temperature cycling a frozen solution is known to facilitate Ostwald ripening and increase the ice crystal size

(Flores & Goff, 1999). Frozen sucrose solutions (20 (w/v)%, -5°C) were heated to -3°C, held for 1 h to assure thermal equilibrium, then cooled back to -5°C and again held for 1 h to return to the starting state (Figure 3.1.7). This cycle was repeated three times, and the ultrasonic velocity measured at the end of each equilibration period. The ultrasonic velocity measurements at -5°C were higher than that at -3°C consistent with the higher ice content at the lower temperature (~50% and 20% respectively). In addition, the ultrasonic velocity at a given temperature increased with cycling. Presumably this change is due to the increase in crystal size on thermal cycling and any complete theory for ultrasonic propagation in a frozen solution must account for this.

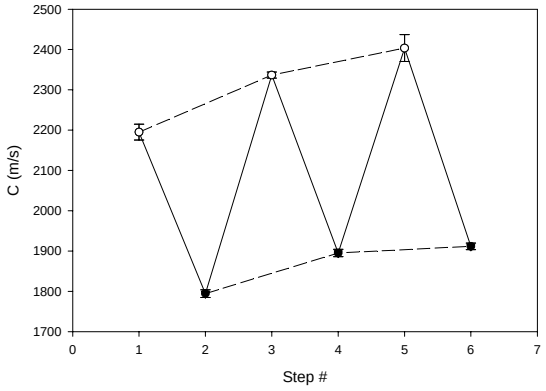

Figure 3.1.7. Ultrasonic velocity in a frozen 20% sucrose solutions during temperature cycling Odd numbered steps correspond to the measurements at -5 ºC (○), and the even numbered ones to those in -3 ºC (●). Solid lines connect consecutive measurements while dotted lines connect the measurements at each temperature.

There are two main groups of theoretical approaches that might be taken to this problem.

i. **Scattering Theory.** Particles with impedances different from those of the continuous phase will scatter sound and sizes approaching the wavelength of sound cause significant velocity dispersion and high attenuation (Povey, 1997). The wavelength of sound in this system would be in the order of millimeters so I would expect significant scattering depending on crystal/bubble/interstitial water number and morphology. The impedances of water, ice and air bubbles are approximately 3.6 $x10^6$ $kgm^{-2}s^{-1}$, 1.4 $x10^6$ $kgm^{-2}s^{-1}$ and zero respectively so the various structures should scatter strongly. Air bubbles in particular can resonate at certain frequencies and cause huge attenuation of ultrasound (Povey, 1997).

ii. **Relaxations at the Ice-Water Interface.** The fluctuating pressure of an ultrasonic wave is associated with a small local temperature variation (~mK). In a partially frozen solution ice is at equilibrium with unfrozen liquid at the same temperature and this small temperature fluctuation would cause a fluctuation in the position of the equilibrium and consequently absorb sound. Akulichev & Bulanaov (1981) proposed a theory to describe these losses as this was cited by McClements *et al*. (1993) to explain the attenuation peak seen in the melting of crystalline *n*-hexadecane emulsion droplets. However, Marshall *et al*. (2002) dismissed the importance of this phenomenon relative to that of scattering in their study of the ultrasonic properties of aqueous crystalline copper (II) sulphate pentahydrate dispersions. It is unclear how important this mechanism is here, but it is impossible to discount.

In summary, a full theoretical description of the ultrasonic properties of a simple solution over a freezing transition is likely to be extremely complex. The early stages are likely to be dominated by scattering from ice crystals. As the crystals form a network, scattering theory becomes more challenging and eventually may be better expressed as the scattering of interstitial fluid in a crystalline continuum. In all cases the size and shape of the scattering particles and the importance of relaxations at the crystal surfaces would vary enormously. While it may be possible to tackle special cases of this problem analytically, a complete solution is probably at present impossible and some variation of the empirical approach taken here may have to suffice.

3.1.4. Conclusions

The ultrasonic velocity of sucrose, glycerol and orange juice solutions are measured as a function of concentration and temperature. Both functions show a characteristic discontinuity upon freezing. The properties of the unfrozen solution could be modeled empirically while the change in velocity on freezing is proportional to the amount of ice formed. A single linear relation was suggested for relating the two for sucrose and orange juice solutions.

Acknowledgements: I am grateful to Supratim Ghosh for assistance with the calorimetric measurements. This work was supported by a grant from USDA-CSREES.

3.1.5 References

1. Akulichev, V.A. & Bulanov, V.N. 1981. Sound propagation in a crystallizing liquid. *Soviet Physics Acoustics*, 27 (5), 377-381.

2. Amarante, A. & Lanoisellé, J. 2005. Heat transfer coefficients measurement in industrial freezing equipment by using heat flux sensors. *Journal of Food Engineering*, 66(3), 377-386.

3. Bilaniuk, N., & Wong, G.S.K. 1993. Speed of sound in pure water as a function of temperature. *The Journal of Acoustical Society of America*, 93(3), 1609-12.

4. Carcione, J. M., Santos, J. E., Ravazzoli, C. L. & Helle, H. B. 2003b. Wave simulation in partially frozen porous media with fractal freezing conditions. *Journal of Applied Physics*, *94*, 7839-7847.

5. Contreras, N.I., Fairley, P., McClements, D.J. & Povey, M.J.W. 1992. Analysis of the sugar content of fruit juices and drinks using ultrasonic velocity measurements. *International Journal of Food Science and Technology*, 27(5), 515-529.

6. Cosenza, L.W., Bringaud, F., Baltz, T. & Vellieux, F.M.D. 2000. Crystallization and preliminary crystallographic investigation of glycosomal pyruvate phosphate dikinase from *Trypanosoma brucei*. *Acta Crystallographica Section D- Biological Crystallography*, 56(12), 1688-1690.

7. Coupland, J.N. 2004a. Low-intensity ultrasound. *Food Research International*, 37(6), 537-543.

8. Coupland, J.N. 2004b. Crystallization in emulsions. *Current Opinion in Colloid and Interface Science*, 7(5-6), 445-450.

9. Coupland, J.N. & Saggin, R. 2003. Ultrasonic sensors for the food industry. *Advances in Food and Nutrition Research*, 45, 101-165.

10. Del Grosso, V.A. & Mader, C. W. 1972. Speed of sound in pure water. *Journal of the*

Acoustical Society of America, 52 (5), 1442-46.

11. Dinçer, İ. 1997. *Heat transfer in food cooling applications*. Taylor & Francis, USA.
12. Flores, A. A. & Goff, H.D. 1999. Recrystallization in ice cream after constant and cycling temperature storage conditions as affected by stabilizers. *Journal of Dairy Science,* 82(7), 1408-15.
13. Hartel, R.W. 2001. Crystallization in foods. Aspen Publishers, USA.
14. Karel, M. & Lund, D.B. 2003. *Physical principles of food preservation*. 2nd ed. Marcel Dekker, Inc, USA.
15. Kell, G.S. 1967. Precise representation of volume properties of water at one atmosphere. *Journal of Chemical and Engineering Data*, 12 (1), 66-69.
16. Lee, S., Pyrak-Nolte, L.J., Cornillon, P., & Campanella, O. 2004. Characterization of frozen orange juice by ultrasound and wavelet analysis. *Journal of the Science of Food and Agriculture*, 84(5), 405-410.
17. Lee, S., Cornillon, P. & Kim, Y.R. 2002. Spatial investigation of the non-frozen water distribution in frozen foods using NMR SPRITE. *Journal of Food Science*, 67(6), 2251-55.
18. Marshall, T., Challis, R.E., Holmes, A.K. & Tebbutt, J.S. 2002. Modeling ultrasonic compression wave absorption during the seeded crystallization of copper (II) sulphate pentahydrate from aqueous solution. *IEEE Transactions on Ultrasonics, Ferroelectrics, and Frequency Control*, 49 (11), 1583- 91.
19. McClements, D.J. 1995. Advances in the application of ultrasound in food analysis and processing. *Trends in Food Science and Technology*, 6(9), 293-299.
20. McClements, D.J. & Fairley, P. 1992. Frequency scanning ultrasonic pulse echo reflectometer. *Ultrasonics*, 30(6), 403-405.
21. McClements, D.J. & Povey, M.J.W. 1987. Solid fat content determination using ultrasonic velocity measurements. *International Journal of Food Science and Technology*, 22(5), 491-499.
22. McClements, D.J. & Povey, M.J.W. 1988a. Comparison of pulsed NMR and ultrasonic velocity techniques for determining solid fat contents. *International Journal of Food Science and Technology*, 23(2), 159-170.

23. McClements, D.J. & Povey, M.J.W. 1988b. Investigation of phase transitions in glyceride/paraffin oil mixtures using ultrasonic velocity measurements. *Journal of the American Oil Chemists` Society*, 65(11), 1791-95.

24. McClements, D.J., Povey, M.J.W. & Dickinson, E. 1993. Absorption and velocity dispersion due to crystallization and melting of emulsion droplets. *Ultrasonics*, 31(6), 433-437.

25. Miles, C. A. & Cutting, C.L. 1974. Technical note: changes in the velocity of ultrasound in meat during freezing. *Journal of Food Technology*, 9(1), 119-122.

26. Mittal, G.S. & Zhang, J. 2000. Prediction of freezing time for food products using a neural network. *Food Research International*, 33(7), 557-562.

27. Petrenko, V.F. & Whitworth, R.W. 1999. *Physics of ice*. Oxford University Press, Great Britain.

28. Ponsawatmanit, R. & Miyawaki, O. 1993. Measurement of temperature-dependent ice fraction in frozen foods. *Bioscience, Biotechnology, Biochemistry*, 57(10), 1650-54.

29. Povey, M.J.W. 1997. *Ultrasonic techniques for fluids characterization*. Academic Press, USA.

30. Saggin, R. & Coupland, J.N. 2002. Measurement of solid fat content by ultrasonic reflectance in model systems and chocolate. *Food Research International*, 35(10), 999-1005.

31. Saggin, R. & Coupland, J.N. 2001. Oil viscosity measurement by ultrasonic reflectance. *Journal of the American Oil Chemists` Society*, 78(5), 509-11.

32. Saggin, R. & Coupland, J.N. 2001. Non-contact ultrasonic measurements in food materials. *Food Research International*, 34(10), 865-870.

33. Sigfusson, H., Ziegler, G.R. & Coupland, J.N. 2004. Ultrasonic monitoring of food freezing. *Journal of Food Engineering*, 62(3), 263-269.

34. Singh, A.P., McClements, D.J. & Marangoni, A.P. Comparison of ultrasonic and pulsed NMR techniques for determination of solid fat content. *Journal of the American Oil Chemists` Society*, 79(5), 431-437.

35. Slie, W.M., Donfor, Jr., A.R. & Litovitz, T.A. 1966. Ultrasonic shear and longitudinal measurements in aqueous glycerol. *Journal of Chemical Physics*, 44(10), 3712-18.

36. Smith, A.C., & Kishoni, D. 1986. Measurement of speed of sound in ice. *AIAA Journal*,

24(10), 1713-15.

37. Young, F.E. & Jones, F.T. 1949. Sucrose hydrates. The sucrose-water phase diagram. *Journal of Physical Chemistry*, 1334-50.

3.2 Ultrasonic Attenuation Measurements in Model Food Solutions

3.2.1 Introduction

In Chapter 3.1, ultrasonic velocity measurements in partially frozen model foods were presented. Ultrasonic velocity increased approximately linearly with ice content in all samples. However, the slope depended on the composition of the samples and therefore was not a universal indicator of ice content. In order to obtain more information on the properties of freezing foods, ultrasonic attenuation was also measured in the same samples.

3.2.2 Materials and Methods

Ultrasonic attenuation was measured using the experimental setup described in Chapter 3.1.

3.2.3 Results

Ultrasonic attenuation was measured in 10-50% sucrose solutions (Figure 3.2.1). Attenuation increased very rapidly immediately after the onset of freezing and remained high as ice content increased. In all cases, attenuation was considerably higher than attenuation of a liquid sample with similar composition which would typically be a few Nepers per meter. However, there was not a clear trend between increasing ice content and attenuation in the samples.

3.2.4 Conclusions

I was unable to relate ice content in partially frozen foods to ultrasonic attenuation. Further investigations are required to explain the change in ultrasonic properties in partially frozen foods.

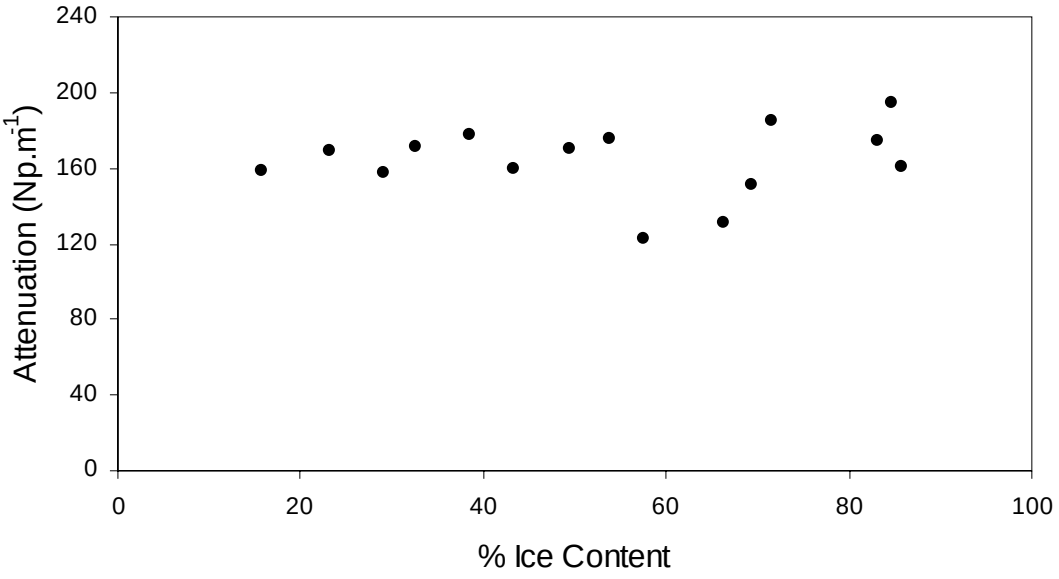

Figure 3.2.1. Ultrasonic attenuation as a function of ice content in partially frozen sucrose solutions (10-50% wt sucrose) prepared as described in Chapter 3.1. The attenuation measurements were taken at temperatures ≤ -8°C.

3.3 Conclusions

In Chapters 3.1 & 3.2, I was unable to use ultrasonic velocity or attenuation measurements as universal indicators in freezing of foods. Based on these observations I conclude ice content is not the sole predictor of these parameters and the influence of other physical properties of the system should also be included in this analysis. Although currently no complete theoretical solution exists for freezing of foods, many partial theories that refer to the influence of heterogeneities or influence of crystallizing entities are present (e.g., scattering and relaxational theories as discussed in Chapter 3.1). It is a complicated task to test the validity of these approaches in partially frozen foods due to the difficulties in controlling or describing crystal size distribution and impingement. Therefore it will be more practical to analyze simpler model systems to develop theory before returning to the evaluation in frozen samples. In Chapter 4 (*i.e.*, Objective 2), *n*-alkane emulsions are studied as model systems to analyze the ultrasonic properties during phase transitions. This selection was made due to the simplicity of the system as well as the previous arguments on the scattering and relaxational losses in melting alkane emulsions (McClements *et al*. 1993).

Reference

1. McClements, D.J., Povey, M.J.W. & Dickinson, E. 1993. Absorption and velocity dispersion due to crystallization and melting of emulsion droplets. *Ultrasonics*, 31(6), 433-437.

Chapter 4

Excess Attenuation in Melting Emulsion Droplets

4.1 Excess Ultrasonic Attenuation due to Solid-Solid and Solid-Liquid Transitions in Emulsified Octadecane

Abstract

The crystallization and melting of emulsified *n*-octadecane (C_{18}) is monitored by microcalorimetry and by ultrasonic (2.25 MHz) velocity and attenuation measurements. During cooling, the lipid showed two thermal events (a large exothermic DSC peak at 12.8°C and a smaller one at 7.8°C) and during heating showed a similarly-spaced pattern in reverse (a minor endothermic DSC peak at 15.9°C and a major DSC peak at 27.3°C). The minor DSC peaks during heating and cooling was attributed to a transition between a rotator phase stable at higher temperatures and a crystal phase stable at lower temperatures. The major DSC peaks were attributed to a transition between the liquid and rotator phases. The major DSC peaks corresponded to small but measurable changes in the speed of sound in the emulsions and the major and minor endothermic DSC peaks during heating corresponded to peaks in ultrasonic attenuation. The peaks in attenuation were not seen during the cooling cycle. Scattering theory provided a good model for the temperature dependent ultrasonic properties of the emulsion with the exception of the peaks in attenuation observed during melting transitions. However, by calculating an effective specific heat, density and cubical expansion coefficient over the melting transition from the microcalorimetry data, it was possible to extend scattering theory to include the excess attenuation on melting.

4.1.1 Introduction

The crystallization and melting of emulsified lipids is of practical interest in the formulation of foods, cosmetics, and drug delivery systems as well as in fundamental studies of the mechanisms of nucleation. Lipid crystallization in fine emulsions differs from crystallization in bulk in two main ways: firstly the structure of the crystals formed is influenced by the curvature of the interface and the presence of a surface layer (Dickinson & McClements, 1995) and secondly any potential nucleation catalysts are compartmentalized into individual droplets and consequently the majority of the oil must nucleate via a much slower homogeneous mechanism (*e.g.*, emulsified alkane droplets typically crystallize 10-15°C below their melting points while bulk alkanes typically show <5°C of supercooling).

Normal alkanes are widely-studied models of lipid crystallization, as they are chemically simple and are available with a wide range of chain lengths. As well as forming a stable crystalline phase, various studies have identified rotator phases in normal alkanes (Wang *et al*. 2003; Shinohara *et al*. 2005; Montenegro & Landfester, 2003; Oliver & Calvert, 1975; Hammami & Mehrotra, 1995; Genovese *et al*. 2006). A rotator phase is defined as lamellar crystals "which exhibit long-range order in the molecular axis orientation and center-of-mass position but lack rotational degrees of freedom of the molecules about their long axis" (Kraack *et al*. 2000). The relatively weak crystalline structures formed can be classified as plastic crystals or highly ordered smectic phases (Sirota *et al*. 1993).

Ultrasound is high frequency (>20 kHz) sound that is often used at low power levels in the nondestructive testing of materials. Measurements of ultrasonic velocity are particularly sensitive to changes in solid fat content and have been widely used to study droplet crystallization (McClements & Povey, 1987, 1988) while the ultrasonic attenuation of suspensions of solid and liquid droplets are usually similar. However, McClements *et al*. (1993)

noted an anomalous attenuation during the melting of emulsified *n*-hexadecane. The attenuation started to increase 7-8°C below the thermodynamic melting point and reached a peak at the melting point, 5-6 times the values measured for either purely solid or purely liquid droplets, before quickly decreasing at higher temperatures. The authors attributed the excess attenuation to a mechanism initially proposed by Akulichev and Bulanov (1981, 1983) who suggested the compressions and rarefactions in the medium due to the passing ultrasonic wave, although small, may perturb the phase equilibrium during the melting processes. The melting/recrystallization of the fat absorbs ultrasonic energy and is responsible for excess attenuation. McClements and co-workers (1993) argued that the excess peak was not seen during crystallization as the emulsified lipid was so deeply supercooled that, once initiated, the transition was complete before it could be measured.

In the present work, I use microcalorimetry to identify the formation and melting of rotator and crystal phases in emulsified octadecane, and show that both the crystal-to-rotator and the rotator-to-liquid melting transitions are associated with an excess ultrasonic attenuation. The excess attenuation can be modeled by incorporating the discontinuity in density and thermal properties at the melting point into scattering theory and does not require the additional theory of Bulanov (1981, 1983).

4.1.2 Materials and Methods

Materials and Sample Preparation. *n*-Octadecane (C_{18}) was obtained from Alfa Aesar (99% purity) and Tween 20 (polysorbate 20, W929150-1) was purchased from Aldrich Chemical Company. The alkane (3 wt%) was mixed with a Tween 20 solution (1 wt%) in a high speed blender (Kinematica GmbH FT10/35, Brinkmann Instruments, Switzerland) to prepare a coarse emulsion which was further homogenized using a two-stage valve homogenizer (1-5 passes, 200 to 600 bar, 10% of which was maintained over the second stage, Niro-Soavi Panda, Model no: 3344, Parma, Italy). In order to keep the oil in a liquid state for homogenization, the equipment was preheated with hot water prior to use. The particle size distribution of the emulsions was

characterized by static light scattering (Horiba LA-920, Irvine, CA, USA) after appropriate dilution. The emulsions were stable over the course of the experiment (i.e., no change in particle size, no visible phase separation) and were not destabilized by the cooling-heating cycles.

Ultrasonic Measurements. The ultrasonic properties of the emulsions were measured as a function of temperature using a modified pulse-echo technique (McClements & Fairley, 1992). An electrical spike signal (Panametrics 500 PR, Waltham, MA, USA) was passed to a broadband ultrasonic transducer (2.25 MHz center frequency, Panametrics, Waltham MA), which converted the energy to ultrasound. The pulse of sound traveled into a Plexiglas delay line, and was partially reflected at the plastic-sample interface. The reflected part of the signal returned through the delay line to the transducer (echo 1) and the transmitted part traveled through the sample (~1 cm), was reflected from the brass plate and returned through the sample and the delay line to the transducer (echo 2). The transducer reconverted the acoustic signal to an electrical signal which was stored for analysis with a digital oscilloscope (LeCroy 9310c, Chestnut Ridge, NY, USA). The time and energy difference between echo 1 and echo 2 were used to calculate the speed of sound and attenuation of the sample.

Aliquots (~20 ml) of emulsion were poured into the ultrasonic measurement cell at 35°C and held for 30 minutes. The samples were then cooled to 0°C at 6 °C/hr and measurements were taken at each integer °C. Additional measurements were taken to increase the resolution of the ultrasonic data around the attenuation peaks. To ensure complete crystallization before the heating cycle, the samples were held at 0°C for 30 minute before reheating at the same rate to the starting temperature.

Differential Scanning Calorimetry. The crystallization and melting thermograms were measured using differential scanning calorimetry (VP-DSC, Microcal, Northampton, MA). Samples were diluted to 0.25 wt% lipid with water prior to analysis so that the signals were within the range of the instrument. Samples (513.1 μl) were run against a similar reference cell filled with water. Samples were heated to 35°C, held for 30 minutes, and cooled to 1°C at 10 °C/hr (to measure any crystallization) then held for a further 30 min and reheated at the same rate to 35°C (to

measure any melting events). The heat capacity data for the water-water scan was subtracted from the sample runs to measure the heat flux due to changes in the lipid phase. In preliminary experiments, I showed that the surfactant solution did not itself show any measurable transitions over this range.

4.1.3 Results

There were two peaks in the cooling thermogram of the C_{18} emulsion; the larger one with an onset of about 16°C and the smaller about 7°C (Figure 4.1.1a). In previous studies of emulsified octadecane crystallization I have only seen a single peak at about 8°C which was taken as homogeneous nucleation of the lipid phase (Cramp *et al*. 2004). However, the earlier studies were conducted with a less-sensitive calorimeter which may have been incapable of detecting the smaller thermal events. The higher temperature peak probably corresponds to the formation of a metastable rotator phase (RO, Sirota & Herold, 1999) which itself transforms to the low-temperature crystalline phase (LO) at 8°C. A C_{18} rotator phase has also been detected in miniemulsion droplets ($\leq$ 0.25 μm) at around 17°C by X-ray crystallography (Montenegro & Landfester, 2003). In the DSC measurements performed on the same systems, these workers detected a double peak on cooling rather than the distinct peaks seen here, but this may have been due to the somewhat faster cooling rate (5°C.min^{-1}) used (Montenegro & Landfester, 2003).

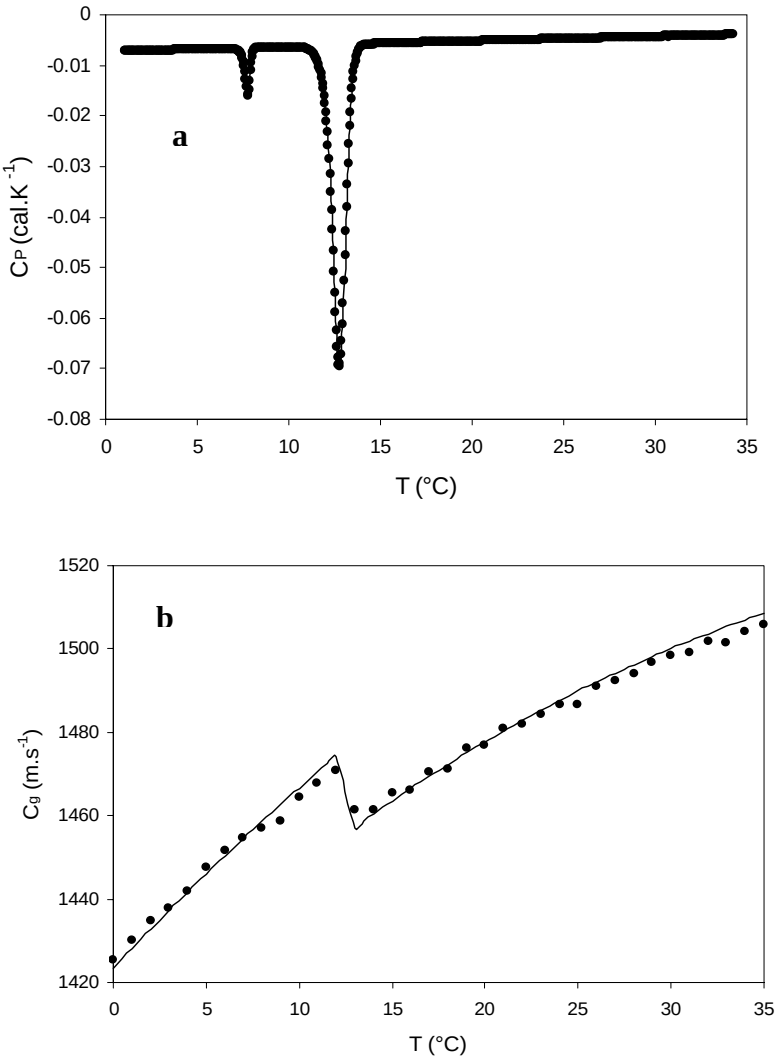

Figure 4.1.1. Crystallization of 3% C_{18} emulsion (d_{32}=0.45 μm) stabilized by 1% Tween 20 as monitored by (a) differential scanning calorimetry, (b) ultrasonic velocity and (c) ultrasonic attenuation measurements. Ultrasonic measurements are made using a 2.25 MHz center frequency transducer. Lines show predictions of ultrasonic properties calculated from scattering theory.

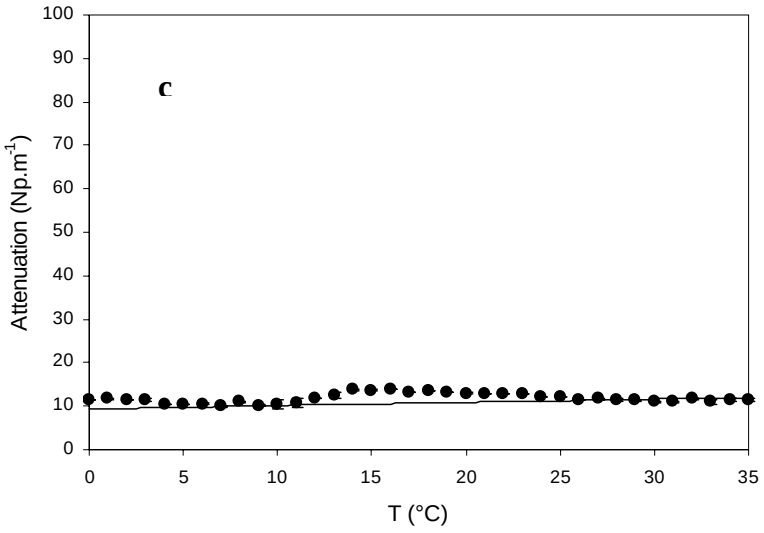

Figure 4.1.1 (continued)

Several workers have attributed multiple exothermic peaks during the cooling of emulsified alkanes to different populations of the fat crystallizing by different mechanisms (*e.g.*, Vanapalli *et al*. 2003). Typically a proportion of the droplets are assumed to contain an active catalytic nucleus and crystallize heterogeneously, while other droplets lack a nucleus and crystallize homogeneously Heterogeneous nucleation occurs at a higher temperature (close to the bulk crystallization temperature) than homogeneous nucleation so two exothermic peaks are seen during cooling. The relative proportion of these peaks depends on the concentration of catalytic impurities in the original fat and the number of droplets. However, I do not expect this phenomenon to be relevant in this case because the major crystallization peak occurs at a degree of supercooling typical of homogeneous nucleation in alkanes and the minor peak occurs at an even lower temperature. Indeed, both peaks occur well below the bulk crystallization temperature which would be characteristic of a heterogeneous nucleation mechanism. Another explanation for the multiple peaks would be impurities in the fat crystallizing as separate phases. Again I do not believe this to be the case here, firstly because the lipid used was of a high purity and secondly, *n*-alkane contaminants tend to co-crystallize with the main lipid fraction rather than as a separate phase with a distinct melting point (data not shown).

The ultrasonic velocity and attenuation of similar C_{18} emulsions were measured as a function of temperature during cooling (Figure 4.1.1b and 4.1.1c, respectively). The ultrasonic velocity in the emulsion decreased with temperature because the speed of sound in water (the major component) also decreases with temperature (Chanamai *et al*. 1998). There was a small discontinuity in ultrasonic velocity at around 15°C corresponding to the crystallization of the lipid phase. Other workers (McClements & Povey, 1987, 1988; McClements *et al*. 1993; Saggin & Coupland, 2002) have typically reported a similar increase in velocity of about 3 $m.s^{-1}$ per percent of lipid crystallizing. The attenuation of the emulsions was largely temperature-independent (10-14 $Np.m^{-1}$) and similar to the values reported by other workers for similar systems (*e.g*., 9 -17 $Np.m^{-1}$ in McClements *et al*. 1993). There was no significant attenuation peak corresponding to droplet crystallization, probably because, as other workers have suggested (McClements *et al*. 1993), the transition in the supercooled droplet is complete before it can be detected. Neither of the ultrasonic measurements could resolve the formation of the RO phase seen in the calorimetric measurements.

The heating thermogram of the emulsions had three distinct events (Figure 4.1.2a); a small transition at about 16°C and a major double peak at 27°C close to the thermodynamic melting point of C_{18} (26.6°C) (Sirota & Herhold, 1999). I attribute the first to a LO→RO transition and the larger double peak to the RO→liquid transition occurring in two stages. Several workers, including recently Povey *et al*. (2006), have suggested that the emulsified lipid closest to the surface is mixed with the hydrophobic portions of the surfactant used and thus has different physical properties than the more pure lipid in the core of the droplet. It is possible that the double peak seen here is due to the melting of first the surface lipid followed by the lipid at the droplet core.

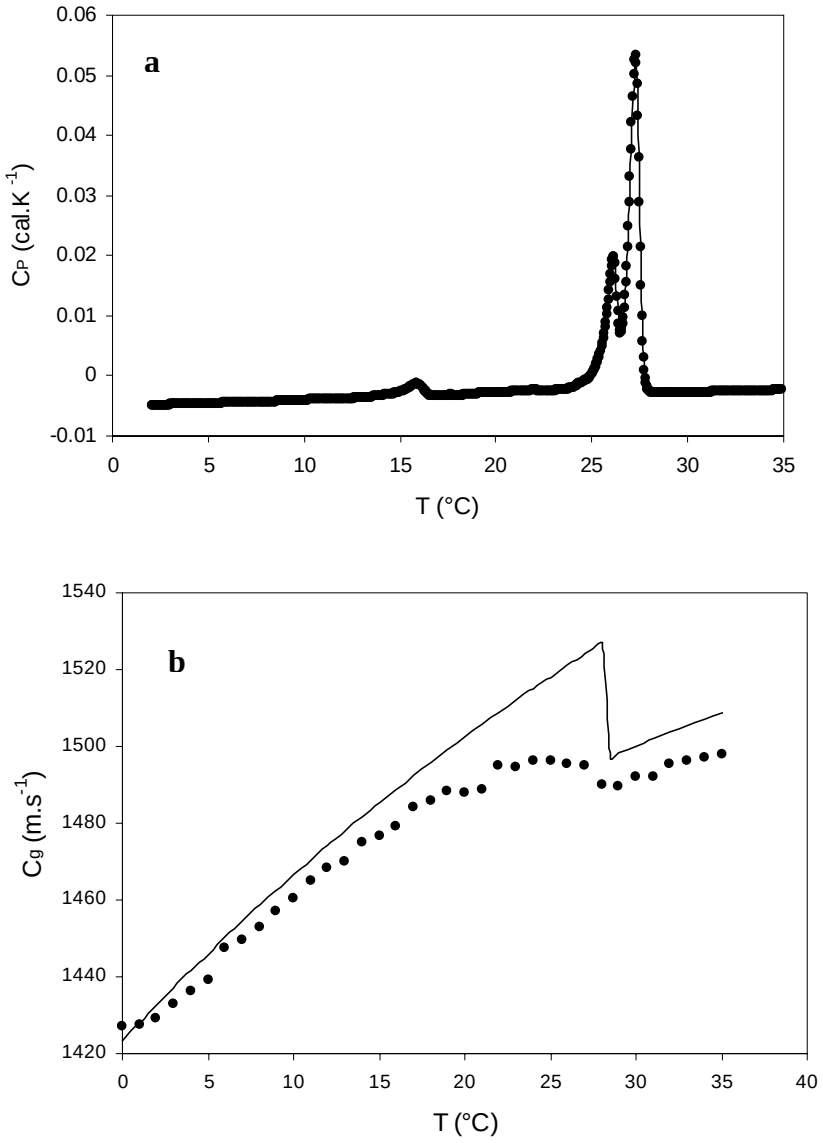

Figure 4.1.2. Melting of 3% C_{18} emulsion (d_{32}=0.45 μm) stabilized by 1% Tween 20 as monitored by (a) differential scanning calorimetry, (b) ultrasonic velocity (c) ultrasonic attenuation measurements. Ultrasonic measurements are made using a 2.25 MHz center frequency transducer. Lines show predictions of ultrasonic properties from calculated scattering theory.

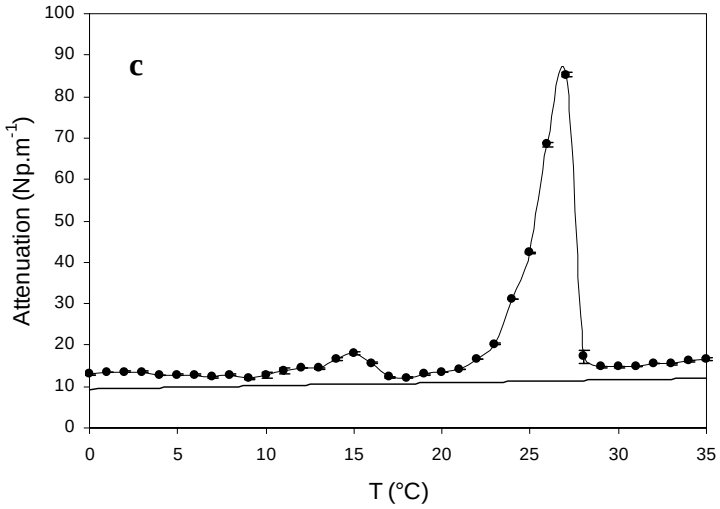

Figure 4.1.2 (continued)

The ultrasonic velocity in the emulsions increased with temperature during heating and there was a small decrease corresponding to the main droplet melting (Figure 4.1.2b). These observations are quantitatively similar to results reported by other workers (McClements *et al*. 1993). I was not able to detect a change in ultrasonic velocity corresponding to the LO→RO transition seen in the thermogram. There were two peaks in ultrasonic attenuation during the heating of the emulsions (Figure 4.1.2c) ; a minor peak between 10°C and 17°C and a larger, peak at around 20-29°C corresponding to the LO→RO and RO→liquid transitions seen in the DSC measurements (Figure 4.1.2a). The ultrasonic measurements were not able to resolve the details in the major melting transition seen by calorimetry; even when the ultrasonic experiment was repeated at a slower scanning rate (1°C/hr) taking measurements every 0.1°C (data not shown).

4.1.4 Discussion

The ultrasonic velocity measurements are similar to those reported elsewhere by other workers and will not be discussed further here, but the attenuation results are more novel and deserve further consideration. Scattering theory provides the most general and widely-used model for ultrasonic attenuation in emulsions (Povey, 1997). Although more complete versions of scattering theory exist to describe a wider range of frequencies and droplet sizes and concentrations (Allegra & Hawley, 1972) the simple formulation (neglecting multiple scattering) suggested by McClements and Coupland (1996) will suffice for the dilute emulsions and large wavelength: droplet size ratio used here. Using this theory and tabulated data for the physical properties of the component phases (Table 4.1.1) the ultrasonic properties of the emulsions were calculated as a function of temperature (Figure 4.1.1b and c, Figure 4.1.2b and c). In general the fits of both velocity and attenuation were good; however scattering theory does not predict the peaks in attenuation seen during melting.

The excess attenuation at melting was qualitatively described by McClements and co-workers (1993) in terms of Bulanov's theories (Akulichev & Bulanov, 1981, 1983). Briefly, the fluctuating pressure/temperature in the passing ultrasonic wave displaces the position of the crystal-melt equilibrium. If the molecular dynamics of the phase transition occurs over a similar timescale as the ultrasonic frequency there is resonance and a large excess attenuation beyond that predicted by scattering theory. However, as I shall show here, it is possible to explain the excess attenuation without invoking additional Bulanov terms into scattering theory by using effective values for the physical properties of the melting crystal droplets.

Table 4.1.1. Physical properties of water and *n*-octadecane (C_{18}) used in the scattering theory[a].

	Water	C_{18}
Ultrasonic velocity, c (m s^{-1})	$3.14643091.\ 10^{-9}\ T^5$ $-1.47800417.\ 10^{-6}\ T^4$ $+3.34198834.\ 10^{-3}\ T^3$ $-5.800852166.\ 10^{-2}\ T^2$ $+5.03711129\ T$ $1.40238754.\ 10^3$ (b)	Liquid phase (f): $1.45.\ 10^3$ $-3.80\ T$ $+2.6.\ 10^{-2}T^2$ Solid phase (g) : $2.16.\ 10^3$ $-\ 1.55.\ 10^1\ T$ $+\ 7.75.\ 10^1\ T^2$
Density, ρ (kg m^{-3})	$-2.10^{-7}\ T^4 + 6.10^{-5}T^3 - 8.8.\ 10^{-3}\ T^2 + 8.4.\ 10^{-2}\ T + 1.\ 10^2$ (c)	Liquid phase (h): $8.02.\ 10^2$ $-\ 8.22.\ 10^{-1}\ T$ $+1.10^{-3}\ T^2$ $-2.10^{-6}\ T^3$ Solid phase (i): $-6.69.\ 10^{-1}\ T + 9.23.\ 10^2$
Viscosity, η (N m^{-2} s)	$-4.10^{-10}\ T^5 +$ $1.10^{-7}\ T^4 - 2.10^{-5}\ T^3 + 1.2.\ 10^{-3}\ T^2 - 5.82.10^{-2}\ T + 1.78$ (d)	$(-9.\ 10^{-7}\ T^3 + 4.\ 10^{-4}\ T^2 -$ $7.65.\ 10^{-2}\ T + 5.3).\ 10^{-3}$ (h)
Specific heat capacity, C_P ($J\ kg^{-1}K^{-1}$)	$6.\ 10^{-10}\ T^6 - 2.10^{-7}T^5$ $+ 3.10^{-5}\ T^4 - 2.8.\ 10^{-3}\ T^3$ $+ 1.38.\ 10^{-1}\ T^2 - 3.66\ T$ $+ 4.22.\ 10^3$ (d)	Liquid phase (i): $-1.10^{-4}\ T^3 + 3.01.\ 10^{-2}\ T^2 +$ $6.13.10^{-1}\ T + 2.19.10^3$ Solid phase (i): $2.6.\ 10^{-3}\ T^3 + 5.55.\ 10^{-2}\ T^2 + 7.7T$ $+ 1.66.10^3$
Thermal conductivity, τ ($Wm^{-1}K^{-1}$)	$4.10^{-13}\ T^6 - 2.10^{-10}\ T^5$ $+ 3.10^{-8}\ T^4 - 2.10^{-6}\ T^3$ $- 2.10^{-6}\ T^2 + 1.8.\ 10^{-2}\ T + 5.62.\ 10^{-1}$ (d)	Liquid phase (e): $1.53.10^{-1}$ Solid phase (j): $1.93.10^{-1}$
Cubical expansion coefficient, β (K^{-1})	$-4.10^{-10}\ T^6 + 2.10^{-7}\ T^5$ $-3.10^{-5}\ T^4 + 3.7.\ 10^{-3}\ T^3$ $- 2.64.\ 10^{-1}\ T^2 + 1.77.\ 10^1\ T$ $- 6.62.10^1.\ 10^{-6}$ (c)	$8.69.10^{-4}$ (e)
Attenuation coefficient, α (Np $m^{-1}\ s^{-2}$)	$2.3.\ 10^{-14}\ f^2$ (e)	$1.16.\ 10^{-13}\ f^2$ (e)

(a) All temperature values are in °C.
(b) Del Grosso, V.A. & Mader, C.W. 1972. *Journal of the Acoustical Society of America*, 52, 1442-46.
(c) Kell, G.S. 1967. *Journal of Chemistry and Engineering Data*, 12, 66-69.
(d) Weast, R.C. 1975. *CRC Handbook of Chemistry and Physics*, 56th ed., CRC Press, Cleveland, OH.
(e) Herrmann, N. & Lemaréchal, P. 1999. *European Physics Journal of Applied Physics*, 5, 127-134.
(f) Defined as a function of T (°C) using the data presented in Dutour, S., Daridon, J.L. & Lagourette, B. 2000. *International Journal of Thermophysics*, 21, 173-184.

(g) Defined experimentally as a function of T (°C).
(h) Defined as a function of T (°C) using the data presented in Caudwell, D.R. *et al*. *International Journal of Thermophysics*, 25, 1339-52.
(i) Defined as a function of T (°C) using the data presented in TRC-TAMU. Thermodynamic Tables – Hydrocarbons (1985).
(j) Approximated from Powell, R.W., Challoner, A.R. 1961. *Industry and Engineering Chem*istry. 53, 581-582.

Firstly, the effective heat capacity (*i.e*., thermal energy required for unit change in temperature) of a material is greater during a melting transition as it must include the enthalpy of fusion. For the pure solid and pure liquid phases, I can use tabulated values for C_p (Table 4.1.1) but during the transition I must add in the heat of fusion from the calorimetry measurements to give an effective specific heat as a function of temperature (Figure 4.1.3a). Secondly, the densities of the solid (ρ_s) and liquid (ρ_l) droplets are simple functions of temperature (Table 4.1.1). During melting, as the solid fat content (%SFC) decreases from 100% to 0% the effective density of the droplet (ρ) can be calculated as the contributions of the solid and liquid components at each temperature:

$$\rho = \rho_s \frac{\%SFC}{100} + \rho_l (1 - \frac{\%SFC}{100}) \qquad [4.1]$$

The solid fat content was calculated from the heat flux curve, assuming the sample was completely solid at the start of the transition and the amount of melting at a given temperature was proportional to the proportion of the enthalpy of fusion released at that temperature (Figure 4.1.3b) allowing a calculation of effective density from Equation 4.1 (Figure 4.1.3c). The cubical expansion coefficient, β, is a simple function of the slope of density with temperature:

$$\beta = -\frac{1}{\rho}\left(\frac{\partial \rho}{\partial T}\right)_P \qquad [4.2]$$

and was calculated from a numerical differentiation of the effective density-temperature curve (Figure 4.3d).

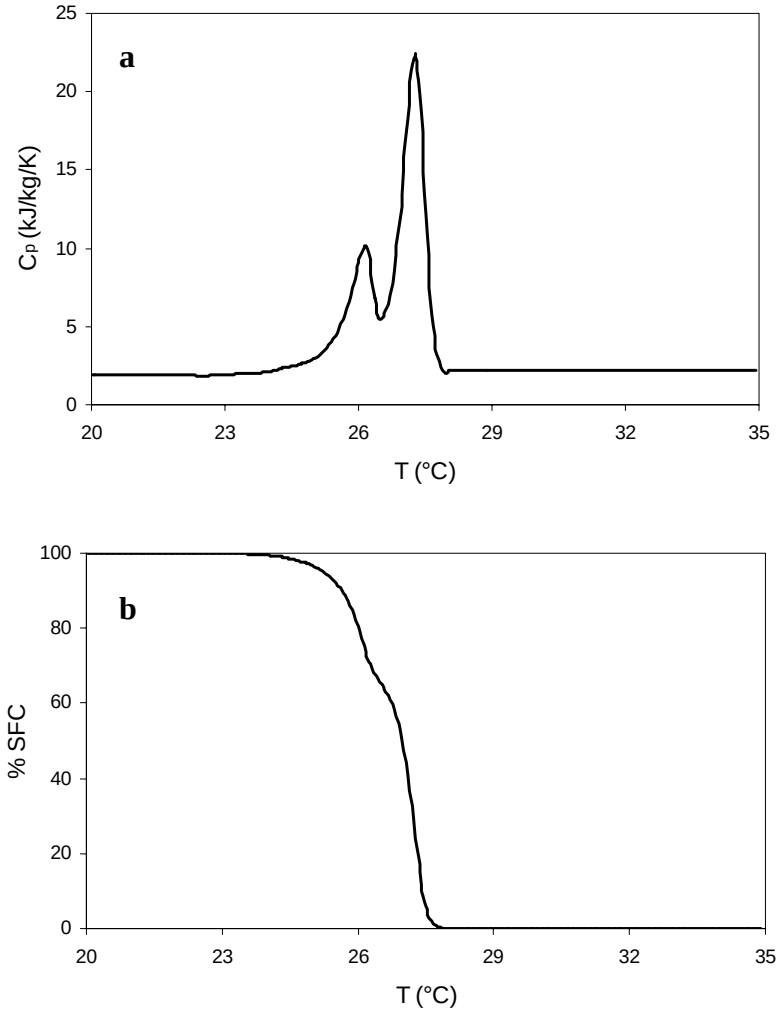

Figure 4.1.3. (a) Heat capacity of *n*-octadecane as a function of temperature calculated from the DSC melting curve for 3% *n*-octadecane-in-water emulsion stabilized by 1% Tween 20 (d_{32} = 0.45 μm). (b) Solid fat content (% SFC) of *n*-octadecane as a function of temperature calculated from the DSC melting curve for 3% *n*-octadecane-in-water emulsion stabilized by 1% Tween 20 (d_{32} = 0.45 μm). (c) Density of *n*-octadecane as a function of temperature calculated from the solid fat content data (Figure 4.1.3b). Dotted lines are the extrapolation of tabulated properties of the pure solid and pure liquid phases. (d) Thermal expansion coefficient of *n*-octadecane as a function of temperature calculated from the density data (Figure 4.1.3c).

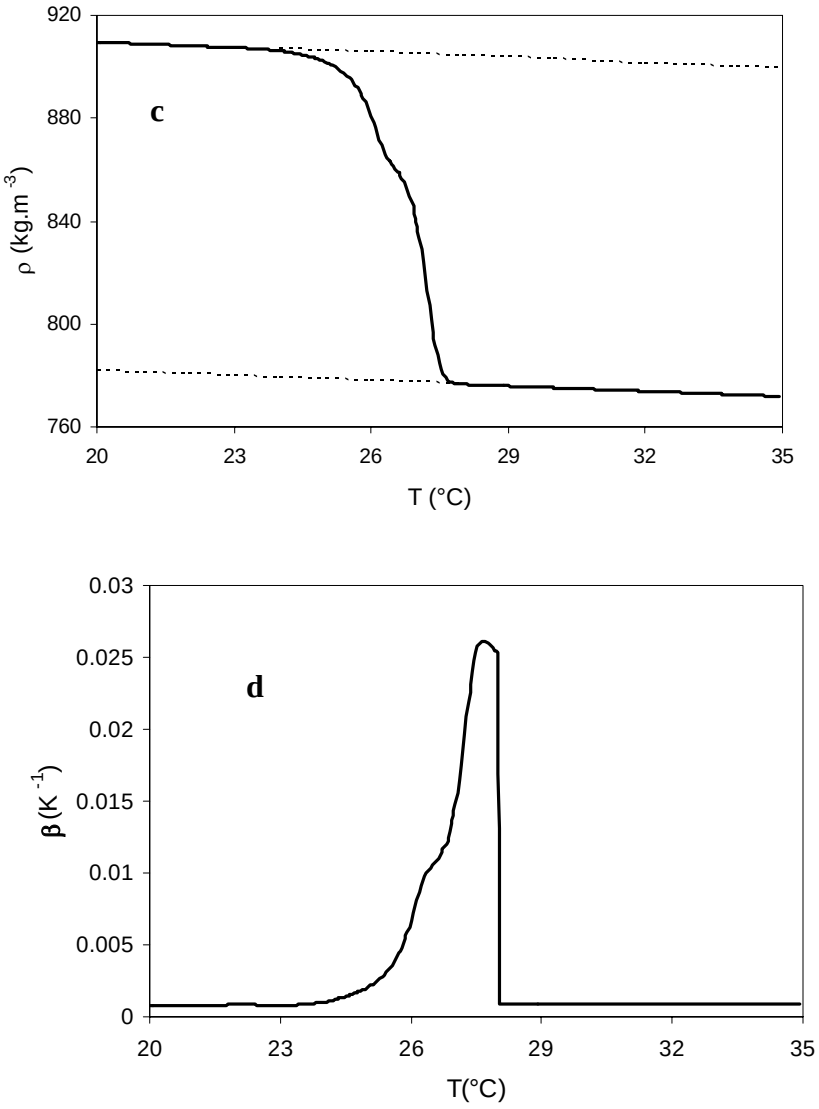

Figure 4.1.3 (continued)

Using the effective values of specific heat, density and cubical expansion coefficient, the ultrasonic attenuation of the melting droplets was once more calculated from scattering theory (Figure 4.1.4). This time there is much better agreement with the experimental measurements and a clear attenuation peak during melting. The theoretically predicted attenuation peak is somewhat larger than the experimental measurement; possibly because it is based on measurements made in a different sample in the microcalorimeter. Another reason is that the physical properties of the rotator phase may have been different than those of the crystalline phase.

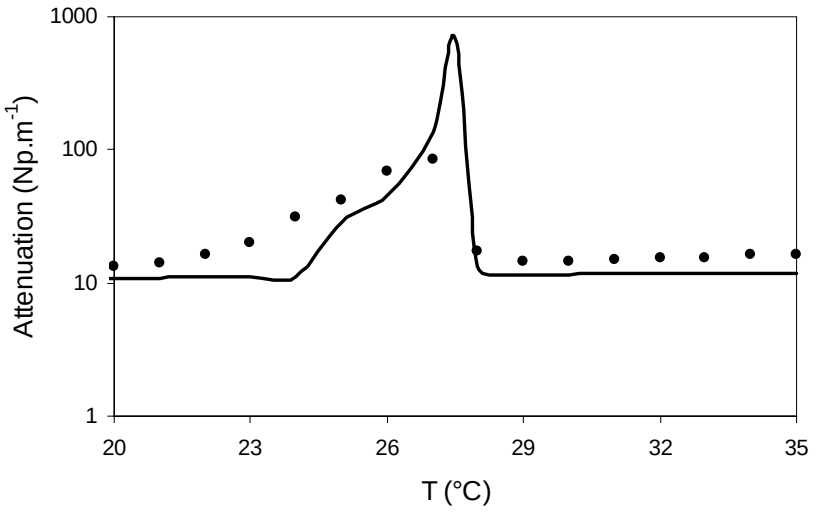

Figure 4.1.4. Detail of the major attenuation peak seen during the heating of a 3% *n*-octadecane-in-water emulsion stabilized by 1% Tween 20 (d_{32} = 0.45 μm) (replotted from Figure 4.1.2c). The line shown is the prediction from scattering theory using effective temperature dependent values for heat capacity, density, and thermal expansion coefficients from Figure 4.1.3.

In another series of experiments, the homogenization conditions were varied to produce emulsions of identical composition but different particle sizes. The ultrasonic attenuation was largely independent of particle size for solid or liquid droplets but increased with decreasing particle size for the melting droplets (Figure 4.1.5). McClements and co-workers (1993) used similar increase in excess in attenuation during melting to argue that the mechanism responsible is largely a surface effect. However, using the effective values of specific heat, density, and cubical expansion coefficient from Figure 4.1.3, I was able to obtain a reasonable prediction of ultrasonic attenuation over a wide particle size range (0.35 to 6.45 μm) without requiring an additional mechanism to account for the losses.

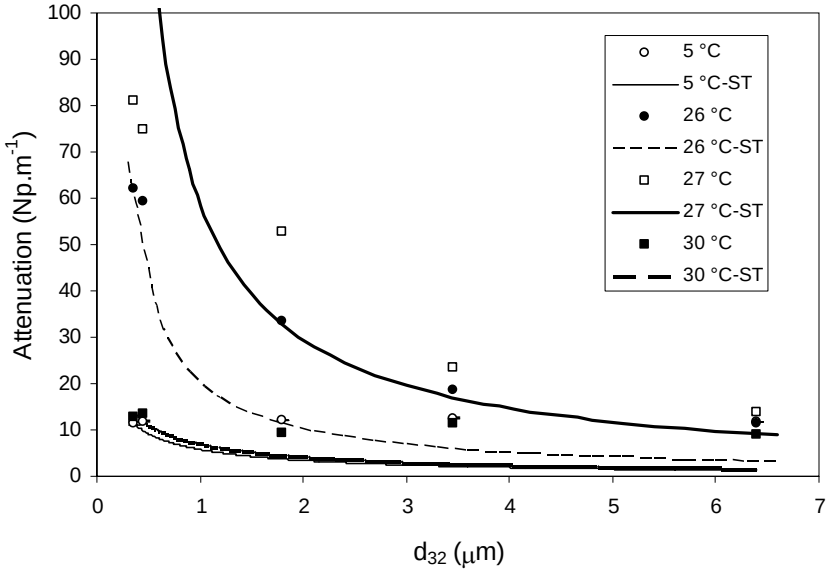

Figure 4.1.5. Effect of particle size on ultrasonic attenuation of 3% C_{18} emulsion stabilized by 1% Tween 20 at the major attenuation peak temperatures (26 and 27 °C), for pure solid samples (5 °C) and for pure liquid samples (30 °C) during the melting scan. Ultrasonic measurements are made using a 2.25 MHz center frequency transducer. Lines show predictions of ultrasonic attenuation from scattering theory (ST) for the tabulated properties purely solid (5°C) and liquid (30°C) droplets as well as the semi-crystalline droplets (26 and 27°C) using data from Figure 4.1.4.

As an ultrasonic wave passes through an emulsion it is scattered by the droplets and the droplets pulsate and oscillate in the passing pressure gradient. The ultrasonic attenuation is the sum of contributions due to the intrinsic properties of the component phases, scattering losses as the sound is directed into different paths by interaction with the droplets, thermal losses due to heat flow between the pulsating droplets and surrounding continuous phase and viscous losses due to the drag the continuous phase exerts on the oscillatory motions of the droplets (McClements & Coupland, 1996). At this combination of droplet size and ultrasonic wavelength (*i.e.*, the long wavelength limit) thermal losses are most significant. Since the physical properties (*i.e.*, density, heat capacity, compressibility) of the dispersed and continuous phases are different, the compression-rarefaction cycles lead to different degrees of heating and cooling in the different phases and consequently to the formation of a thermal wave at the droplet-continuous phase interface which decays as it moves into each phase. The distance over which maximum thermal wave amplitude is reduced to e^{-1} of its original value is referred as the thermal skin depth:

$$\delta_t = \sqrt{\frac{2 \cdot \tau}{\omega \rho C_P}} \qquad [4.3]$$

where, δ_t is the thermal skin depth, ω is the angular frequency, τ is the thermal conductivity, ρ is the density and C_P the heat capacity.

The calculation of thermal attenuation will depend on the number of thermal skin depths within both phases. For example, thermal skin depth in both water and oil phases for a 3% *n*-octadecane emulsion with a particle size of 0.45 μm are both approximately 0.1 μm (at 25°C and 2.25 MHz), therefore thermal attenuation wave intensity suffers an e^4 (~55) fold reduction over the diameter of a single droplet. The relationship between thermal skin depth and droplet radius, r, is expressed in the complex ratio, b (Allegra & Hawley, 1972):

$$b = (1+i)\frac{r}{\delta_t} \qquad [4.4]$$

The thermal attenuation, $\alpha_{T,}$ can be calculated from the b parameter as:

$$\alpha_T = \frac{i3\phi k_1 H(\gamma - 1)}{2b_1^{\,2}}\left(1 - \frac{\beta_2 \rho_1 C_{P,1}}{\beta_1 \rho_2 C_{P,2}}\right)^2 \qquad [4.5]$$

where subscripts 1 and 2 represent continuous and dispersed phases, respectively, k is the complex wavenumber, ϕ is the volume fraction of the dispersed phase, and γ is the ratio of specific heats ($C_{P,1}/C_{V,1}$) and H is given by:

$$H = \left(\frac{1}{1 - i.b_1} - \frac{\tau_1}{\tau_2} \cdot \frac{\tan(b_2)}{\tan(b_2) - b_2}\right)^{-1} \qquad [4.6]$$

Using this formulation I can begin to understand the mechanism by which melting leads to the observed increase in attenuation. I will examine the relevant parameters, density, specific heat and cubical expansion coefficient in turn.

When the density of a droplet increases, the thermal skin depth decreases (Equation 4.3) which, in turn, increases the thermal attenuation (Equation 4.5). The effect of changing the density alone on the ultrasonic attenuation of an emulsion is calculated using Equation 4.3; all other physical properties are held constant as those of liquid octadecane at 20°C while the oil density is increased from that of the pure solid to the pure liquid (~17% change) (Figure 4.1.6). The change in attenuation due just to changes in density are minimal (*i.e.*, within 2 $Np.m^{-1}$) and do not significantly contribute to the peak measured experimentally.

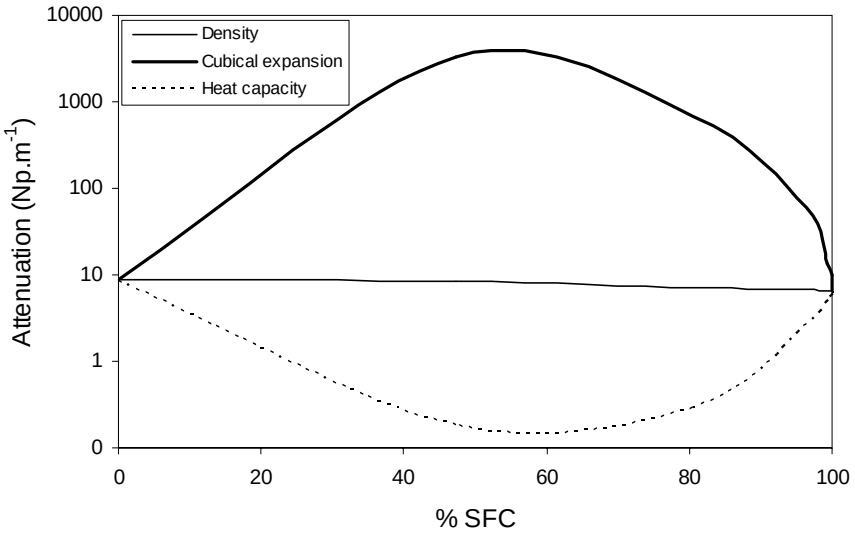

Figure 4.1.6. Scattering theory prediction of attenuation as heat capacity (C_P), density (ρ) and cubical expansion coefficient (β) vary as a function of % SFC. When one parameter was varied, the other two were held constant at their 20°C value (100% SFC).

Although the specific heats of the liquid and solid phases are only slightly different from one another, the effective specific heat during melting is 6-7 times greater than either of these values and may have a larger effect on attenuation. A large heat capacity also reduces the thermal skin depth (Equation 4.5) which consequently increases the thermal attenuation. However, specific heat also plays a role in the quadratic term of Equation 4.3, $\left(1-\frac{\beta_2\rho_1 C_{P,1}}{\beta_1\rho_2 C_{P,2}}\right)$, which defines the temperature difference between the two phases. A droplet with a large specific heat will decrease this term, and hence thermal attenuation of the emulsion. The effects of changing specific heat independently on the thermal attenuation of an octadecane emulsion are calculated in Figure 4.1.6 and it can be seen that the attenuating effect of specific heat on the thermal skin depth is completely overcome by anti-attenuating effect on the temperature gradient term and the large effective specific heat during melting in fact decreases the attenuation of the emulsion – the opposite of the effect seen in practice.

Finally, I consider the effects of the large peak in cubical expansion coefficient also during melting (Figure 4.1.6). A large cubical expansion coefficient increases the temperature difference driving the thermal wave (*i.e.*, the quadratic term in Equation 4.5) and hence the thermal attenuation. Once more I look at the effect of changing this term independently and I see that the large cubical expansion coefficient of a melting droplet is greater than the effects of specific heat and is responsible for the measured attenuation maximum. The larger cubical expansion coefficient causes a partly melted droplet to change its size more vigorously in the passing ultrasonic wave, and consequently creates a larger temperature gradient and more thermal losses.

Three parameters in thermal attenuation calculations are frequency dependent: wavenumber for the continuous phase (k_1), number of thermal skin depths for the continuous phase (b_1) and parameter H. As frequency increases, all three parameters increase which causes thermal attenuation to increase. However α/f^2 decreases with frequency in a form similar to that seen in the experimental data of McClements and co-workers (1993).

4.1.5 Conclusions

In this work I use the well-characterized melting and crystallization of a simple emulsified alkane to reveal new detail on the mechanisms of ultrasonic losses associated with a phase transition. This study is not the first to investigate the crystallization, melting and rotator phase transition phenomena in emulsified alkanes but I am able to use this well-characterized system to offer some novel conclusions.

Firstly, the excess attenuation measured during a droplet melting transition is directly related to the changing thermophysical properties of the system and scattering theory. This work has implications for the use of ultrasound to characterize other semi-crystalline systems, particularly lipids. Ultrasonic velocity measurements are widely used to estimate the solid fat content of emulsified lipids and it may be possible to combine these measurements with simultaneous ultrasonic attenuation measurements to estimate the enthalpy changes associated with phase transitions. However, even with the combined measurements, these calculations would be challenging as they require detail on the densities and thermal properties of the phases involved close to the transition.

Secondly, although the presence of a rotator phase in bulk and emulsified alkanes has become widely accepted since Sirota and Herhold's original work in 1999 (Sirota & Herhold, 1999) it is still interesting to see further evidence in another experimental system. It is particularly interesting here that the formation of the rotator phase on melting produced a small but measurable increase in ultrasonic attenuation. Previously, rotator phases have been typically detected only by X-ray scattering. The formation of a rotator phase is just one simple example of a solid-solid phase transition and the findings of this work suggest that any first order phase

transition associated with an abrupt change in density (*i.e*., large effective cubical expansion coefficient) can lead to excess attenuation. The ultrasonic attenuation in bulk semi-crystalline fats is exceptionally high and has been attributed to a variety of mechanisms including scattering from voids in the lipid or from elements of crystal microstructure (Singh *et al*. 2002). In melting mixtures of lipids, the SFC typically changes over a broad temperature range with several associated solid-solid transitions that could contribute to the high attenuation often reported (Saggin & Coupland, 2004; Martini *et al*. 2005a, b).

4.1.6 References

1. Dickinson, E. & McClements, D.J. 1995. *Advances in Food Colloids*, Blackie Academic & Professional, New York, NY.
2. Wang, S., Tozaki, K., Hayashi, H., Hosaka, S. & Inaba, H. 2003. Observation of multiple phase transitions in *n*-$C_{22}H_{46}$ using a high resolution and super-sensitive DSC. *Thermochimica Acta*, 408, 31-38.
3. Shinohara, Y., Kawasaki, N., Ueno, S., Kobayashi, I., Nakajima, M. & Amemiya, Y. 2005. Observation of the transient rotator phase of *n*-hexadecane in emulsified droplets with time resolved two-dimensional small- and wide-angle x-ray scattering. *Physics Review Letters*, 94, Art. No. 097801.
4. Montenegro, R. & Landfester, K. 2003. Metastable and stable morphologies during crystallization of alkanes in miniemulsion droplets. *Langmuir*, 19(15), 5996-6003.
5. Oliver, M.J. & Calvert, P.D. 1975. Homogeneous nucleation of *n*-alkanes measured by differential scanning calorimetry. *Journal of Crystal Growth*, 30(3), 343-351.
6. Hammami, A. & Mehrotra, A.K. 1995. Thermal behaviour of polymorphic *n*-alkanes: effect of cooling rate on the major transition temperatures. *Fuel*, 74(1), 96-101.
7. Genovese, A., Amarasinghe, G., Glewis, M., Mainwaring, D. & Shanks, R.A. 2006. Crystallization, melting, recrystallization and polymorphism of *n*-eicosane for application as a phase change material, *Thermochimica Acta*, 443(2), 235-244.
8. Kraack, H., Sirota, E.B. & Deutsch, M.J. 2000. Measurements of homogeneous nucleation in normal-alkanes. *Journal of Chemistry Physics*, 112(15), 6873-85.
9. Sirota, E.B., King, Jr., H.E., Singer, D.M. & Shao, H.H. 1993. Rotator phases of the normal alkanes: an x-ray scattering study. *Journal of Physical Chemistry*, 98(7), 5809-24.
10. McClements, D.J. & Povey, M.J.W. 1987. Solid fat content determination using

ultrasonic velocity measurements. *International Journal of Food Science and Technology*, 22(5), 491-499.

11. McClements, D.J. & Povey, M.J.W. 1988. Comparison of pulsed NMR and ultrasonic velocity techniques for determining solid fat contents. *International Journal of Food Science and Technology*, 23(2), 159-170.
12. McClements, D.J., Povey, M.J.W. & Dickinson, E. 1993. Absorption and velocity dispersion due to crystallization and melting of emulsion droplets. *Ultrasonics*, 31(6), 433-437.
13. Akulichev, V.A. & Bulanov, V.N. 1981. Sound propagation in a crystallizing liquid. *Soviet Physics Acoustics*, 27(5), 377-381.
14. Akulichev, V.A. & Bulanov, V.N. 1983. Crystallization nuclei in liquid in a solid field, *International Journal of Heat and Mass Transfer*, 26(2), 289-300.
15. McClements, D.J. & Fairley, P. 1992. Frequency scanning ultrasonic pulse echo reflectometer, *Ultrasonics*, 30(6), 403-405.
16. Cramp, G.L., Docking, A.M., Ghosh, S. & Coupland, J.N. 2004. On the stability of oil-in-water emulsions to freezing. *Food Hydrocolloids*, 18(6), 899-905.
17. Sirota, E.B. & Herhold, A.B. 1999. Transient phase-induced nucleation, *Science*, 283(5401), 529-532.
18. Vanapalli, S.A., Palanuwech, J. & Coupland, J.N. 2003. Stability of emulsions to dispersed phase crystallization: effect of oil type, dispersed phase volume fraction, and cooling rate. *Colloids and Surfaces A*, 204(1-3), 227-237.
19. Chanamai, R., Coupland, J.N. & McClements, D.J. 1998. Effect of temperature on the ultrasonic properties of oil-in-water emulsions, *Colloids and Surfaces A*, 139(2), 241-250.
20. Saggin, R. & Coupland, J.N. 2002. Measurement of solid fat content by ultrasonic reflectance in model systems and chocolate. *Food Research International*, 35(10), 999-1005.
21. Sirota, E. B. & Herhold, A.B. 1999. Transient rotator phase induced nucleation in *n*-alkane melts. *Polymer*, 41(25), 8781-89.
22. Povey, M.J.W., Hindle, S.A., Aarflot, A. & Hoiland, H. 2006. Melting point

depression of the surface layer in *n*-alkane emulsions and its implications for fat destabilization in ice cream. *Crystal Growth Design*, 6(1), 297-301.

23. Povey, M.J.W. 1997. *Ultrasonic techniques for fluid characterization*. Academic Press, San Diego, CA, 1997.
24. Allegra, J.R. & Hawley, S.A. 1972. Attenuation of sound in suspensions and emulsions: theory and experiments. *Journal of Acoustical Society of America*, 51 (5B), 1545-64.
25. McClements D.J. & Coupland, J.N. 1996. Theory of droplet size distribution measurements in emulsions using ultrasonic spectroscopy. *Colloids and Surfaces A*, 117(1), 161-170.
26. Singh, A.P., McClements D.J. & Marangoni, A.G. 2002. Comparison of ultrasonic and pulsed NMR techniques for determination of solid fat content. *Journal American Oil Chemists` Society*, 79(5), 431-437.
27. Saggin, R. & Coupland, J.N. 2004. Shear and longitudinal ultrasonic measurements of solid fat dispersions. *Journal of American Oil Chemists` Society,* 81(1), 27-32.
28. Martini, S., Bertoli, C., Herrera, M.L., Neeson, I. & Marangoni, A. 2005a. *In situ* monitoring of solid fat content by means of pulsed nuclear magnetic resonance spectrometry and ultrasonics. *Journal of American Oil Chemists` Society,* 82(5), 305-312.
29. Martini, S., Bertoli, C., Herrera, M.L., Neeson, I. & Marangoni, A. 2005b. Attenuation of ultrasonic waves: influence of microstructure and solid fat content. *Journal of American Oil Chemists` Society,* 82(5), 319-328.

4.2 The Effect of Emulsifier Type and Droplet Size on Phase Transitions in Emulsified Even Numbered *n*-Alkanes

Abstract

Phase transitions in emulsified even numbered *n*-alkanes (C_{16}, C_{18} and C_{20}) are studied as a function of droplet size (0.15-3.45 μm) and surfactant type (polyoxyethylene sorbitan monolaurate or caseinate) using microcalorimetry (DSC) and ultrasonic attenuation measurements (2.25 MHz). Two DSC exothermic peaks were observed during the heating of C_{18} and C_{20} emulsions stabilized by Tween 20: a minor peak around 15°C and 25°C respectively, and a major double peak about 10°C higher. I tentatively attribute the minor peak to crystal-rotator phase transition, and the split major peak to melting of the surface and core of the droplets. The C_{16} emulsions showed similar behavior for the major melting peak (15°C), but the minor peak was absent - possibly as the sample was not cooled enough to cause the rotator phase to enter the low temperature crystalline state. For similar sodium caseinate stabilized emulsions of C_{18} and C_{20}, the minor peak was much less pronounced (~25%) which I attribute to the lack of compatibility between the alkane and protein molecules. There were two ultrasonic attenuation peaks for the melting of C_{18} and C_{20} and one for C_{16} corresponding to the DSC peaks. In all cases, the magnitude of the attenuation decreased with increasing particle size. Using an extended scattering theory approach I was able to relate the changes in ultrasonic attenuation to the changes in the effective physical properties of the alkane molecules during melting.

4.2.1 Introduction

The crystallization and melting behavior of the dispersed phase in oil-in-water emulsions has attracted considerable interest both as it is important to the functionality of certain commercial products (*e.g.*, whipped cream) but also as it provides a means to study the basics of nucleation and melting without the complication of crystal growth (Coupland, 2004). Crystallization of emulsified lipids typically requires much more extensive supercooling than the same lipid in bulk, because each droplet must nucleate independently and the influence of heterogeneous catalysts is minimized. For example, Montenegro *et al*. (2003), showed the crystallization temperature of hexadecane in a miniemulsion (218 nm) was 16°C lower than that of the bulk sample, whereas the melting point decreased only slightly (*i.e.*, 0.7°C) (Montenegro & Landfester, 2003). The phase behavior of emulsified lipids is affected by the surfactant present at the oil-water interface. Katsuragi *et al*. (2001) argued that if the hydrophobic portion of a small molecule surfactant is structurally similar to the lipid itself, it may catalyze droplet crystallization. On the other hand, the hydrophobic tails of the surfactant can act as impurities for the lipid adjacent to the surface so reducing its melting temperature and consequently, the fat in fine emulsions sometimes melts in two events at different temperatures (*i.e*., core and surface) (Povey *et al*. 2006).

Normal alkanes are frequently used as model lipids for emulsion crystallization studies as they are readily available over a range of chain lengths to a good degree of purity. Medium chain, even carbon numbered alkanes in emulsions typically crystallize in a triclinic form, although this can be modified by the addition of high-melting, hydrophobic emulsifiers (Ueno, 2003). However, in recent work I used temperature scanning microcalorimetry to identify a small thermal event occurring about 12°C below the major melting/crystallization peak of emulsified octadecane (Chapter 4.1). I tentatively attributed this to the melting/formation of a rotator phase as an intermediate between the high temperature liquid and low temperature

crystal. A rotator phase is defined as lamellar crystals "which exhibit long-range order in the molecular axis orientation and center-of-mass position but lack rotational degrees of freedom of the molecules about their long axis" (Kraack *et al*. 2000). There was also an excess ultrasonic attenuation on heating the octadecane emulsions associated with the crystal-rotator and rotator-liquid phase transitions (Chapter 4.1). As the droplets melt, their effective specific heat and thermal expansion coefficient are instantaneously very high as they include contributions from the enthalpy of fusion and changing solids content respectively. By incorporating these terms into scattering theory, it was possible to model the excess attenuation during melting.

In the present work, I extend this investigation to consider a wider range of emulsion samples prepared with different surfactants (*i.e*., one protein, one small molecule surfactant), oils (*i.e.*, three different *n*-alkanes), and particle sizes. I combine sensitive microcalorimetric measurements of the enthalpy transitions in the samples with ultrasonic attenuation measurements. My aims are to identify the factors affecting the small transition attributed to the rotator phase as well as the main melting and crystallization events and to demonstrate excess ultrasonic "melting" attenuation in a wider range of samples.

4.2.2 Materials and Methods

Materials and Sample Preparation. *n*-Octadecane (C_{18}) and *n*-Eicosane (C_{20}) were obtained from Alfa Aesar (99% purity). Tween 20 (polyoxyethylene sorbitan monolaurate, W929150-1) and sodium caseinate were purchased from Aldrich Chemical Company. *n*-Hexadecane (C_{16}) was obtained from Fisher Scientific Company. The alkane (3 wt%) was mixed with a Tween 20 (1 wt%) or sodium caseinate (0.5% wt) solution in a high speed blender (Kinematica GmbH FT10/35, Brinkmann Instruments, Switzerland) to prepare a coarse emulsion which was further homogenized using a two-stage valve homogenizer (1-5 passes, 200 to 600 bar, 10% of which was maintained over the second stage, Niro-Soavi Panda, Model no: 3344, Parma, Italy). In order to keep the oil in a liquid state for homogenization, the equipment was preheated with hot water prior to use. The particle size distribution of the emulsions was characterized by static light

scattering (Horiba LA-920, Irvine, CA, USA) after appropriate dilution. The emulsions were stable over the course of the experiment (i.e., no change in particle size, no visible phase separation) and were not destabilized by the cooling-heating cycles.

Ultrasonic Measurements. The ultrasonic attenuation of the emulsions was measured as a function of temperature using a modified pulse-echo technique. An electrical spike signal (Panametrics 500 PR, Waltham, MA, USA) was passed to a broadband ultrasonic transducer (2.25 MHz center frequency, Panametrics, Waltham MA), which converted the energy to ultrasound. The pulse of sound traveled into a Plexiglas delay line, and was partially reflected at the plastic-sample interface. The reflected part of the signal returned through the delay line to the transducer (echo 1) and the transmitted part traveled through the sample (~1 cm), was reflected from the brass plate and returned through the sample and the delay line to the transducer (echo 2). The transducer reconverted the acoustic signal to an electrical signal which was stored for analysis with a digital oscilloscope (LeCroy 9310c, Chestnut Ridge, NY, USA). The time and energy difference between echo 1 and echo 2 were used to calculate the speed of sound and attenuation of the sample.

Aliquots (~20 ml) of C_{16}, C_{18}, and C_{20} emulsions were poured into the ultrasonic measurement cell at 30, 35, and 45°C, respectively, and held for 30 minutes, then cooled to 0°C at 6°C.hr^{-1} and measurements were taken at each integer °C. Additional measurements were taken to increase the resolution of the ultrasonic data around the attenuation peaks. To ensure complete crystallization before the heating cycle, the C_{16} samples were held at -5°C and the C_{18} and C_{20} emulsions at 0°C for 30 minutes before reheating at the same rate to the starting temperature. The aqueous phase of the emulsions did not freeze under these conditions.

Differential Scanning Calorimetry. The crystallization and melting thermograms were measured using differential scanning calorimetry (VP-DSC, Microcal, Northampton, MA). Samples were diluted to 0.25 wt% lipid with water prior to analysis so that the signals were within the range of the instrument. Samples (513.1 μl) were run against a similar reference cell filled with water. C_{16}, C_{18}, and C_{20} samples were heated to 30, 35, 45°C, respectively, held for 30 minutes, and cooled to 0.5°C at 10 °C/hr then held for a further 30 min and reheated at the same rate to 30, 35,

and 45°C for C_{16}, C_{18}, and C_{20} samples. The heat capacity data for the water-water scan was subtracted from the sample runs to measure the heat flux due to changes in the lipid phase. In preliminary experiments, I showed that Tween 20 and sodium caseinate solutions did not exhibit any measurable transitions over this range.

4.2.3 Results and Discussion

Melting Thermograms. The melting behavior of coarse (d_{32}=3.45 μm), intermediate (d_{32}=0.45 μm) and fine (d_{32}=0.15 μm) emulsions of C_{16}, C_{18} and C_{20} stabilized by Tween 20 were monitored by microcalorimetry (Figure 4.2.1). There was a single, large endothermic peak corresponding to the melting of C_{16} whose maximum increased with droplet size (*i.e.*, 16.9, 17.3, and 17.7°C for fine, intermediate, and coarse emulsions respectively, Figure 4.2.1a). Various authors (Montenegro *et al*. 2003; Montenegro & Landfester, 2003) have noted a small increase in melting temperature with droplet size and this is usually attributed to a reduction in surface curvature and crystal structure. The peak for the larger droplets was larger, and occurred over a narrower temperature range while the finer droplets had broader melting peaks preceded by a smaller maximum at approximately 15°C. My observations are similar to those reported for *n*-hexadecane and *n*-octadecane miniemulsions (Montenegro *et al*. 2003; Montenegro & Landfester, 2003). Various workers (*e.g.*, Povey *et al*. 2006) have suggested that there are two populations of lipid in an emulsion droplet. The lipid closest to the surface would be mixed with the alkyl tails of the surfactant and have a lower melting point (corresponding to the minor peak in DSC) while the remaining core lipid is effectively pure and would melt at a higher temperature (corresponding to the major peak in the DSC). I suggest that the minor peak seen here corresponds to the surface lipid and has a lower melting point while the large peak corresponds to the purer lipid in the core of the droplets. In smaller droplets there is a higher proportion of the lipid at the surface, so the ratio of the size of the smaller to larger peak increases.

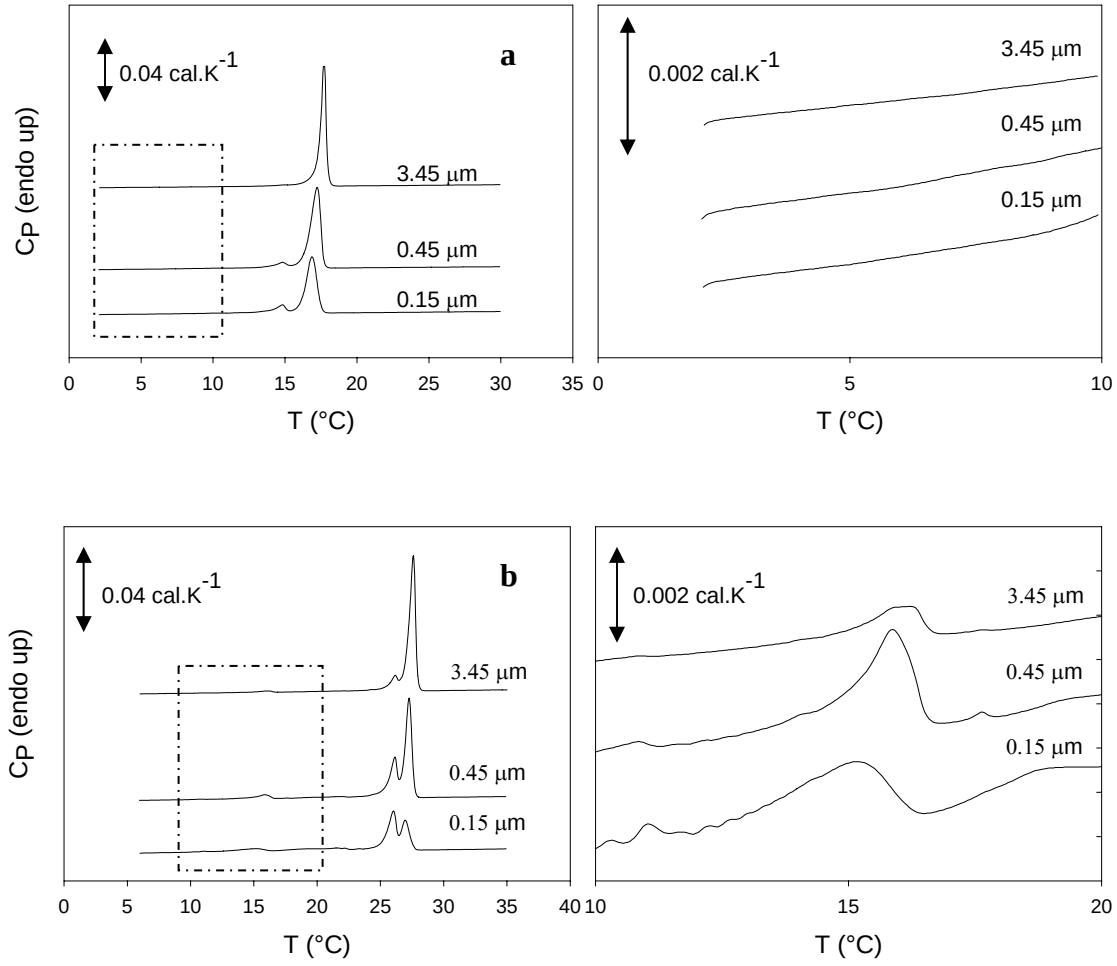

Figure 4.2.1. Heating thermograms for 0.25% emulsions of (a) C_{16}, (b) C_{18}, (c) C_{20} stabilized by 1% Tween 20 recorded at a scanning rate of 10 °C/hr. The figures to the right are higher resolution zooms of the boxed area of the main, data sets shown on the left.

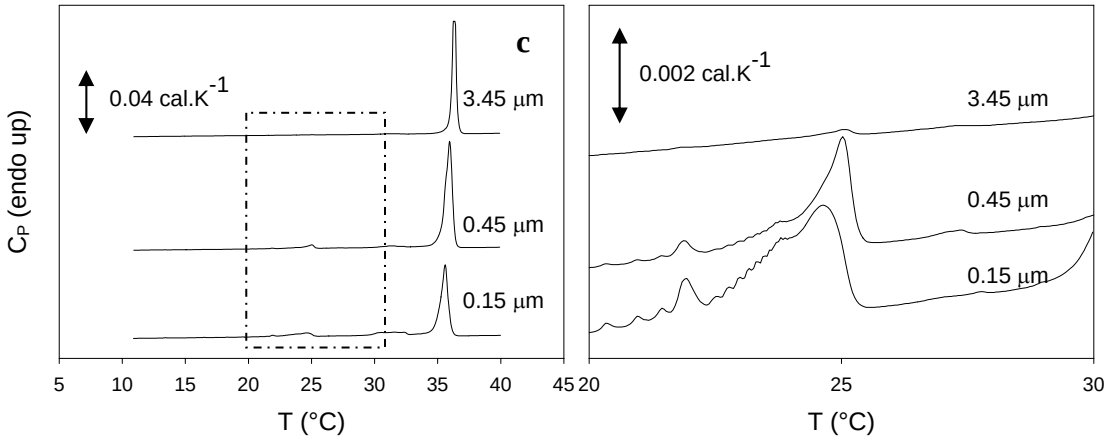

Figure 4.2.1 (continued)

The C_{18} droplets melted at a higher temperature than the C_{16} droplets because of the stronger intermolecular forces between the larger alkanes (Figure 4.2.1b). However, similar trends were seen in the data, *i.e.*, a single bimodal melting peak with the proportion of the enthalpy in the lower-temperature peak decreasing with increasing droplet size). The Tween-stabilized C_{20} droplets melted at still higher temperatures, but in this case, the minor peak was less pronounced (Figure 4.2.1c).

In the sodium caseinate stabilized emulsions (Figure 4.2.2), the major melting peak occurred at a similar temperature to the corresponding Tween-stabilized emulsions, but there was only a single peak rather than the bimodal peak seen with Tween-stabilized emulsions. This is consistent with my hypothesis that the minor peak in the Tween-stabilized emulsions is due to the lipid mixed with surfactant alkyl groups. Proteins lack the long hydrophobic chains of surfactant and sodium caseinate is known to have little effect on the crystallization properties of lipid droplets (Skoda & van den Tempel, 1963; Palanuwech & Coupland, 2003). Consequently, in the caseinate stabilized emulsions there is only one population of lipid and a single DSC peak. The end point temperature for the melting of the emulsion samples was not influenced by the

type of surfactant used and in each case was close to the tabulated values of the thermodynamic melting points (Gallant & Yaws, 1993).

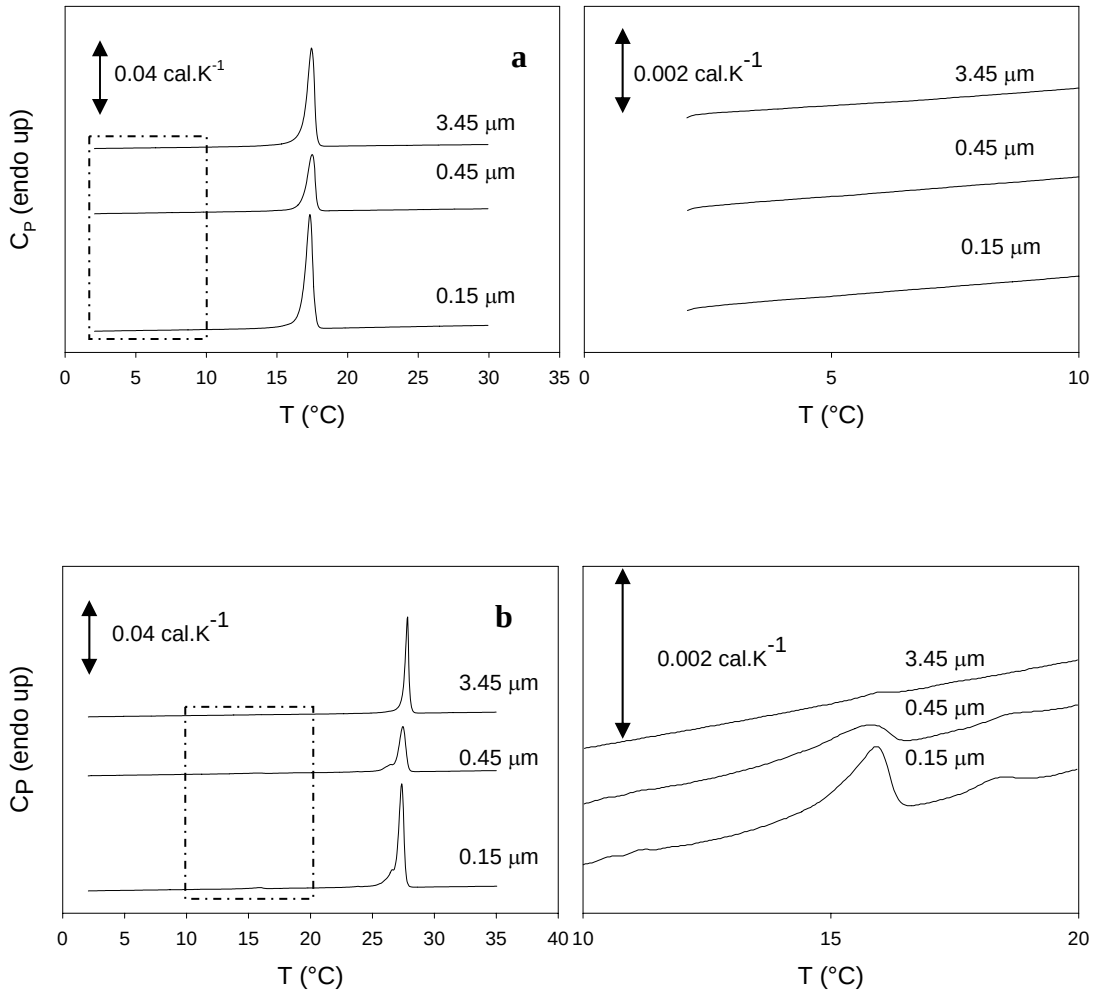

Figure 4.2.2. Heating thermograms for 0.25% emulsions of (a) C_{16}, (b) C_{18}, (c) C_{20} stabilized by 0.5% sodium caseinate recorded at a scanning rate of 10 °C/hr. The figures to the right are higher resolution zooms of the boxed area of the main, data sets shown on the left.

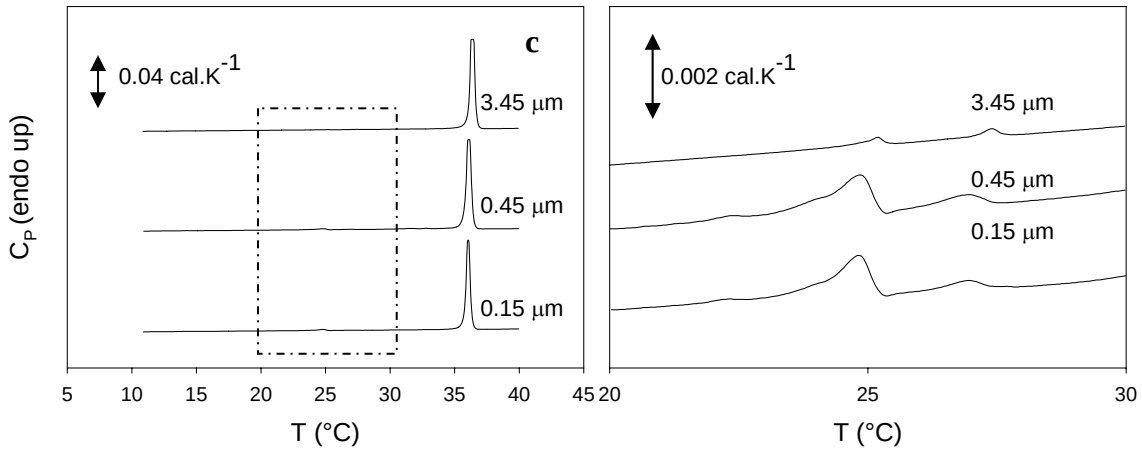

Figure 4.2.2 (continued)

There was a second, minor endothermic peak for the Tween stabilized C_{18} and C_{20} droplets at around 15°C and 25°C respectively (Figure 4.2.1b and 4.2.1c). The peak was detectable but much smaller in the corresponding caseinate-stabilized droplets and occurred at a similar temperature in each case (Figure 4.2.2). No corresponding minor peak was seen in the C_{16} emulsions. To increase the resolution of this small peak I repeated the experiments with more concentrated emulsions (5 wt% C_{18} or C_{20}, d_{32} = 0.52 μm) (Figure 4.2.3). (Because more of the lipid was going through the transition in this case it was possible to resolve greater detail although it was not possible to simultaneously measure the major peak due to limitations in the dynamic range of the instrument.)

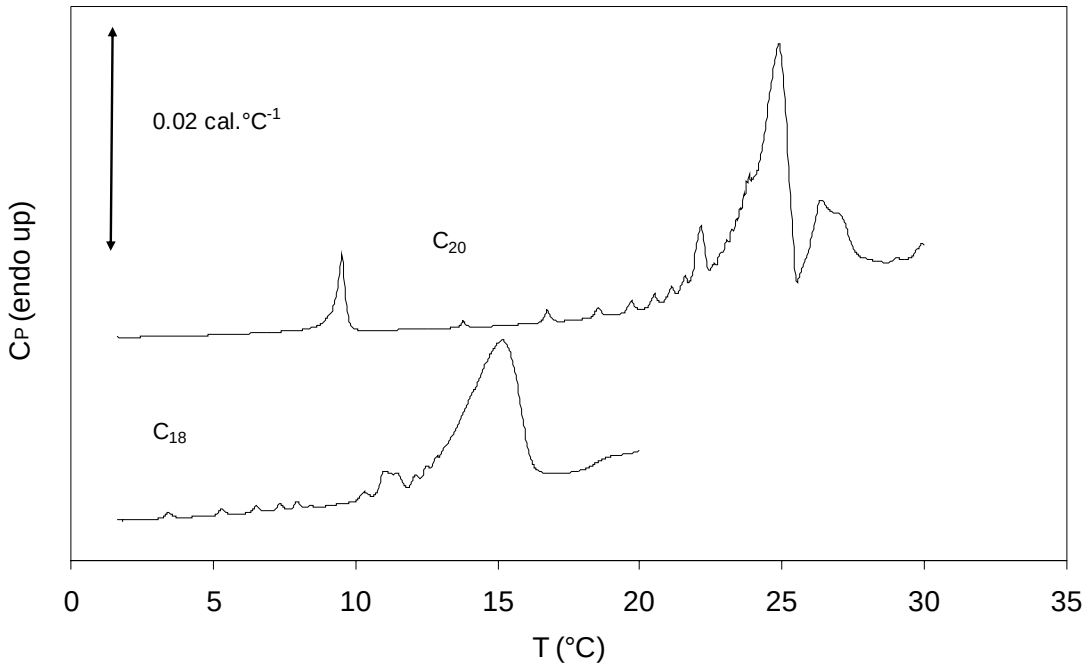

Figure 4.2.3. Heating thermograms for 5% emulsions of C_{18}, C_{20} stabilized by 1% Tween 20 (d_{32} = 0.52 μm) recorded at a scanning rate of 10 °C/hr. Data are similar to Figure 4.2.1, but the more concentrated emulsion reveals detail of the crystal-rotator transition.

Because the position of the minor peak approximately corresponded to the major melting endotherm of the next smaller even *n*-alkane used, I initially suspected it could be due to the presence of a contaminant. However, mixtures of similarly-sized alkanes (*i.e.*, C_{16} and C_{18} and C_{18} and C_{20}) co-crystallize with a melting point between the melting points of the pure components and not as independent phases (data not shown). I therefore attribute the minor peak to a solid-solid phase transition, and tentatively attribute it to the melting of a crystal phase (probably triclinic according to Montenegro & Landfester, 2003) to form a rotator phase. A rotator phase has been previously observed in these alkanes as an intermediate between the liquid and crystalline phases (Sirota, & Herhold, 1999, 2000). Montenegro and Landfester (2003) used X-ray diffraction to show that transition from the stable crystalline phase to the rotator phase occurred at 15.3°C for C_{18} emulsions (d=125 nm), and at 24.1°C for C_{20} emulsions (d=129 nm). The end points of the thermal transitions reported here occurred at similar temperatures (17°C

and 26°C) respectively, despite the slower scanning rate (10°C hr^{-1} against the 300°C hr^{-1} used by Montenegro & Landfester, 2003). Sirota and Herhold (1999, 2000) used a comparable scanning rate to the one used here (*i.e.*, 3°C hr^{-1}) in their X-ray studies of rotator phase formation in bulk alkanes, however in that work the phase transitions occurred at 27°C and 32°C respectively. Montenegro and Landfester (2003) did not observe a rotator phase for bulk or emulsified C_{16}.

Ueno and co-workers (2003) saw a similar minor DSC peak a few degrees below the major crystallization/melting peak in emulsified *n*-hexadecane (φ=20%, 0.9 μm; octadecane and eicosane were also studied but the data were not reported) stabilized by 1% Tween 20 but only in the presence of a hydrophobic additive. Alkanes typically crystallize in the triclinic form but the additive favored alternative crystal habits and, using coupled X-ray measurements, these authors were able to attribute the minor peak to a polymorphic phase transition. They saw no evidence of a rotator phase, perhaps because their scanning rate was relatively fast (2°C min^{-1}) or due to a lack of sensitivity in their measurement apparatus. I do not believe the polymorphic phase transition detected by Ueno *et al*. (2003) is responsible for the minor peak in my work as although I used the same lipid and surfactant I did not use the additive.

Cooling Thermograms. Cooling thermograms for C_{18} and C_{20} are shown in Figure 4.2.4 and 4.2.5 for Tween 20 and sodium caseinate stabilized samples respectively. (Because C_{16} has a crystallization onset of approximately 2°C, and the microcalorimeter used cannot safely be cooled below 0°C, the main crystallization peak could not be observed fully using this apparatus and is not reported here. However, by holding all samples for 30 minutes at 0.5°C I am confident that the C_{16} droplets were completely crystallized prior to beginning the heating cycle.) In most respects, the patterns seen in melting were repeated in reverse on cooling. As expected, there was an offset of about 10-15°C between the melting and crystallization points of the emulsified lipids because the finely dispersed oil must largely nucleate homogeneously (Dickinson & McClements, 1995). Interestingly, there was a small peak in the large caseinate stabilized C_{20} droplets close to the melting point of the fat (*i.e.*, less supercooling). This is probably because a significant fraction of the largest droplets contained a nucleation catalyst and

therefore could nucleate heterogeneously at a higher temperature (Palanuwech & Coupland, 2003).

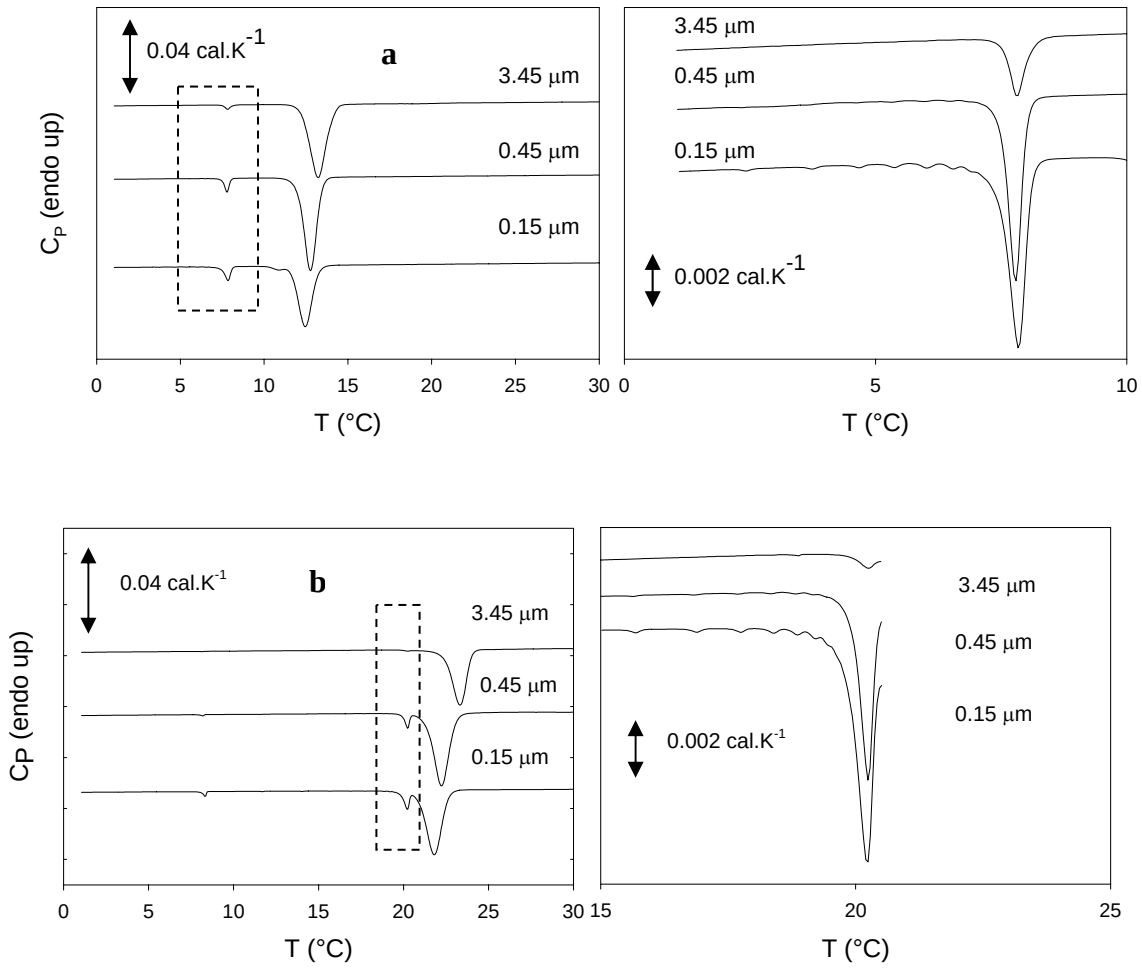

Figure 4.2.4. Cooling thermograms for 0.25% emulsions of (a) C_{18}, (b) C_{20} stabilized by 1% Tween 20 recorded at a scanning rate of 10 °C/hr. The figures to the right are higher resolution zooms of the boxed area of the main, data sets shown on the left.

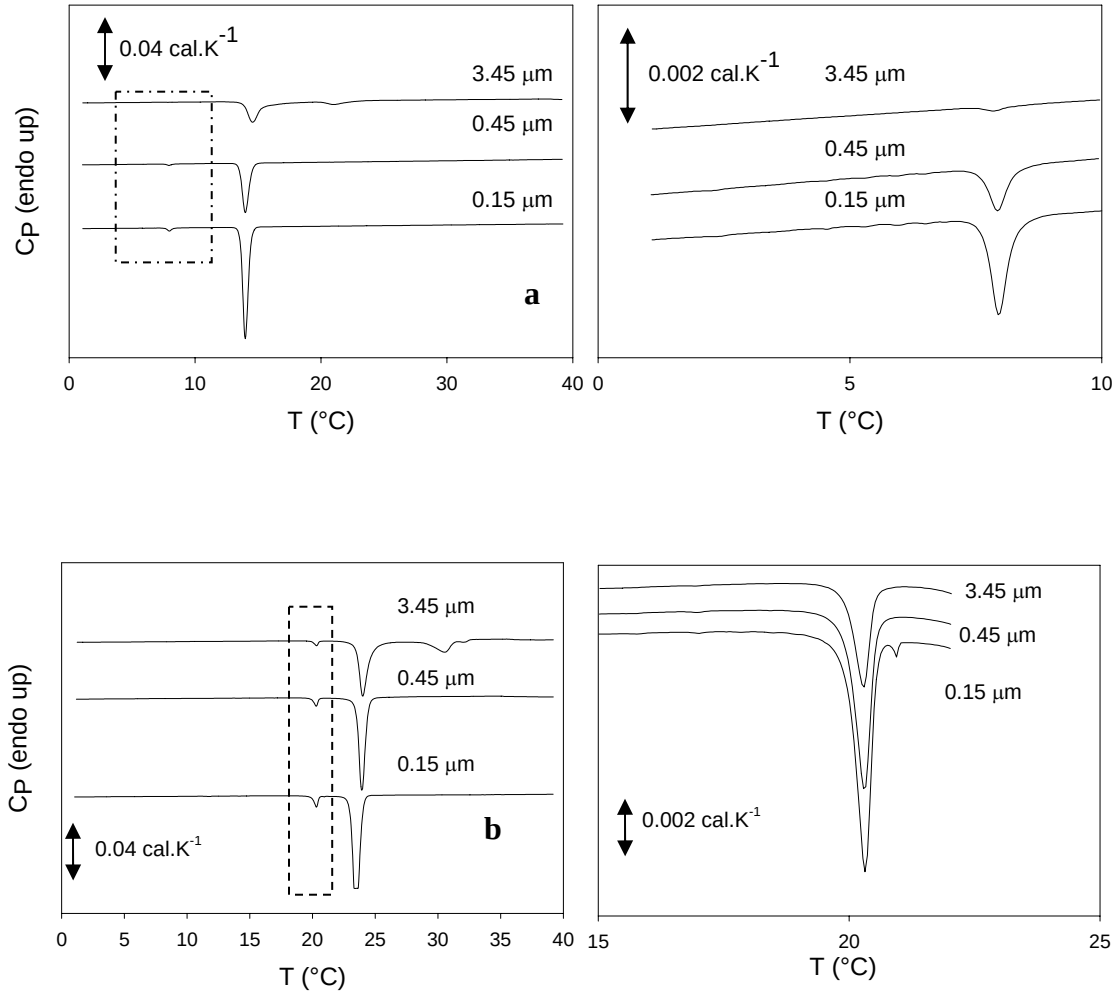

Figure 4.2.5. Cooling thermograms for 0.25% emulsions of (a) C_{18}, (b) C_{20} stabilized by 0.5% sodium caseinate recorded at 10 °C /hr. The figures to the right are higher resolution zooms of the boxed area of the main, data sets shown on the left.

The caseinate stabilized droplets crystallize about 1°C above the corresponding Tween stabilized droplets (Figures 4.2.4 & 4.2.5). This may be related to my earlier suggestion that the hydrophobic tails of the Tween act as an impurity in the oil and depress its crystallization temperature. However, perhaps due to differences in cooling rate, this observation is different from those of Skoda and Van den Tempel (1963) and Palanuwech and Coupland (2003) who noted that Tween-stabilized emulsions tended to crystallize at higher temperatures than caseinate-stabilized droplets.

In some Tween-stabilized emulsions (notably C_{20} but also C_{18}) there was a small shoulder approximately 1.5°C after the major crystallization peak. This minor peak was not identified in earlier studies perhaps due to the superior sensitivity of the instrument used here and the slow heating rates. I suggest that this small peak corresponds to the freezing of the surface monolayer where freezing temperature was depressed due to the protrusion of Tween alkyl chains. Despite this, most of the main crystallization peaks were unimodal, presumably because due to the deep supercooling, once crystallization had been initiated it rapidly spread throughout the droplet. Increasing particle sizes reduced the relative significance of this minor peak because of a reduction in surface: volume ratio of the lipid.

There was a smaller exothermic peak approximately 4-6 °C below the major peaks for all samples (Figure 4.2.4 and 4.2.5). The position of the peak was unaffected by the type of surfactant or the droplet size but the size of the peak decreased with increasing droplet size (and was largely absent in the largest droplets). These minor peaks were larger for the Tween-stabilized emulsions than for the caseinate-stabilized emulsions. This can mostly be attributed to the interactions between the emulsifier and oil molecules. Increasing surface area can be expected to increase the extent of these interactions. The symmetry between the properties of this peak and the properties of the minor endotherm seen on heating, leads us to attribute it to a rotator-crystal phase transition. I hypothesize that the major peak is a liquid to rotator phase transition and the minor peak is a rotator to crystal transition. It is a possibility that the absence of a minor crystal-rotator phase transition on heating C_{16} droplets is not an intrinsic property of the smaller lipid but rather because I was not able to cool those samples far enough to convert

them into the low temperature crystal form. In Figure 4.2.6, I present a DSC melting scan (10 to 35°C) for an octadecane sample. Small droplets (d_{32} = 0.2 μm) were selected to make any minor peaks more pronounced. Since the sample was not cooled below the rotator phase transition temperature (approximately 7.8°C), no rotator phase transition peak was observed. Previously, Shinohara *et al.* (2005) noted that hexadecane droplets (mean size 32.6 μm) crystallize into the triclinic phase through the transient rotator phase. Their results were slightly different than that of mine, since rotator to triclinic phase transitions in my DSC measurements were always characterized with a separate minor peak rather than a small shoulder within the major DSC peak (*i.e.*, no surface freezing). Due to instrumental limitations, I was unable to observe the rotator phase transitions in hexadecane emulsions. Extrapolating from the larger lipids I expect the rotator to crystal transition in the C_{16} would occur between about -5 to -10°C. This difference could be in part be explained by the difference in particle size.

Ultrasonic Attenuation Measurements. Ultrasonic attenuation (at 2.25 MHz) of *n*-alkane emulsions stabilized with Tween 20 and sodium caseinate were measured as a function of temperature during heating (Figure 4.2.7 and 4.2.8) and cooling (data not reported). The attenuation coefficient of the emulsions with larger droplets (*i.e.*, 3.45 μm) was low (<10 $Np.m^{-1}$) and could not be reliably measured by this technique so the data are not reported. The attenuation of solid and liquid droplets was largely temperature independent and unaffected by the nature of the interfacial material. Importantly there were excess attenuation peaks during heating at temperatures corresponding to the major and minor melting peaks seen in the DSC thermograms (Figures 4.2.1 and 4.2.2). The maximum peak attenuation was always the lowest in the largest droplets and was always less in the caseinate-stabilized emulsions compared to the Tween-stabilized emulsions. There were no peaks corresponding to the crystallization of the emulsion droplets on cooling (data not shown).

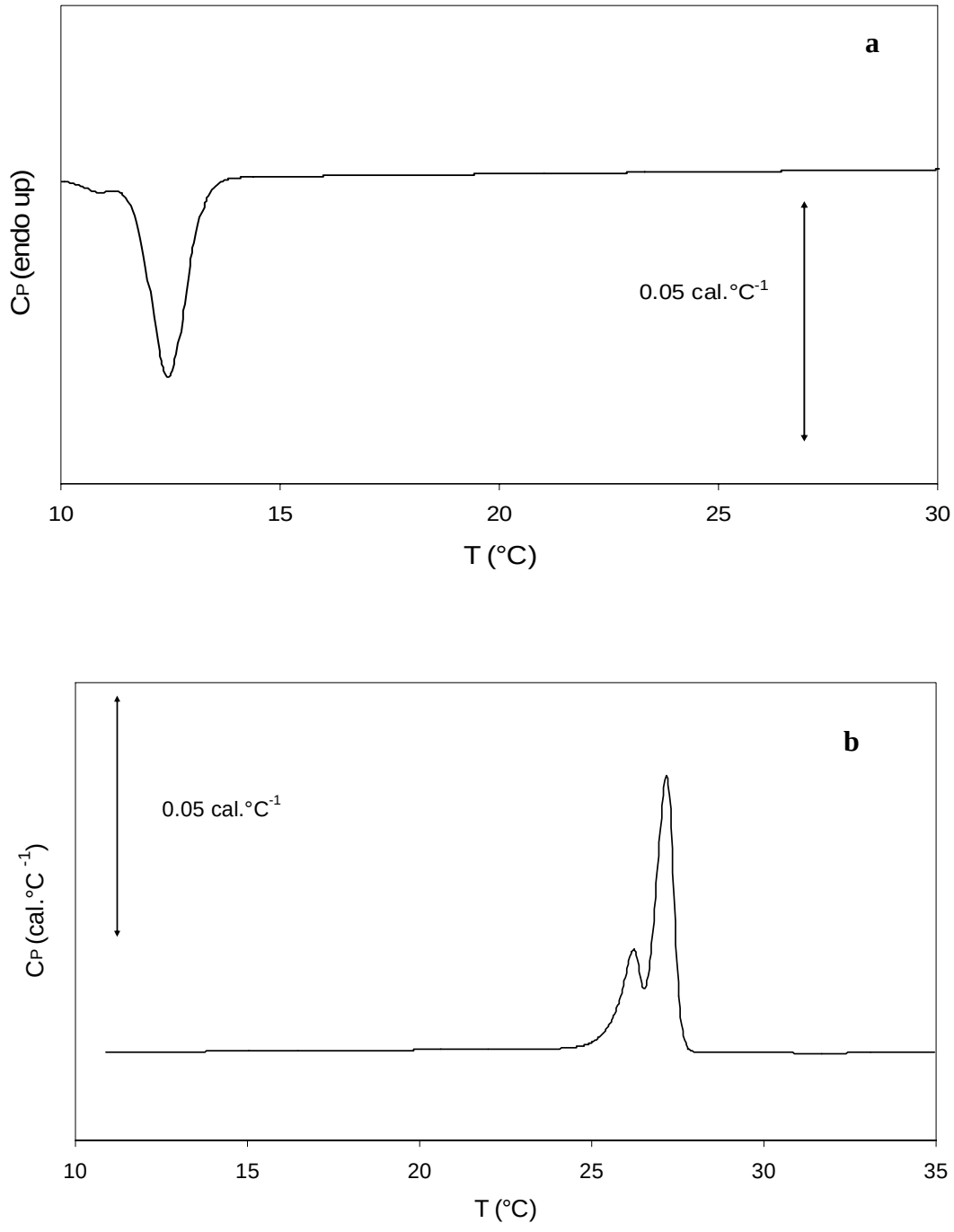

Figure 4.2.6. Thermograms of a 0.25% C_{18} emulsion of by 1% Tween 20 (d_{32} = 0.2 μm). Samples were (a) cooled to 10°C at 10 °C/hr then (b) reheated to 35°C at the same rate.

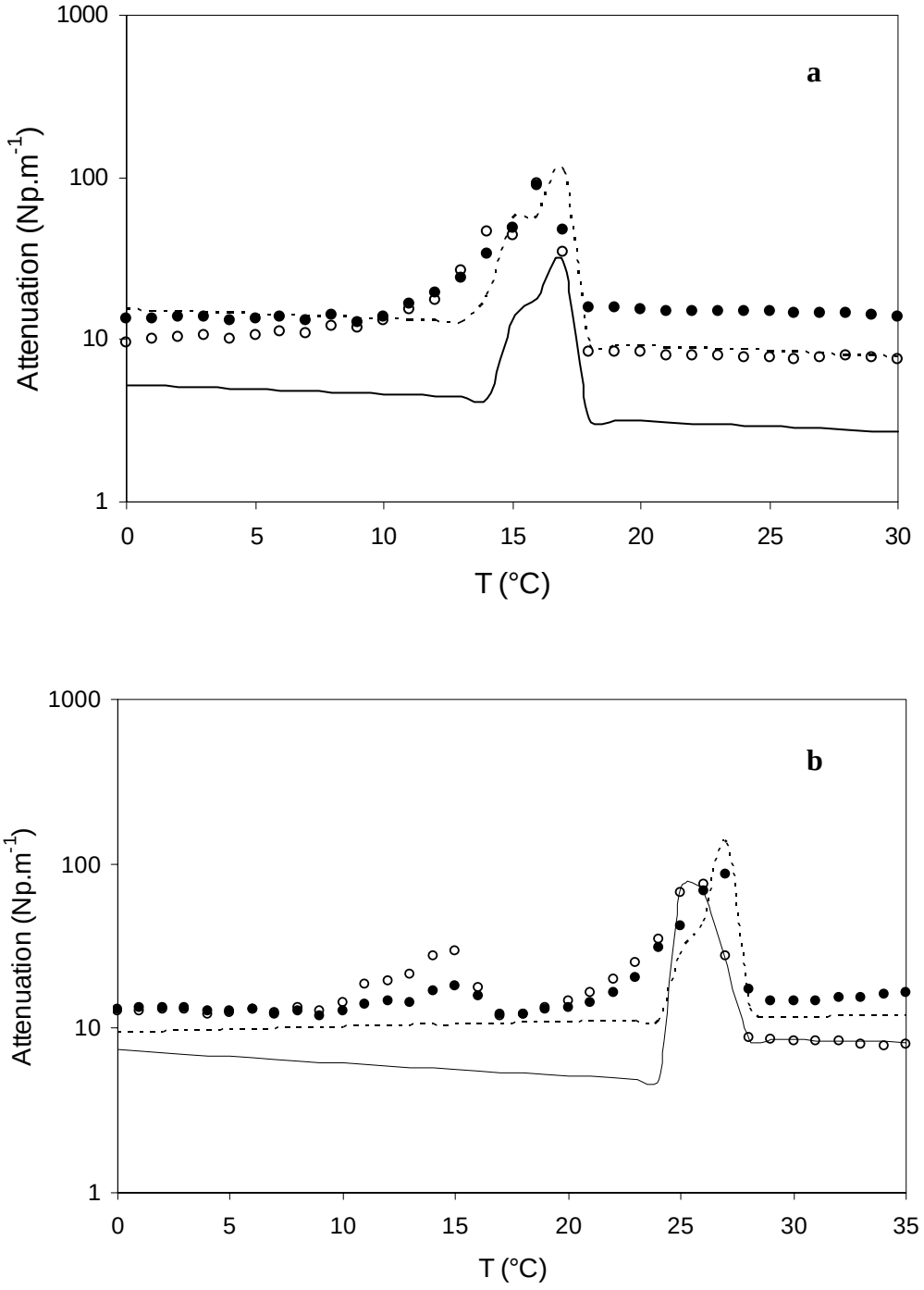

Figure 4.2.7. Ultrasonic attenuation as a function of temperature during heating (6 °C/hr) of 3% emulsions (○: 0.15 μm, ●: 0.45 μm) of (a) C_{16}, (b) C_{18}, (c) C_{20} stabilized by 1% Tween 20. Lines represent predictions from scattering theory (see text for details). Broken lines are used for 0.15 μm samples, solid lines are used for 0.45 μm samples.

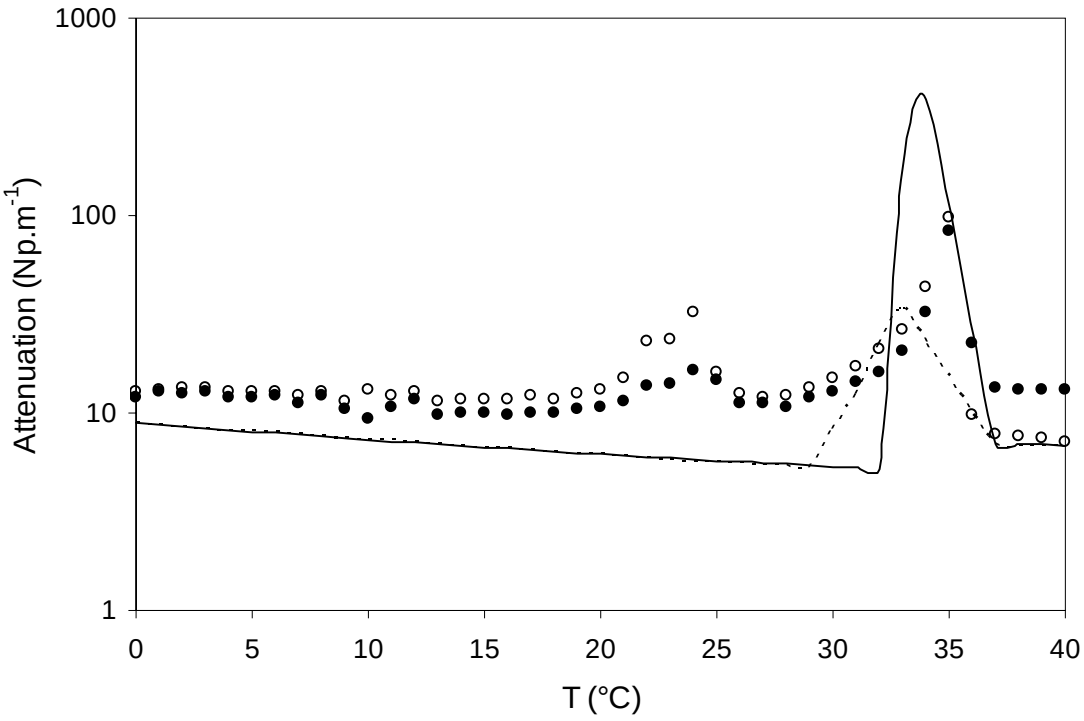

Figure 4.2.7 (continued)

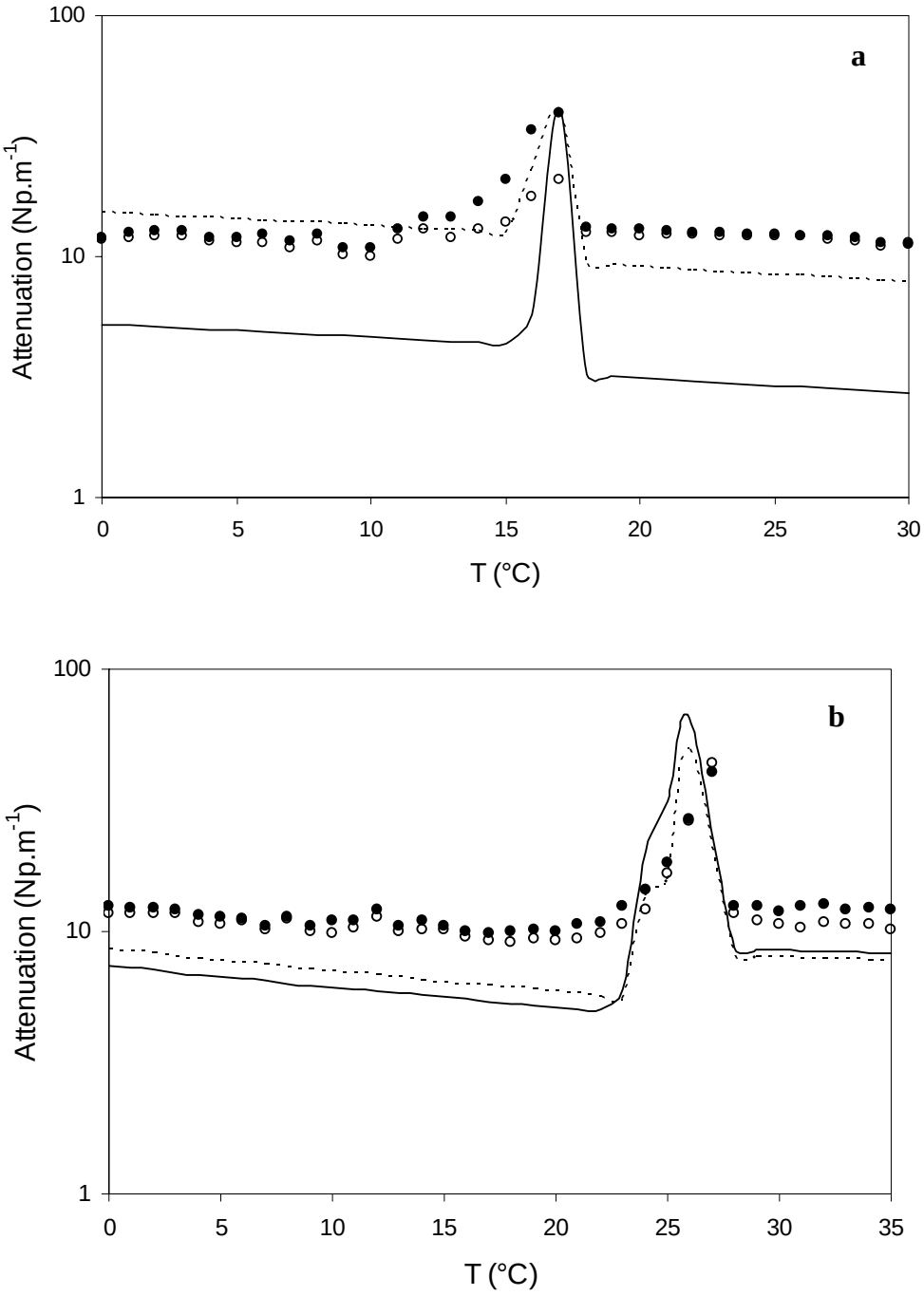

Figure 4.2.8. Ultrasonic attenuation as a function of temperature during heating (6 °C/hr) of 3% emulsions (○: 0.15 μm, ●: 0.45 μm) of (a) C_{16}, (b) $C_{18,}$ (c) C_{20} stabilized by 0.5% sodium caseinate. Lines represent predictions from scattering theory (see text for details). Broken lines are used for 0.15 μm samples, solid lines are used for 0.45 μm samples.

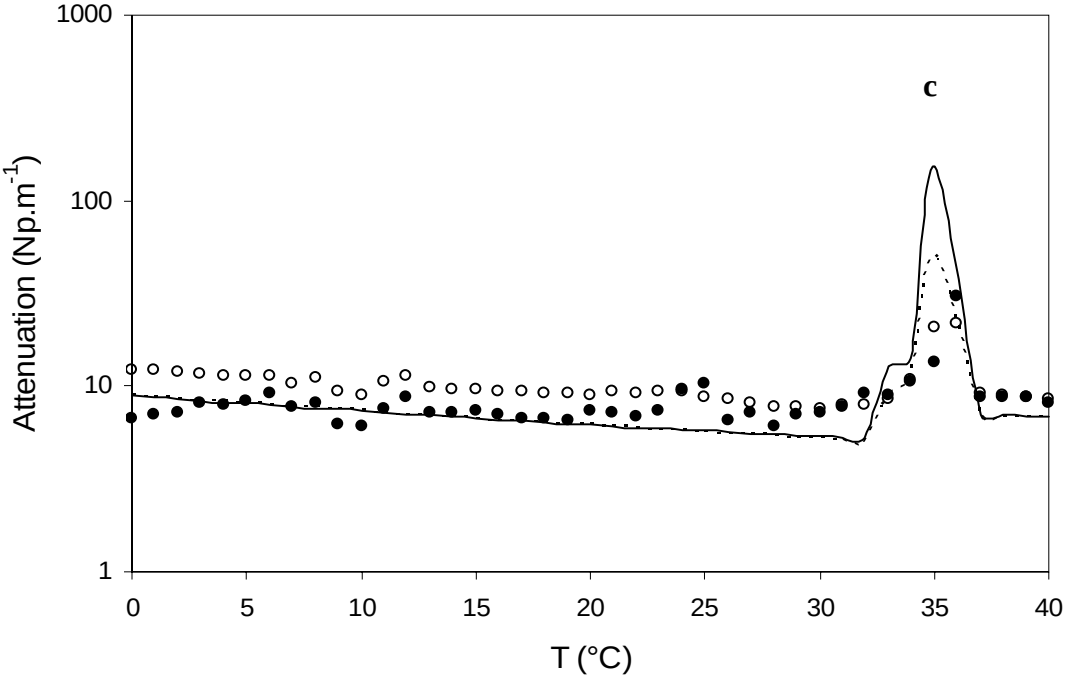

Figure 4.2.8 (continued)

The measured ultrasonic attenuation of an emulsion has contributions from the intrinsic attenuation of the component phases and from scattering by the droplets. The droplets pulsate and oscillate in the passing pressure wave, scattering sound in different directions and converting a proportion of the ultrasonic energy to heat as the droplet movement is not elastic. Good theoretical expressions have been developed for all of these terms and it is possible to predict the ultrasonic properties of an emulsion as a function of the physical properties of the component phases and the size and number of droplets (McClements & Coupland, 1996). Ultrasonic attenuation (unlike ultrasonic velocity) is only slightly affected by changes in temperature and even though the physical properties of solid and liquid droplets are different, ultrasonic attenuation is typically only slightly affected by droplet melting (*i.e.*, < 2 $Np.m^{-1}$). However, during the phase transition the changing solid fat content means the instantaneous specific heat of the lipid phase is very much higher as it now includes a contribution from the enthalpy of fusion. By incorporating an effective value of specific heat (and by a similar logic density and

thermal expansion coefficient) into scattering theory, I have been able to model the attenuation peaks seen during the melting of Tween stabilized *n*-octadecane emulsions (Chapter 4.1). Corresponding attenuation peaks are not seen during crystallization as the droplets are deeply supercooled before nucleation so crystallization is complete before a measurement can be made. I use the same theory here to model the attenuation during due to the melting of a larger set of emulsions including a variety of *n*-alkanes (C_{16}, C_{18}, and C_{20}), droplet sizes (0.15, and 0.45 μm) and emulsifying agents (Tween 20 and sodium caseinate). My theory shows reasonable agreement with the experimental data for all of these systems (Figure 4.2.7 and 4.2.8).

The Tween-stabilized droplets had a higher excess attenuation on melting than the corresponding caseinate droplets. The excess attenuation observation is primarily due to the co-existence of solid and liquid alkane molecules in the droplets. I argued from my DSC data that there is evidence that the surface lipid in the Tween-stabilized emulsion is mixed with the alkyl tails of the surfactant and tends to remain liquid over a wider temperature range and this phenomenon could also be responsible for the greater attenuation in these samples. Furthermore, the peaks are larger for smaller droplets where the proportion of the lipid affected by the interface is greater.

A similar attenuation peak was observed at the temperatures where the crystalline phase converted to a rotator phase as the melting enthalpy needed for the crystal-rotator transition and the density differential between the phases contributes to the increased attenuation of the samples. The attenuation peak is again larger for the Tween-stabilized samples than for the caseinate-stabilized samples and increased with decreasing particle size.

4.2.4 Conclusions

In the present work, I used microcalorimetry and ultrasonic attenuation measurements to investigate the thermal transitions in emulsified alkanes during cooling and heating as a function of alkane chain length, surfactant type and droplet size. The significant conclusions of this work are that (i) alkane droplet crystallization and melting is a two-step process proceeding via an intermediate, probably rotator, phase, (ii) there is an excess ultrasonic attenuation during droplet melting that decreases with increasing droplet size, and this finding is coherent with my extended scattering theory approach, (iii) surfactant molecules can act as crystal modifiers or stabilizers during the crystallization and melting of emulsified lipids, and affect the magnitude of the thermal transitions and excess ultrasonic attenuation.

Although my measurements are of emulsions of simple alkanes, the physical transformations in the lipid responsible for the excess attenuation will also occur in more complex, lipid-continuous systems such are margarine and chocolate. Semi-crystalline lipids such as these frequently have unexpectedly high ultrasonic attenuation (McClements *et al*. 1993) and while this can be attributed by scattering from the structural elements, it seems reasonable that the excess attenuation described here could also contribute. If this is the case, I would expect fats with a broad melting curve (*e.g*., milkfat in butter) would have a lower excess attenuation than those with a steeper melting curve (*e.g*., cocoa butter in chocolate) at a similar solids level. Solid fat content can be calculated from ultrasonic velocity measurements using a volume-weighted average of the properties of the solid and liquid phases but ultrasonic attenuation, while easily measured simultaneously, is not often used in these sensors (McClements & Povey, 1987). If the excess attenuation theory described here can be validated for complex, lipid continuous samples it may be possible to combine velocity and attenuation measurements to give a more complete ultrasonic characterization of semicrystalline lipids.

Furthermore, as originally suggested by McClements *et al*. (1993), the dynamics of melting can be determined from the frequency dependence of attenuation data.

Acknowledgement. The project was supported by the National Research Initiative of the USDA Cooperative State Research, Education and Extension Service, grant number 2003-35503-13852.

4.2.5 References

1. Coupland, J.N. 2004. Crystallization in emulsions. *Current Opinion in Colloid Interface Science*, 7(5-6), 445-450.
2. Montenegro, R., Antionetti, M., Mastai, Y. & Landfester, K. 2003. Crystallization in miniemulsion droplets. *Journal of Physical Chemistry B*, 107(21), 5088-94.
3. Montenegro, R. & Landfester, K. 2003. Metastable and stable morphologies during crystallization of alkanes in miniemulsion droplets. *Langmuir*, 19(15), 5996-6003.
4. Katsuragi, T., Kaneko, N. & Sato, K. 2001. Effects of addition of hydrophobic sucrose fatty acid oligoesters on crystallization rates of *n*-hexadecane in oil-in-water emulsions. *Colloids and Surfaces B*, 20(3), 229-237.
5. Povey, M.J.W., Hindle, S.A., Aarflot, A. & Hoiland, H. 2006. Melting point depression of the surface layer in *n*-alkane emulsions and its implications for fat destabilization in ice cream. *Crystal Growth and Design*, 6(1), 297-301.
6. Ueno, S., Hamada, Y. & Sato, K. 2003. Controlling polymorphic crystallization of *n*-alkane crystals in emulsion droplets through interfacial heterogeneous nucleation. *Crystal Growth and Design*, 3(6), 935-939.
7. Kraack, H. Sirota, E.B. & Deutsch, M.J. 2000. Measurements of homogeneous nucleation in normal-alkanes. *Journal of Chemical Physics*, 112(15), 6873-85.
8. Skoda, W. & van den Tempel, M. 1963. Crystallization of emulsified triglycerides. *Journal of Colloid Science*, 18(6), 568-584.
9. Palanuwech, J. & Coupland, J.N. 2003. Effect of surfactant type on the stability of oil-in-water emulsions to dispersed phase crystallization. *Colloids and Surfaces A*, 223(1), 251-262.
10. Gallant, R.W. & Yaws, C.L. 1993. Physical properties of hydrocarbons and other chemicals,

vol.3. Gulf Publishing Company, Houston, TX.

11. Sirota, E.B. & Herhold, A.B. 2000. Transient rotator phase induced nucleation in *n*-alkane melts. *Polymer*, 41(25), 8781-89.
12. Sirota, E.B. & Herhold, A.B. 1999. Transient phase-induced nucleation. *Science*, 283 (5401), 529-532.
13. Dickinson, E. & McClements, D.J. 1995. Advances in Food Colloids. Blackie Academic & Professional, New York, NY.
14. Shinohara, Y., Kawasaki, N., Ueno, S., Kobayashi, I., Nakajima, M. & Amemiya, Y. 2005. Observation of the transient rotator phase of *n*-hexadecane in emulsified droplets with time-resolved two-dimensional small- and wide-angle X-ray scattering. *Physics Review Letters*, 94, (097801-1)-(097801-4).
15. McClements, D.J. & Coupland, J.N. 1996. Theory of droplet size distribution measurements in emulsions using ultrasonic spectroscopy. *Colloids and Surfaces A*, 117(1), 161-170.
16. McClements, D.J., Povey, M.J.W. & Dickinson, E. 1993. Absorption and velocity dispersion due to crystallization and melting of emulsion droplets. *Ultrasonics*, 31(6), 433-437.
17. McClements, D.J. & Povey, M.J.W. 1987. Solid fat content determination using ultrasonic velocity measurements. *International Journal of Food Science and Technology*, 22(5), 491-499.

4.3 Conclusions

In Chapters 4.1 & 4.2, ultrasonic attenuation in melting emulsions was investigated. Although attenuation in purely solid and purely liquid droplets was very low and could be predicted by scattering theory; over the melting range, attenuation increased considerably and deviated from scattering theory predictions. This observation was previously attributed to relaxational loss mechanism (McClements *et al*. 1993). In Chapter 4.1, I developed an extended version of scattering theory which predicted ultrasonic attenuation in melting emulsions. In Chapter 4.2, I tested the applicability of my theory to melting alkane emulsions as the oil and emulsifier type, and particle size changed. In all cases, the agreement between the theory and experiments was reasonably good. The excess losses were attributed to the rapid changes in thermophysical properties of melting droplets.

As indicated in Chapter 3.3, the investigations in alkane emulsions were carried out in order to understand the physical basis for the excess attenuation observed during the phase change. I hypothesize that the same mechanism contributes to the high attenuation in partially frozen solutions (Chapter 3.2) where ice crystals and saturated solutions are at equilibrium. If scattering by ice crystals was solely responsible for the attenuation, we would expect a single simple relation between the ice content and ultrasonic attenuation. Scattering losses increase with the concentration of scattering objects in the system raised to a power (*i.e.*, ice content^{n}), where the exponent (n) is dependent on material properties (Povey, 1997). However if relaxational losses play a role then we would expect any excess attenuation to be dependent on the amount of crystals that undergo a phase transition with unit change in temperature (*i.e.*, $\frac{\partial([ice])}{\partial T}$). Therefore, total attenuation would be expected to be a function of ice content and change in ice content with temperature:

$$\alpha = a.\,[\text{Ice content}]^{n} + b.\,\frac{\partial[\text{Ice content}]}{\partial T} \qquad [4.7]$$

where a, n, and b are sample specific constants. Based on this formulation I expect that if there are two samples with similar ice contents than the one with the greater rate of change in ice content with temperature would have the higher attenuation. I will test the excess attenuation hypothesis (Equation 4.7) in partially frozen sucrose solutions with varying ice content in Chapter 5.

References

1. McClements, D.J., Povey, M.J.W. & Dickinson, E. 1993. Absorption and velocity dispersion due to crystallization and melting of emulsion droplets. *Ultrasonics*, 31(6), 433-437.

2. Povey, M.J.W. 1997. Ultrasonic techniques for fluids characterization. Academic Press, USA.

Chapter 5

Ultrasonic Properties of Partially Frozen Sucrose Solutions

Abstract

Ultrasonic velocity and attenuation were measured as a function of temperature (-10°C to 0°C) in partially frozen sucrose solutions (25-50%) which had either been degassed under vacuum or not prior to freezing. Ultrasonic velocity increased approximately linearly with ice content in all cases and was somewhat affected by the initial sucrose concentration and degassing. The high ultrasonic attenuation in frozen systems was determined mainly by the presence of air bubbles and only weakly by ice content.

5.1 Introduction

During phase transitions the physical properties, including ultrasonic properties, of materials change rapidly. For example, the ultrasonic velocity in ice (approximately 3900 $m.s^{-1}$) (Smith & Kishoni, 1986) is higher than that in water (approximately 1400 $m.s^{-1}$) (Bilaniuk & Wong, 1993). Recent studies have tried to exploit these changes to build an ultrasonic sensor for the characterization of partly frozen food. Lee *et al.* (2004) measured the ultrasonic velocity and ice content (by NMR) in frozen orange juice samples (0 to -50°C), but they did not suggest a simple relationship between ice content and ultrasonic velocity. Sigfusson *et al*. (2004) measured the ultrasonic properties of a block of food parallel to the direction of heat flux during freezing. They were able to reflect part of an ultrasonic pulse from the moving ice front and from that calculate the proportion of the food frozen. I measured ultrasonic velocity in partially frozen solutions of sucrose, glycerol, and orange juice (Chapter 3.1). The velocity increased rapidly at the onset of freezing and the magnitude of the change in velocity was approximately linear with ice content. While the attenuation was high in these samples it was not reported. Indeed, to my knowledge there has been no systematic study of the ultrasonic attenuation in frozen solutions and no general mechanism proposed for ultrasonic propagation.

One possible mechanism for ultrasonic losses in frozen solutions is scattering by the crystals themselves or by the grain boundaries between the crystals. Scattering losses increase with the concentration of scattering objects in the system (*i.e*., ice crystals) raised to a power (Povey, 1997) so I would expect a single simple relationship between ice content and ultrasonic attenuation (assuming microstructure remained constant). The scattering may be more complex in frozen solutions where there is a phase equilibrium between crystals and unfrozen solvent phase. McClements *et al*. (1993) reported very high attenuation during the melting of crystalline

emulsion droplets and I have recently repeated and expanded their findings (Chapter 4). The attenuation is due to the perturbation of the equilibrium between the crystalline phase and solvent phase due to the small temperature fluctuation caused by the passing ultrasonic wave (Akulichev & Bulanov, 1981, 1983). Consequently there are periodic shifts in the equilibrium which is characterized by the melting and crystallization of a tiny amount of the crystalline phase. Since the process is inefficient, part of the ultrasonic energy will become out-of-phase and be recorded as an increase in attenuation. I hypothesize that the same mechanism is a contribution to the high attenuation in partially frozen solutions where ice crystals and saturated solutions are at equilibrium. If these relaxational losses play a role then the magnitude of the effect to be dependent on the amount of crystals that undergo a phase transition with unit change in temperature (*i.e*., the slope of the melting curve) .

Another factor potentially contributing to the ultrasonic attenuation in frozen solutions is the presence of air bubbles formed on freezing. Since the solubility of gases is significantly higher in water than in ice, bubbles are known to form upon freezing (Carte, 1961). Bubbles pulsate when the ultrasonic frequency corresponds to a critical bubble radius causing large losses of acoustic energy (Feuillade, 1995). The extent of bubble formation on freezing can be reduced by degassing the liquid solution (Carte, 1961).

In this study, I will investigate ultrasonic propagation in partially frozen sucrose solutions with varying ice content. I will also consider the potential effects of entrapped air by comparing samples prepared with and without prior degassing.

5.2 Materials and Methods

Ultrasonic Measurements: The ultrasonic measurements were carried out using a modified pulse-echo technique. An electrical spike signal (Panametrics 500 PR, Waltham, MA) was passed to a 2.25 MHz broadband ultrasonic transducer (Panametrics V606), which converted the energy to ultrasound. The pulse of sound traveled into a Plexiglas delay line, and was partially

reflected at the plastic-sample interface. The reflected part returned through the delay line to the transducer and the transmitted part traveled through the sample (~1 cm), was reflected from the brass plate and returned through the sample and the delay line to the transducer. The transducer reconverted the acoustic signal to an electrical signal, which was stored for analysis with a digital oscilloscope (LeCroy 9310c, Chestnut Ridge, NY, USA).

Sample Preparation: Anhydrous sucrose (Grade I, > 98% purity) was obtained from Sigma Chemical Company (St. Louis, MO). Sucrose solutions (25-50% by wt) were stirred for 1 hour and either immediately placed in the sample container (non-degassed samples) or degassed for 15 min using a Microvac vacuum unit (Microcal, Northampton, MA) and placed in the sample container (degassed samples). All the samples were rapidly frozen at -20°C and held there for approximately 30 min after the onset of nucleation. The samples were then heated to -10°C, held overnight then slowly heated from -10°C to 0°C at a heating rate of $1°C.hr^{-1}$. Ultrasonic measurements were carried out at intervals during the final heating cycle.

5.3 Results

The ice content in the samples was calculated from the temperature and composition using a sucrose-water phase diagram (Young & Jones, 1949) (Figure 5.1). In this analysis I assume the system has reached thermodynamic equilibrium which seems reasonable as they had been aged for at least 24 hrs prior to measurement and the unfrozen phase did not become glassy. There was a small and steady reduction in ultrasonic velocity during cooling and increase with sucrose concentration before the onset of freezing (Figure 5.2). At the onset of freezing there was a discontinuity and ultrasonic velocity increased rapidly then at a decreasing rate with further decreases in temperature. The temperature of the discontinuity was estimated by fitting separate empirical functions to the ultrasonic data above and below freezing and calculating their intersection point. The temperature of the discontinuity in the ultrasonic velocity curves corresponded to the published melting point of sucrose solutions (Figure 5.1) suggesting the samples were indeed at thermodynamic equilibrium. These results are similar to my earlier studies (Chapter 3.1) although the quantitative agreement is not perfect; perhaps because these experiments were conducted during heating while the earlier measurements were performed during the cooling cycle and thus are more dependent on variability in ice nucleation kinetics. Degassing only affected the velocity of the 30% sucrose samples while the velocity in frozen 40% and 50% sucrose solutions were similar if they had been degassed or not.

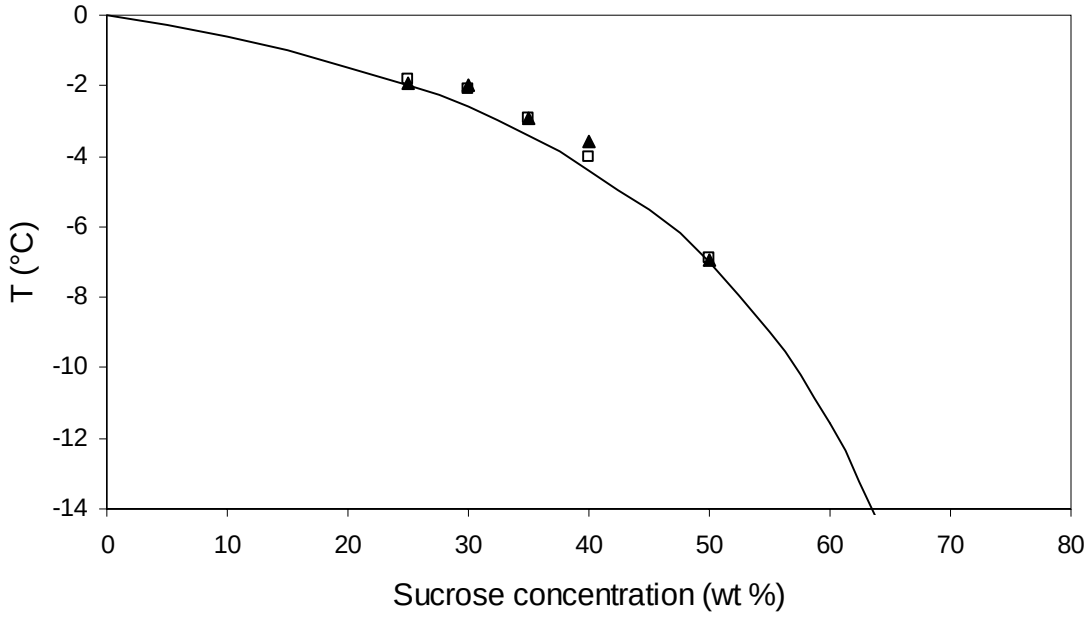

Figure 5.1. Sucrose water phase diagram (calculated from data provided in Young & Jones (1949)). Points show the temperature of the discontinuity in the ultrasonic velocity (□) or attenuation (▲) temperature curves at the melting point (from Figure 5.2 and 5.4).

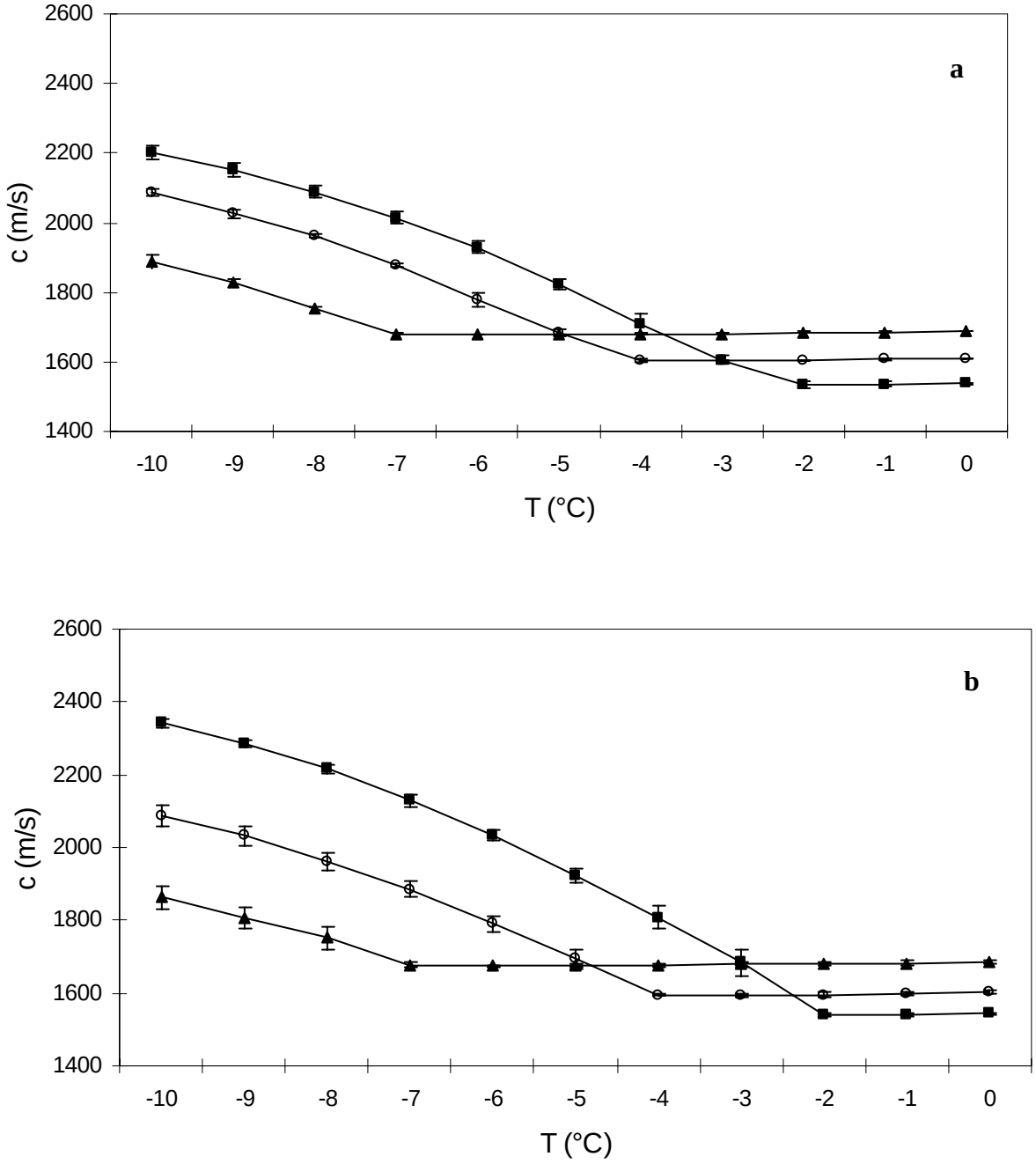

Figure 5.2. Ultrasonic velocity in partially frozen sucrose solutions (■) 30%, (○) 40%, (▲) 50% prepared with (a) or without (b) degassing.

The change in velocity upon freezing (*i.e.*, the difference between the measured velocity at a given temperature and the extrapolation of the linear velocity-temperature relation for similar liquid samples) increased with ice content (Figure 5.3) for all samples and the magnitude of the increase in velocity on freezing increased with sucrose concentration. The higher the sucrose concentration, the lower the degree of supercooling at the nucleation temperature and thus the larger the average final crystal size (Hartel, 2001) so possibly the microstructure of the frozen solid is influencing the ultrasonic propagation. As the samples are at thermodynamic equilibrium, the composition of the unfrozen phase would be the same in all cases.

Ultrasonic attenuation was high in all frozen samples (Figure 5.4). The attenuation was the highest at -10°C and decreased with increasing temperature until close to the melting point, when attenuation decreased more rapidly. After the completion of melting, the attenuation was very low (approximately 1-2 $Np.m^{-1}$). The sudden drop in attenuation on melting corresponded to the thermodynamic melting point on the phase diagram (Figure 5.1). At a given temperature the 30% sucrose solutions had higher attenuation than the more concentrated samples (40% and 50%) due to the lower ice contents in the more concentrated solutions. There was not a clear trend between the ice content and attenuation however degassing substantially reduced the attenuation of the frozen solutions (Figure 5.5).

If scattering was solely responsible for ultrasonic losses in frozen solutions I would expect a single function relating ice content and ultrasonic attenuation and clearly this is not the case. If the excess attenuation model was correct then I had hypothesized that if there were two samples with similar ice contents then the one with the higher rate of change in ice content with temperature would have the higher attenuation. However, this too was found not to be the case. For example, a 40% sucrose solution at -6°C and a 50% sucrose at -10°C had approximately the same ice content (12.1% and 13%, respectively) and attenuation (98.4 and 95.7 $Np.m^{-1}$) yet the slope of the melting curve in the former case is more than double that in the latter (7.6 % $°C^{-1}$ and 3.4 % $°C^{-1}$) . I conclude that ultrasonic losses in frozen foods are primarily due to the presence of air bubbles and not scattering from ice crystal or relaxational models proposed. The

sudden increase of attenuation on freezing is more connected with the formation of a bubble phase trapped in the ice than the formation of the ice in itself. Further cooling beyond the freezing point will increase the amount of ice but the bubbly matrix and hence the attenuation will remain largely unchanged.

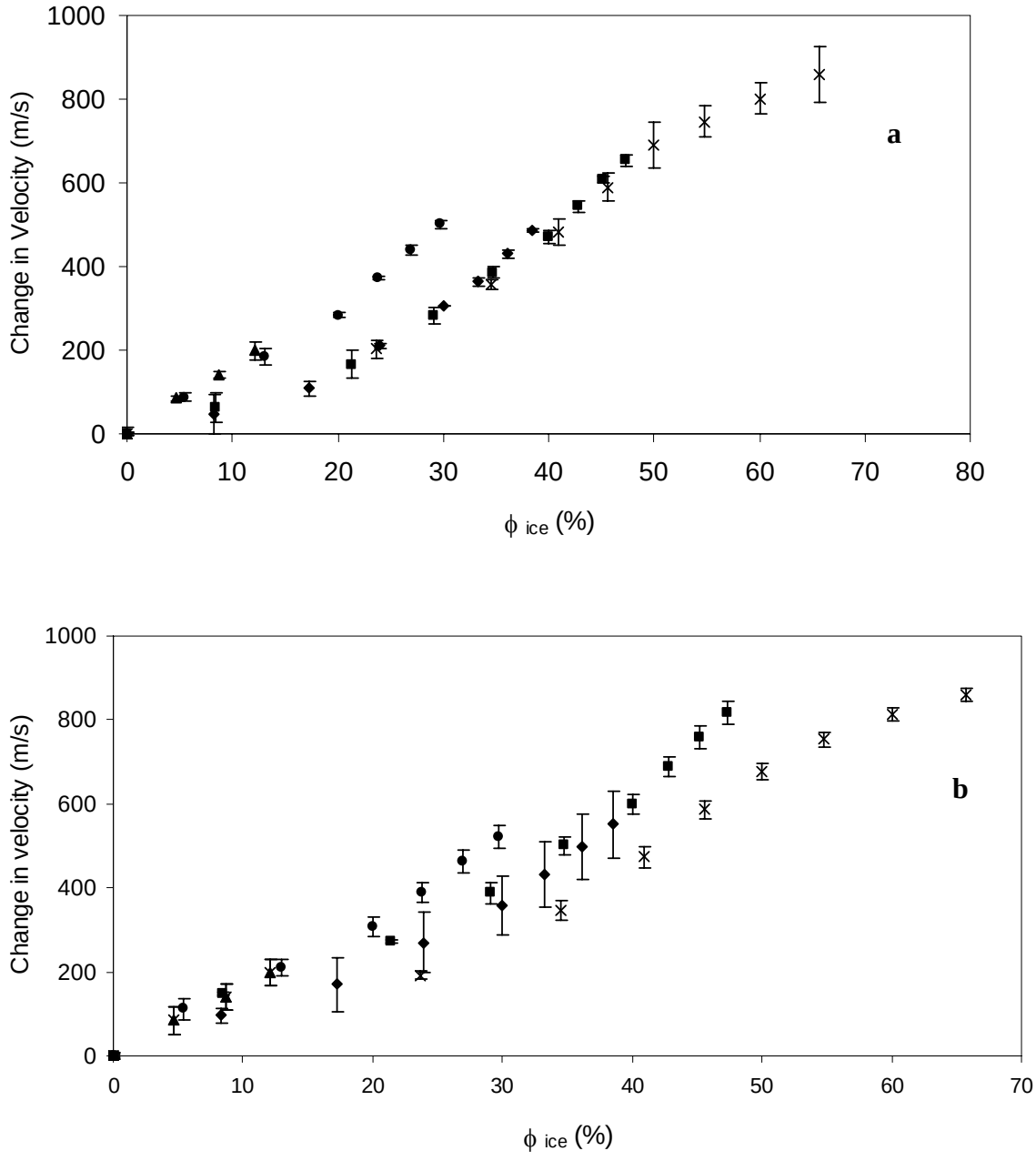

Figure 5.3. Change in ultrasonic velocity on freezing as a function of ice content in partially frozen sucrose solutions (x: 25%, ■: 30%, ♦: 35%, ●: 40%, ▲: 50% sucrose) prepared with (a) or without (b) degassing.

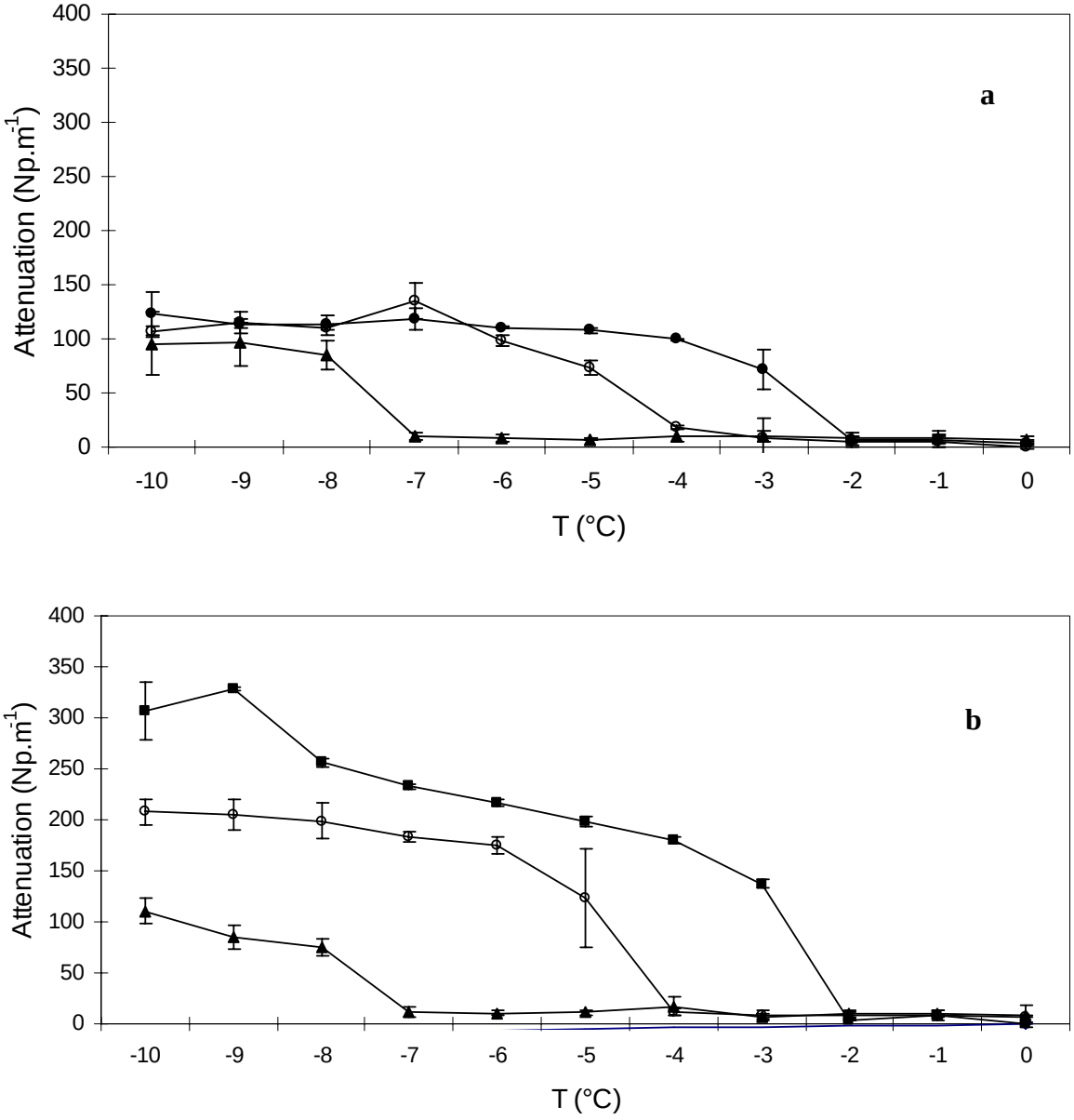

Figure 5.4. Ultrasonic attenuation in partially frozen sucrose solutions (■) 30%, (○) 40%, (▲) 50%) prepared with (a) or without (b) degassing.

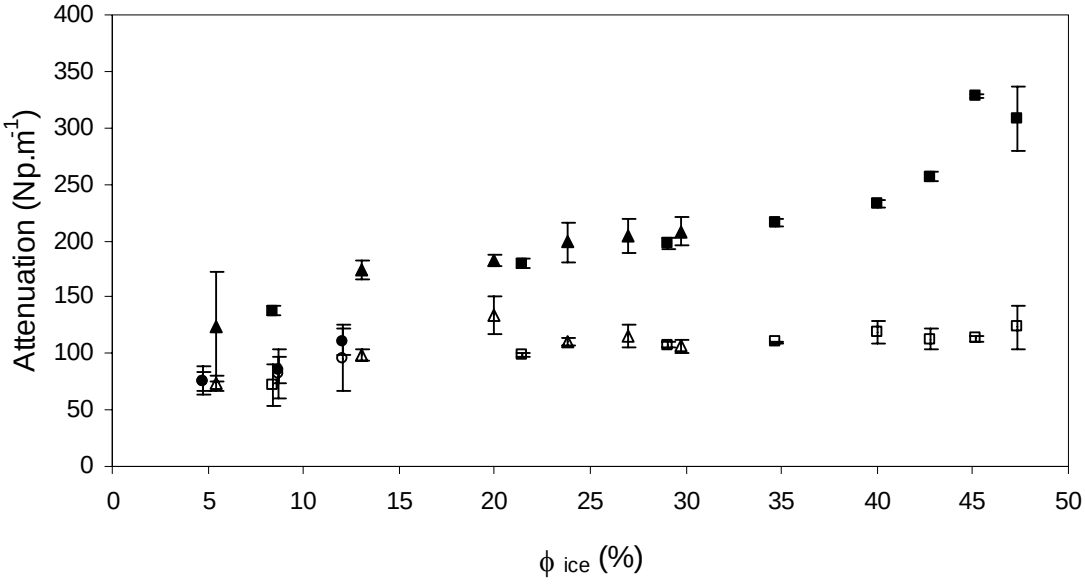

Figure 5.5. Ultrasonic attenuation as a function of ice content in partially frozen sucrose solutions (■:30%, ▲: 40%, ●: 50%) prepared with (open points) or without (filled points) degassing.

5.4 Conclusions

Similar to my earlier studies (Chapter 3.1) I found an approximately linear relation between ice content and the increase in ultrasonic velocity upon freezing. This relation may not be adequate as a sensor for ice content however as the velocity was also somewhat affected by the solution composition and degassing. Attenuation in frozen samples was dominated by the presence of air bubbles and had no strong dependence on ice content. To my knowledge these are the first systematic reports of ultrasonic attenuation in frozen solutions. Sudden changes in ultrasonic velocity and attenuation were indicative of the completion of melting of all solutions and could be used to easily establish the phase boundary.

Acknowledgement. The project was supported by the National Research Initiative of the USDA Cooperative State Research, Education and Extension Service, grant number 2003-35503-13852.

5.5 References

1. Akulichev, V.A. & Bulanov, V.N. 1981. Sound propagation in a crystallizing liquid. *Soviet Physics Acoustics*, 27(5), 377-381.
2. Akulichev, V.A. & Bulanov, V.N. 1983. Crystallization nuclei in liquid in a solid field. *International Journal of Heat and Mass Transfer*, 26(2), 289-300.
3. Bilaniuk, N. & Wong, G.S.K. 1993. Speed of sound in pure water as a function of temperature. *Journal of the Acoustical Society of America*, 93(3), 1609-12.
4. Carte, A.E. 1961. Air bubbles in ice. *Proceedings of the Physical Society*, 77 (3), 757-768.
5. Feuillade, C. 1996. The attenuation and dispersion of sound in water containing multiply interacting air bubbles. *Journal of the Acoustical Society of America*, 99(6), 3412-30.
6. Hartel, R.W. 2001. Crystallization in foods. Aspen Publishers, USA.
7. Lee, S., Pyrak-Nolte, L.J., Cornillon, P. & Campanella, O. 2004. Characterization of frozen orange juice by ultrasound and wavelet analysis. *Journal of the Science of Food and Agriculture*, 84 (5), 405-410.
8. McClements, D.J. & Coupland, J.N. 1996. Theory of droplet size distribution in emulsions using ultrasonic spectroscopy. *Colloids and Surfaces A: Physicochemical and Engineering Aspects*, 117 (1-2), 161-170.
9. McClements, D.J., Povey, M.J.W. & Dickinson, E. 1993. Absorption and velocity dispersion due to crystallization and melting of emulsion droplets. *Ultrasonics*, 31(6), 433-437.
10. Povey, M.J.W. 1997. Ultrasonic techniques for fluids characterization. Academic Press, USA.
11. Sigfusson, H., Ziegler, G.R. & Coupland, J.N. 2004. Ultrasonic monitoring of food freezing. *Journal of Food Engineering*, 62(3), 263-269.
12. Smith, A.C. & Kishoni, D. 1986. Measurement of speed of sound in ice. *AIAA*

Journal, 24(10), 1713-15.

13. Young, F.E. & Jones, F.T. 1949. Sucrose hydrates. The sucrose-water phase diagram. *Journal of Physical Chemistry*, 1334-50.

Chapter 6

Conclusions

The overall goal of my thesis was to relate the ultrasonic properties of frozen foods and related crystalline systems to their composition and structure. In order to accomplish this goal the specific objectives of my research were to:

1) Investigate the effect of ice content on the ultrasonic properties of model frozen solutions,
2) Investigate the excess attenuation documented by McClements *et al.* (1993) for melting lipids in emulsion droplets and suggest a mechanism for the losses that may be responsible for the very high attenuation in frozen samples.
3) Measure the attenuation in model frozen foods and interpreting relevance of the losses in terms of the mechanism hypothesized in Objective 2.

Objective 1: Ice content dependence of ultrasonic properties of model frozen foods

The first objective of the study was to investigate the effect of ice content on the ultrasonic properties of model frozen foods. The preliminary set of experiments reported in Chapter 3 focused on the ultrasonic velocity measurements in partially frozen model food solutions (*i.e.*, sucrose and glycerol solutions, and diluted orange juice) as a function of temperature and composition. Velocity was found to be proportional to ice content for a given sample, and the correlation was particularly strong at low temperatures where ice content changed only slowly with temperature (Chapter 3.1). Ultrasonic attenuation increased with ice content and frequency

but was very high and hard to measure at even moderate ice contents (Chapter 3.2). Since ultrasonic velocity or attenuation measurements were not universal indicators of ice content, the influence of other physical properties on the ultrasonic propagation was studied. Due to their relative simplicity, emulsions were chosen as model systems for further work.

Objective 2: Excess attenuation in melting emulsion droplets

The second objective of the study was to investigate the excess attenuation documented by McClements *et al.* (1993) for melting lipids in emulsion droplets and suggest a mechanism for the losses that may be responsible for the very high attenuation seen. In order to explain this observation, a modified form of scattering theory was developed based on the calculation of effective thermophysical properties (*i.e.*, heat capacity, density and thermal expansion coefficient) of the dispersed phase over the melting range (Chapter 4.1). Amongst these parameters the thermal expansion coefficient is shown to be the most important in determining the attenuation of melting crystals. The validity of this approach was shown in a variety of systems using different oil and emulsifier types and varying particle size (Chapter 4.2). I hypothesized that the same mechanism could contribute to the high attenuation in partially frozen solutions.

Objective 3: Ultrasonic losses in model frozen foods

The third objective of the study was to measure the ultrasonic properties in model frozen foods and interpret relevance of the losses in terms of the mechanism hypothesized in Objective 2. This was accomplished in Chapter 5. Ultrasonic velocity and attenuation was measured in partially frozen sucrose solutions. The ultrasonic losses were interpreted in terms of the mechanism hypothesized in Objective 2. In all cases, ultrasonic velocity increased approximately linearly with ice content, but the initial sucrose concentration, extent of supercooling, and ice microstructure influenced velocity as well. Attenuation was a weak function of ice content and

was primarily determined by the extent of degassing. Earlier I had hypothesized that the ultrasonic losses in partially frozen foods would be due to ice crystal loading (*i.e.*, scattering losses) and ultrasonic perturbation of phase equilibrium between ice crystals and saturated solutions (*i.e.*, relaxational losses). My final set of experiments disproved this hypothesis.

Unlike model frozen foods, excess losses were dominant in melting emulsion droplets. This difference between emulsion droplets and frozen foods might be in part due to the differences in crystal size. Emulsion droplets are much smaller in size (*i.e.*, micron scale) and larger in number compared to crystal grains in frozen foods which can approach millimeter range. Scattering losses are known to generally increase with decreasing particle size at a constant volume concentration of scatterers (Allegra & Hawley, 1972). On the other hand, the calculations of Akulichev & Bulanov (1981, 1983) suggested that excess losses decrease with particle size, since small fluctuations in temperature and pressure have greater influence on smaller particles. Consequently, the small crystals in the emulsion would be more affected by the excess losses compared to the large ice crystals. In a related study, Marshall *et al*. (2002) used scattering theory (Allegra & Hawley 1972) to accurately predict the changes in ultrasonic velocity and attenuation during the seeded crystallization of copper (II) sulfate pentahydrate. This is coherent with the findings from my work on frozen sucrose solutions (Chapter 5), since no indication of excess losses existed. The authors used seed crystals that had a central crystal size of approximately 200 μm, much larger than the emulsion droplets studies in Chapter 4 although similar to the typical crystal size in the ice studied in Chapters 3 & 5 and ~ 3% of the solution weight was crystallized, similar to the droplets in Chapter 4 but less than the ice crystals in Chapters 3 & 5. It seems a general observation that the excess attenuation mechanism is less relevant for larger crystals.

In addition to size differences the overall structural characteristics of the emulsions and model frozen foods investigated in the current work are quite different. The emulsions are fairly dilute systems where contact between crystals are largely avoided, whereas frozen foods have a complex, granular structure that is frequently (although not periodically) interrupted by grain boundaries and liquid inclusions from the freeze-concentrated phase. The density of water

decreases during freezing, whereas solidified lipids are denser than liquid ones. In addition, heat capacity and heat of fusion for water is higher than lipids, and its cubical expansion coefficient is approximately six times lower. These differences could account for the changes in excess ultrasonic losses.

Implications

One of the motivations of this work was to assess the feasibility of using ultrasonic sensors to monitor the freezing of foods. A first requirement for a sensor would be that it should be possible to make ultrasonic measurements in the samples. While frozen samples are very highly attenuating, it is possible to make measurements as long as the attenuation was not too high (*i.e.*, ice content <50% and degassed). Where measurement was possible, attenuation increased rapidly at the onset of freezing and was not a strong function of the absolute ice content (Chapter 5), so it was not possible to relate attenuation to ice content. In most cases, however, velocity increased approximately linearly with ice content, but due to the variations in crystal size, crystal impingement and presence of air bubbles, relating ultrasonic velocity to structure in model frozen foods was also challenging.

All the measurements in this study were carried out in contact mode which is not readily applicable to on-line monitoring of solid foods. While non-contact, air-coupled transducers are becoming more available their implementation will remain a challenge due to the large acoustic mismatch between air and frozen foods and the rough surfaces in frozen samples. In conclusion, the potential for ultrasonic sensors in the monitoring of online freezing operations is limited.

While frozen foods in general may be too complex for ultrasonic characterization a practically important and low ice content system where my findings (Chapters 3 & 5) are relevant are ice slurries. Ice slurries are used in a array of applications such as industrial cleaning, home or office cooling systems, medical applications that require rapid cooling of tissues or organs and artificial snow making (Bellas & Tassou, 2005). For example, ultrasonic

parameters have been used as process control tools in the determination of cleaning efficiency using ice slurries (Shire *et al*. 2005). When an ice slurry is employed in a cooling operation, the amount that melts per unit time determines the process efficiency which can be optimized through the selection of flow rate and ice concentration in the slurries using ultrasonic velocimetry. The velocity difference that can be expected between a partially frozen and completely melted slurry is possibly in the order of a few hundreds of meters per second.

Aside from the challenges and benefits of relating ice content to ultrasonic parameters, there are several other practical implications of my work.

Determination of freezing and melting point: Freezing of foods is characterized by an induction time due to the supercooling required for nucleation. In all cases investigated in the current work, ultrasonic velocity and attenuation increased rapidly at the onset of freezing. Therefore, freezing point of frozen foods can be determined monitoring the abrupt changes in velocity and attenuation. Similarly, at the melting point, ultrasonic velocity and attenuation decrease rapidly. The attainment of constant attenuation and velocity could be used to characterize the completion of melting at a constant temperature.

Long-term storage of frozen foods: The changes in crystal content over long storage periods can be monitored qualitatively, if not quantitatively, using ultrasonics. Unless the position of the attained phase equilibrium changes over storage time, ultrasonic properties can be expected to remain constant. However, thermal fluctuations in storage rooms can cause recrystallization, and/or change the ice content in frozen products which can be monitored using ultrasonic sensors.

References

1. Akulichev, V.A. & Bulanov, V.N. 1981. Sound propagation in a crystallizing liquid. *Soviet Physics Acoustics*, 27(5), 377-381.

2. Akulichev, V.A. & Bulanov, V.N. 1983. Crystallizing nuclei in liquid in a sound field. *International Journal of Heat and Mass Transfer*, 26(2), 289-300.

3. Allegra, J.R. & Hawley, S.A. 1972. Attenuation of sound in suspensions and emulsions: Theory and experiments. *Journal of the Acoustical Society of America*, 51(5), 553-565.

4. Bellas, I. & Tassou, S.A. 2005. Present and future applications of ice slurries. *International Journal of Refrigeration*, 28(1), 115-121.

5. Marshall, T., Challis, R.E., Holmes, A.K. & Tebbutt, J.S. 2002. Modeling ultrasonic compression wave absorption during the seeded crystallization of copper (II) sulphate pentahydrate from aqueous solution. *IEEE Transactions on Ultrasonics, Ferroelectrics, and Frequency Control*, 49(11), 1583-91.

6. McClements, D.J., Povey, M.J.W. & Dickinson, E. 1993. Absorption and velocity dispersion due to crystallization and melting of emulsion droplets. *Ultrasonics*, 31(6), 433-437.

7. Shire, S., Quarini, J. & Ayala, R.S. 2005. Ultrasonic detection of slurry ice flows. *Proceedings of the Institute of Mechanical Engineers – Part E: Process Mechanical Engineering*, 219, 217-225.

Appendix

Surface Melting in Alkane Emulsion Droplets as Affected by Surfactant Type

Abstract

The influence of surfactant type (Tween 20, Tween 40, Tween 60, Tween 80, Brij 58, Triton X-100, SDS, STS) on the crystallization and melting characteristics of emulsified (mean droplet diameter 0.52 μm) *n*-octadecane and *n*-eicosane were studied using microcalorimetry. The melting point (~37°C) of the eicosane droplets was higher than the crystallization point (~24°C) and was not affected by the surfactant selected indicative of purely homogeneous nucleation. There was a similar separation between the crystallization (~14°C) and melting (~ 28°C) point of the emulsified octadecane however the details of the transitions was affected by the surfactant selected. For Tween 40 and Brij 58-stabilized droplets there was a split peak on crystallization which I attribute to a surface heterogeneous nucleation mechanism. Only these surfactant-alkane combinations had a split peak on melting. The size of the lower temperature fraction decreased with droplet size suggesting another surface effect. However, the size of the surface layer was calculated to be many times the length of the surfactant tail suggesting the crystal structure was somehow modified by the nucleation mechanism.

A.1. Introduction

The thermodynamic melting point of an alkane is determined by the balance between the intermolecular bonds broken (*i.e.*, enthalpy loss) and loss of order (*i.e.*, entropy gain) in moving from a crystalline to liquid state. The thermodynamic crystallization temperature is determined by the same factors but is frequently kinetically limited by the need to form a crystal nucleus and is consequently observed at a lower temperature than melting. The magnitude of supercooling in alkanes is much greater when the lipid is present in fine emulsion droplets where each droplet must nucleate independently and frequently via a homogeneous mechanism.

Crystal nucleation in emulsified droplets is also affected by the interfacial surfactant material present. Surfactants that have similar alkyl chain lengths as the emulsified lipid have been shown to increase the crystallization point of emulsion droplets, presumably by ordering the lipid adjacent to the surface and reducing the barrier to nucleation (Skoda & van den Tempel, 1963; McClements *et al*. 1993). Alternatively, surface crystallization of the surfactant itself can facilitate nucleation in the lipid contained (Kaneko *et al*. 1999) which may be seen as a small endothermic peak in a differential scanning calorimetry thermogram immediately before the major lipid crystallization peak (Awad & Sato, 2002). On the other hand, Povey *et al*. (2006) suggested that the surfactant tail groups act as an impurity in the lipid close to the surface and can hence lower the crystallization temperature of that portion of the fat. In all cases the magnitude of any surface effects increases with decreases in droplet size.

In most investigations the influence of surfactants on droplet lipid melting has been found to be minimal, since at reasonably slow heating rates, melting occurs at the thermodynamic melting point (McClements *et al*. 1993); there are however some exceptions to this rule. First, the higher Laplace pressure in very fine droplets has the effect of lowering their melting point

(Montenegro & Landfester, 2003) although for this effect to be significant the droplets would have to be considerably smaller than typical macroemulsions (i.e., possibly < 0.5 μm, Montenegro *et al*. 2003). Secondly, the surface crystalline lipid is present in a mixture with the hydrophobic moieties of the surfactant and is hence a less pure material and should therefore have a lower melting point than similar crystalline lipids in the core of the droplet. There have been limited experimental investigations of this hypothesis but recently, Povey *et al.* (2006) were able to use ultrasonic velocity measurements to detect differences in the melting transition due to changes in the surfactant.

The goal of the present work is to investigate the effects of lipid-surfactant interfacial interactions on the melting behavior of lipids. I use microcalorimetry to make careful measurements of the melting (and crystallization) transitions in emulsified alkanes as a function of droplet size and surfactant type and conclude that the lipid closest to the surface will melt before the core lipid if it is compatible with the hydrophobic portion of the surfactant.

A.2. Materials and Methods

Materials and Sample Preparation. *n*-Octadecane (C_{18}) and *n*-Eicosane (C_{20}) were obtained from Acros Organics (Morris Plains, NJ). Tween 20, Brij 58, and Triton X-100 were purchased from Sigma Aldrich Chemical Company (St. Louis, MO). Tween 40 and Tween 60 were obtained from MP Biomedicals, Inc (Solon, OH). Sodium tetradecyl sulfate (STS) solution (27%) was purchased from Pfaltz & Bauer, Inc (Waterbury, CT). Tween 80 and sodium dodecyl sulfate (SDS) were purchased from Fisher Scientific (Pittsburgh, PA).

To prepare the emulsions, varying amounts of alkane and surfactant were mixed with water at 50°C (to ensure the lipid was liquid during homogenization), stirred for 30 minutes and emulsified using a 250 W ultrasonic processor (Vibracell, Sonics & Materials, Danbury, CT, USA) equipped with a stainless steel probe (½ in) at the highest power setting with a 50% duty

cycle. The process time was adjusted (<2.5 min) to produce emulsions with a mean diameter (d_{32}) of 0.52 ± 0.01 μm.

The particle size distribution of the emulsions was characterized by static light scattering (Horiba LA-920, Irvine, CA, USA) after appropriate dilution. The emulsions were stable over the course of the experiment (*i.e.*, no change in particle size, no visible phase separation) and were not destabilized by the cooling-heating cycles. The emulsions were diluted in water to produce a final oil concentration of 0.25% and surfactant concentration of 1%. If necessary, the samples were heated before the sonication procedure in order to keep the oil in a liquid state.

In another series of experiments, octadecane emulsions with a wider mean particle size range (0.19 to 5.58 μm) were prepared using Tween 40. For the preparation of these samples, in addition to the ultrasonic processor, a high speed blender (Kinematica GmbH FT10/35, Brinkmann Instruments, Switzerland) and a two-stage valve homogenizer (1-5 passes, 200 to 600 bar, 10% of which was maintained over the second stage, Niro-Soavi Panda, Model no: 3344, Parma, Italy) were used as necessary. In order to keep the oil in a liquid state for homogenization, the homogenizer was preheated with hot water prior to use.

Differential Scanning Calorimetry. The crystallization and melting thermograms were measured using differential scanning calorimetry (VP-DSC, Microcal, Northampton, MA). Samples diluted to 0.25 wt% lipid with water prior to analysis were used so that the signals were within the range of the instrument. Samples (513.1 μl) were run against a similar reference cell filled with water. C_{18} and C_{20} samples were heated to 35 and 45°C, respectively, held for 30 minutes, and cooled to 0.5°C at 10 °C.hr^{-1} then held for a further 30 min and reheated at the same rate to 35, and 45°C for C_{18} and C_{20} samples. The heat capacity data for the water-water scan was subtracted from the sample runs to measure the heat flux due to changes in the lipid phase. In preliminary experiments, I showed that the surfactant solutions did not themselves show any measurable thermal transitions over this range.

A.3 Results and Discussion

Crystallization. The cooling thermograms of eicosane emulsions (0.25 wt% o/w, 0.52 μm) stabilized by various surfactants are shown in Figure A.1. The calorimetry was extremely reproducible with typical standard deviations in onset and peak temperature of 0.1 and 0.2°C respectively. All small-molecule surfactant stabilized eicosane samples crystallized with a characteristic double peak with the larger portion having an onset at about 24°C and the minor portion at 20.5°C. The major peak in all samples was tentatively attributed to the formation of the rotator phase (R) and the minor one to the rotator phase (R) to low temperature crystalline phase (LO) transition (Chapters 4 & 5). For all samples the major peak was about 15°C below the thermodynamic melting point of octadecane (*i.e.*, 28.2°C, Vargaftik, 1975) suggesting the lipid crystallized via a homogeneous nucleation mechanism. Interestingly the nucleation of eicosane was not affected by the surfactant used.

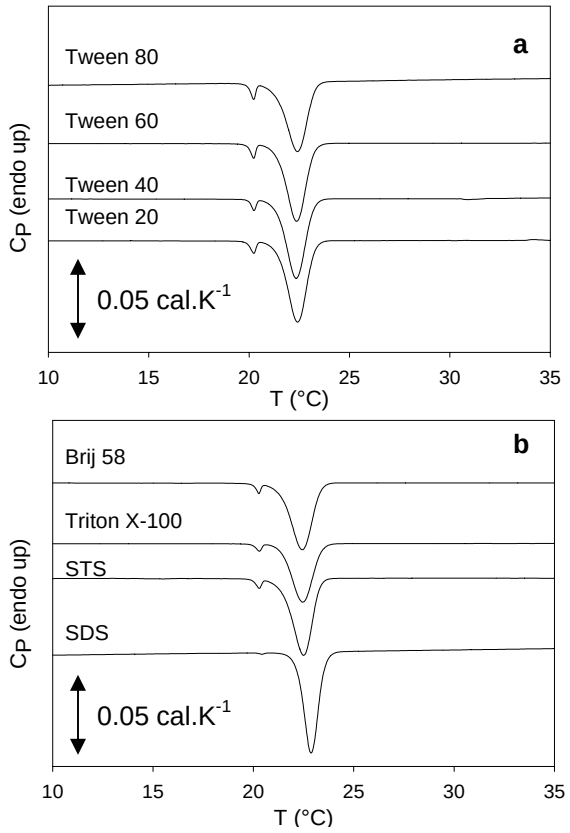

Figure A.1. Cooling thermograms of 0.25% *n*-eicosane emulsions stabilized by (a) Tween emulsifiers (1%), (b) non-Tween emulsifiers (1%) recorded at a scanning rate of 10°C.h^{-1}. The mean particle size (d_{32}) for all samples is 0.52 μm.

In my earlier work (Chapters 4 & 5) I reported similar thermograms for emulsions of hexadecane, octadecane and eicosane stabilized with either Tween 20 or sodium caseinate. In that work I pointed to the minor peak in the eicosane samples at 20.5°C as the crystallization of a surface layer immediately following the larger crystallization peak of the core of the droplet. In the light of the larger data set available in this work (Figure A.1, see 20-25°C range) I now believe this attribution was incorrect and the minor peak is indeed a rotator to crystal phase transition in the lipid. All samples showed a peak at approximately the same temperature although the peak size was somewhat different. The previously published discussion (Chapter 5)

may be particularly confusing as the zoom shown in Figure 5.4b of that work focuses on the wrong temperature range.

Similar experiments were conducted using octadecane droplets stabilized by the same range of surfactants (Figure A.2). For most surfactants used there was a single endothermic peak with a maximum at 12.7°C (*i.e.*, Tween 80, Tween 60, Tween 20, Triton X-100, SDS). Other surfactants had a similar peak at a higher temperature (~16°C, Tween 40 and Brij 58) and the exothermic peak for this group overlapped with another small exothermic transition at still higher temperatures. One surfactant, STS, had a lower crystallization peak (11°C maximum). There was a small but reproducible exothermic peak at 7°C in all emulsions except those prepared with STS where it may not have been evident because it overlapped with the long tail on the major peak. At present I can offer no good mechanism for the low crystallization onset of the STS samples.

The major peak in all samples was tentatively attributed to the formation of the rotator phase (R) and the minor one (*i.e.*, 7°C for octadecane) to the rotator phase (R) to low temperature crystalline phase (LO) transition (Chapter 4 & 5). For all samples the major peak was about 15°C below the thermodynamic melting point of octadecane suggesting the lipid crystallized via a homogeneous nucleation mechanism. The two samples crystallizing at higher temperatures (*i.e.*, Brij 58 and Tween 40) may have had their nucleation catalyzed by the presence of the surfactant. The ability of a surfactant layer to catalyze nucleation in emulsion droplets has been widely observed (*e.g.*, McClements *et al*. 1993) and is usually attributed by an ordering of the surface lipid by the orientated surfactant molecules at the interface. According to McClements *et al*. (1993), when the lipid and surfactant tail had a similar carbon number they would be compatible and the droplet would tend to crystallize at a higher temperature. The alkyl chain length for the Tween surfactants are 12, 16 and 18 carbons for Tween 20, Tween 40, and Tween 60, respectively so according to the McClements theory I would expect the crystallization temperatures of the Tween 60-stabilized emulsion to be highest. However in my work, Tween 40-stabilized octadecane droplets had the highest crystallization temperature while Tween 60 and Tween 20-stabilized droplets were lower and similar to one another. The lower compatibility of

Tween 60 is possibly due to its longer alkyl chain length (*i.e.*, > 16 carbons) which lowers the efficiency of adsorption due to coiling of the surfactant molecule (Rosen, 1989).

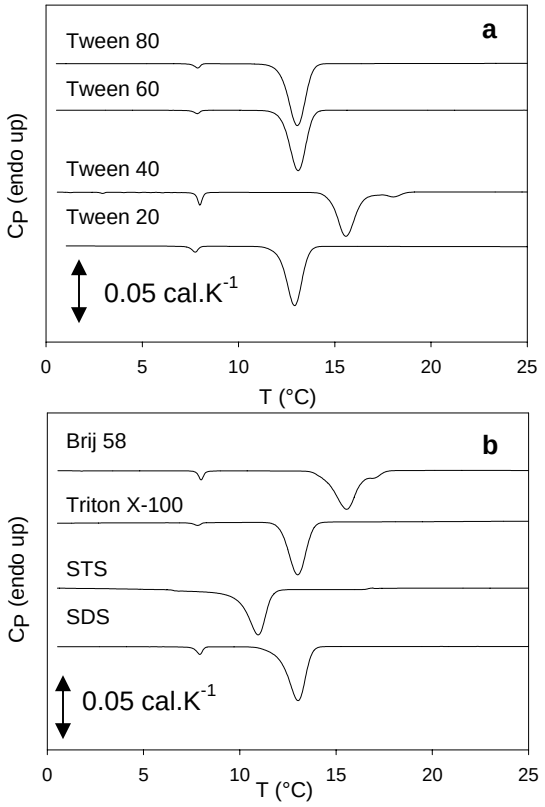

Figure A.2. Cooling thermograms of 0.25% *n*-octadecane emulsions stabilized by (a) Tween emulsifiers (1%), (b) non-Tween emulsifiers (1%) recorded at a scanning rate of 10°C.h^{-1}. The mean particle size (d_{32}) for all samples is 0.52 μm.

Other workers using less-sensitive calorimetric methods have not reported the double peak associated with surface-catalyzed nucleation (*i.e.*, Tween 40 and Brij 58 samples). I suggest that the small peak at high temperatures is due to the crystallization of a surface layer adjacent to the surface. Once formed, the surface crystals rapidly nucleate the core lipid and give rise to the larger peak. In the lower-onset samples (*i.e.*, Tween 80, Tween 60, Tween 20, Triton X-100, SDS) which crystallize by a purely homogeneous mechanism there is effectively one population of lipid droplets unaffected by the surface material. Nucleation occurs somewhere in the bulk of the droplet and the crystal grows from there. It is striking that the minor peak (at 7°C)

that I tentatively assigned to a rotator to crystal phase transition is unaffected by the presence of the surface layer, even in those samples where the surfactant could catalyze a liquid to rotator transition. The minor transition must therefore initiate in the bulk of the lipid droplet for all samples.

An alternative explanation of the split-peak and higher onset of the Tween 40 and Brij 58 samples would be that a phase transition in the surfactant catalyzed the nucleation of the droplets (see Povey *et al*. 2006 for a similar argument using a high-melting hydrophobic surfactant). However I was not able to detect any thermal events in solutions of the surfactant suggesting that some interaction involving the octadecane must be important.

Melting. The heating thermograms of eicosane emulsions (0.25 wt% o/w, 0.52 μm) stabilized by various surfactants are shown in Figure A.3. The calorimetry was extremely reproducible with typical standard deviations in onset and end point temperature of 0.1 and 0.3°C respectively. There was a large, unimodal, endothermic peak independent of surfactant type with an end point of approximately 37°C corresponding to the thermodynamic melting point of these lipids (36.9°C, Vargaftik, 1975). Figure A.3 shows 15-40°C range of the thermograms and reveals a minor peak at 25°C for all samples. While not clearly visible on the scale of the main figure, the higher resolution zoom (5% o/w emulsions) to Figure A.3 shows the 0-30°C region. I have previously identified this peak in eicosane as a crystal to rotator phase transition (Chapters 4 & 5). Once again the solid-solid transition is unaffected by surfactant. STS samples were observed to have an additional peak approximately around 13.5°C.

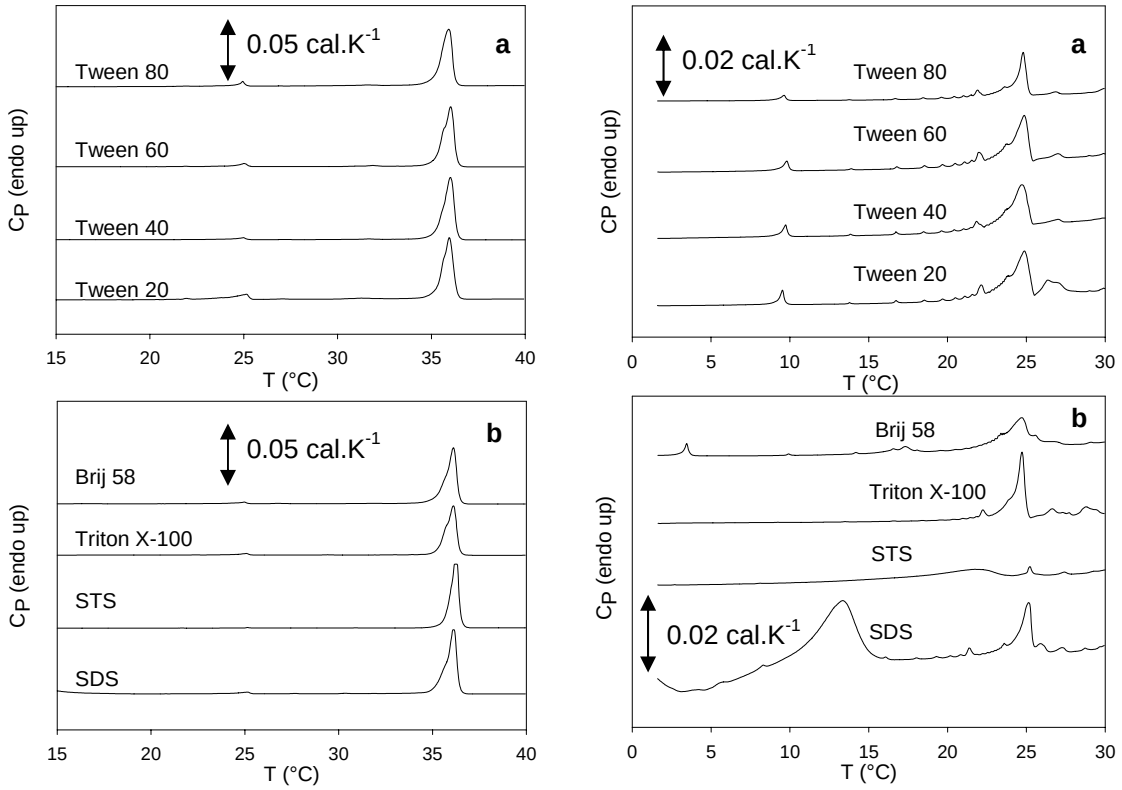

Figure A.3. Heating thermograms of 0.25% *n*-eicosane emulsions stabilized by (a) Tween emulsifiers (1%), (b) non-Tween emulsifiers (1%) recorded at a scanning rate of 10°C.h^{-1}. The figures to the *right* are the higher resolution zooms (5% emulsion) of the main data sets shown on the *left*. The mean particle size (d_{32}) for all samples is 0.52 μm.

The major melting endothermic peak for the octadecane samples was typically more complex, however the end temperature (approximately 28°C) corresponds well with the thermodynamic melting point (28.2°C, Vargaftik, 1975) (Figure A.4). Once more there was a very minor peak at 15°C seen shown in the zoomed region (0-20°C) of Figure A.4 which I attribute to a crystal to rotator phase transition for most of the small-molecule surfactant that were investigated here, mainly for Tween 40 and Brij 58.

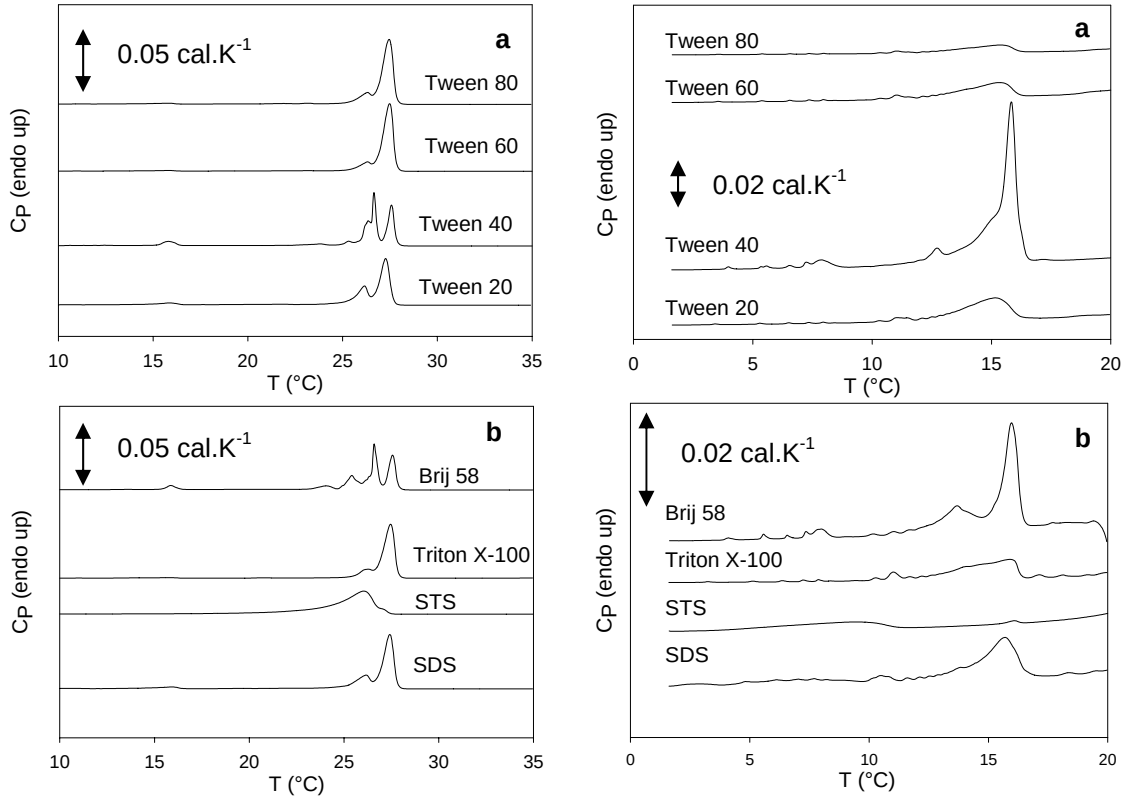

Figure A.4. Heating thermograms of 0.25% *n*-octadecane emulsions stabilized by (a) Tween emulsifiers (1%), (b) non-Tween emulsifiers (1%) recorded at a scanning rate of 10°C.h^{-1}. The figures to the *right* are the higher resolution zooms (5% emulsion) of the main data sets shown on the *left*. The mean particle size (d_{32}) for all samples is 0.52 μm.

There are clear parallels in the details of the major melting transitions with the groupings seen in the crystallization behavior of the same systems. The samples that crystallized with a single peak at the lower temperatures (*i.e*., Tween 80, Tween 60, Tween 20, Triton X-100, SDS) had a bimodal melting transition (minor peak at low temperatures, major peak at high temperatures). The samples with higher crystallization temperatures (*i.e*., Tween 40 and Brij 58) had at least one more peak in the melting transition suggesting there were several populations of lipid going through transitions. The STS samples are an outlier with a lower melting point and a low crystallization point than the other surfactants studied.

Calorimetric studies of alkane droplet melting have rarely shown anything but a single transition. However some workers have suggested there may be two populations of lipid present in a crystalline droplet – a core of "pure" material and a surface layer contaminated with the hydrophobic tails of the surfactant. For example, Walstra and van Beresteyn (1975) suggested there should be a reduction in the melting point of emulsified lipids if the emulsifiers act as impurities in the lipid phase. Povey *et al*. (2006) used sensitive ultrasonic velocity measurements to show that the onset of melting in hexadecane droplets occurred several degrees below the thermodynamic melting point and attributed this to an interaction with the hydrophobic tails of the Tween 20 surfactant used (Kaneko *et al*. 1999).

Surface Effects on Droplet Melting. A novel finding of this work is the details of both the melting and crystallization of alkane droplets depend on an interaction between the lipid and surfactant. Phase transitions in eicosane droplets are relatively simple and not affected by the surfactant while crystallization in octadecane droplets, presumably because the hydrophobic tails of the surfactant are closer in size to the lipid molecules, is strongly affected. Although only some surfactants (*i.e*., Tween 40 and Brij 58, both of which have a C_{16} tail length) can catalyze octadecane droplet nucleation and lead to a split and higher crystallization peak, all samples studied had a split peak in melting. If I assume the surfactant is functional at the droplet surface then the proportion of the total melting enthalpy at the lower temperatures should decrease with droplet size (specific surface area).

To test this hypothesis, I measured the crystallization and melting thermograms of a range of Tween 40-stabilized octadecane emulsions with the same composition but different droplet sizes. The size of the lower temperature crystallization peak (data not reported) and the high-temperature melting peak increased with droplet size (Figure A.5a). This effect can be seen more systematically by dividing the enthalpy into two populations by simply drawing a construction line to the baseline from the minima between the high and low melting peaks (Figure A.5b, a similar approach was taken for the crystallization transition but these data are more generally understood and are not reported). This general trend of the surface-affected

fraction increasing with decreasing droplet size is expected and, according to this approach, the surface melting fraction (SM %) can be calculated from DSC thermograms:

$$SM(\%) = \frac{A_{molten}}{A_{molten} + A_{core}} \times 100 \qquad [A.1]$$

where A represents area under the DSC melting curve (Figure A.5c) for the molten phase and the droplet core as indicated by the corresponding indices. How does this model correspond to the size of the real structures involved? A highly schematic model of a small droplet surrounded by a layer of surfactant is provided in Figure A.5d (Povey *et al*. 2006). The measured diameter of the droplet is given by D. The size of the surfactant headgroup is relatively small (for Tween 20 ~ 1.4 nm**,** Mandal *et al*. 1985) so this can be taken as the size of the lipid phase itself. The lipid phase is divided into two volumes: the inner oil (diameter d) is effectively pure and its contribution to the surface melting enthalpy would correspond to A_{core} above while the section closest to the interface is affected by the surfactant and corresponds to A_{molten} above. Accounting for the density changes associated with the phase transition the surface melting fraction can be expressed in terms of the geometry of this model:

$$SM(\%) = \frac{D^3 - d^3}{d^3} \cdot \frac{\rho_{liquid}}{\rho_{crystal}} \cdot 100 \qquad [A.2]$$

where, ρ is the density of the subscripted alkane phase. The distance (D-d)/2 is the thickness of the surface layer and for melting of *n*-octadecane droplets (Figure A.5c) this value increased with droplet diameter (from 44 nm when the mean particle size (d_{32}) was 190 nm, to 195 nm for the droplets with a mean particle size of 4840 nm. (Considering the full size distribution function instead of just the mean values made little difference to these calculations). Povey *et al*. (2006) proposed that the thickness of the surface layer would correspond to the length of the hydrophobic portion of the surfactant acting as a contaminant in the surface oil (~4 nm for

Tween 40, Sato & Ueno, 2001). Clearly the actual surface values are much larger and droplet size dependant. While the chemistry of the surfactant is important, its influence extends much further into the droplet than the physical size of the molecule.

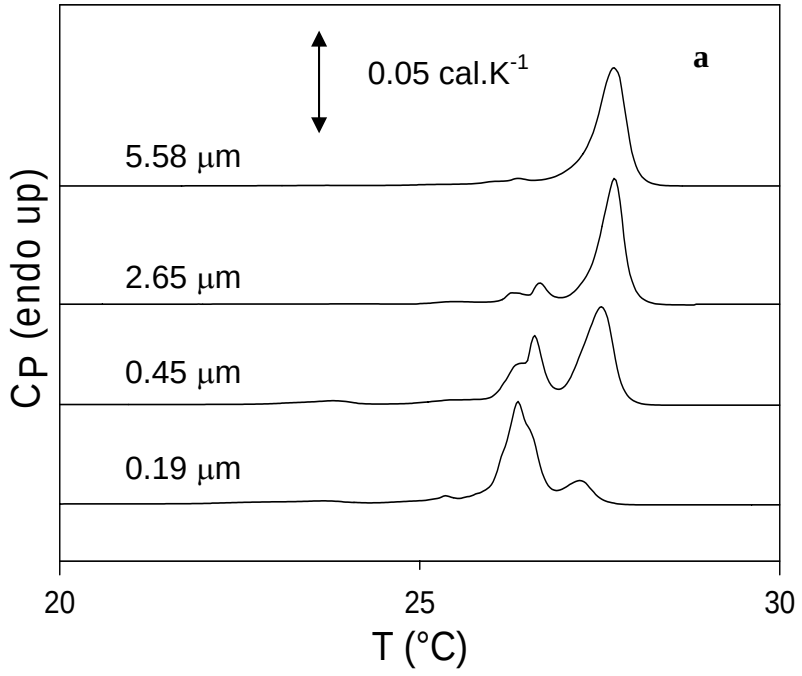

Figure A.5. (a) Heating thermograms of 0.25% *n*-octadecane emulsions stabilized by Tween 40 (1%) as affected by the particle size (0.19 μm to 5.58 μm). (b). The demonstration of the separation of surface melting and droplet core melting processes. (c). A simple physical model of a droplet (diameter D) with a pure lipid core (diameter d). (d). The surface melting (%) characteristics of 0.25% *n*-octadecane emulsions stabilized by Tween 40 (1%) as affected by the particle size (0.19 μm to 5.58 μm).

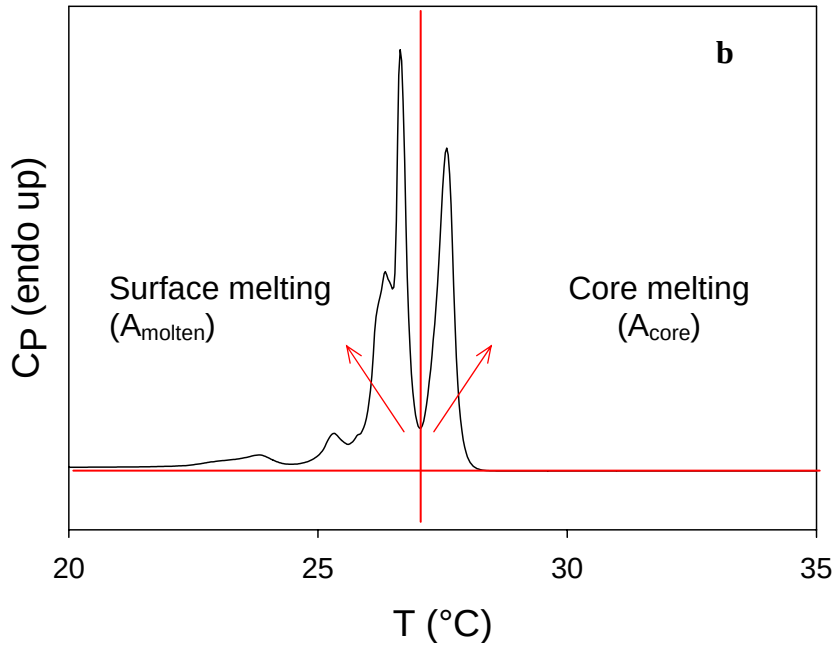

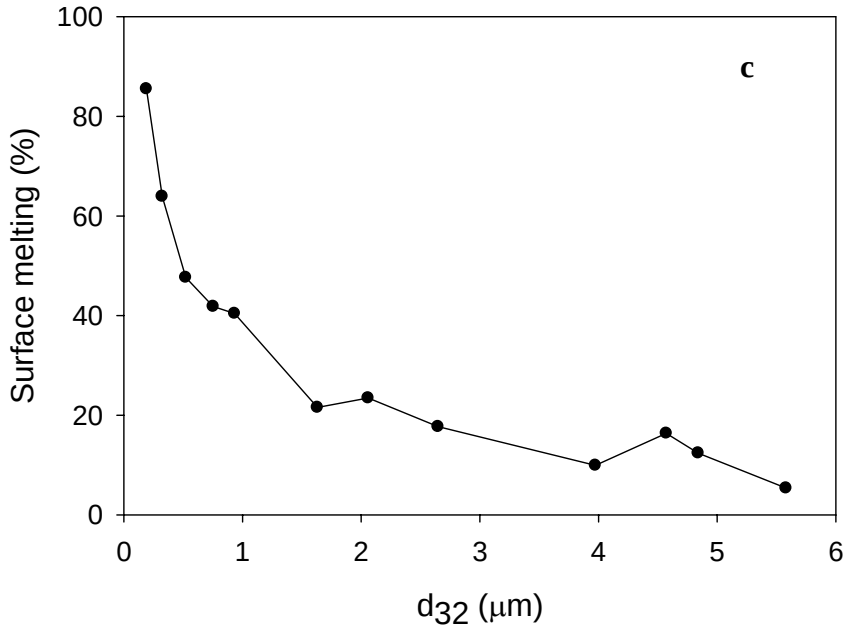

Figure A.5 (continued)

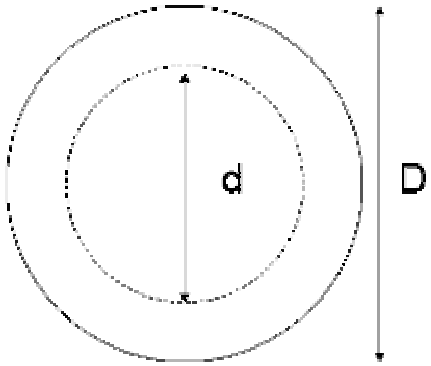

d

Figure A.5 (continued)

An alternative explanation may be that differences in the nucleation pattern lead to differences in droplet melting. I have argued that the emulsions showing a significant, size dependant double peak on melting were those whose crystallization was itself catalyzed at the surface (*i.e*., Brij 58 and Tween 40 stabilized octadecane). It could be that because these lipids nucleate from the impure surface layer, the structure of the crystals formed is somehow different than the structure of the crystals formed by from nucleation in pure alkanes. The different crystal structure would propagate further into the core of the droplet than the physical size of the surface layer and could explain the relatively large surface thickness from my earlier calculations. A second contributing factor could be the physical constraints imposed on crystal structure by the droplet surfaces. It is well-known that the confinement of oil molecules in droplets can alter the polymorphic behavior (Montenegro & Landfester, 2003; Ueno *et al*. 2003) and cause defects in crystal structure when nucleation activating impurities are present (Sonoda *et al*. 2006).

A.4. Conclusions

The melting and crystallization of emulsified eicosane is largely unaffected by the surfactant selected while similar octadecane droplets can show an additional high temperature

crystallization transition and low temperature melting transition with certain surfactants (Brij 58 and Tween 40). I propose that these surfactants are somehow molecularly compatible with the lipid and can catalyze nucleation from the droplet surface. The crystals nucleating at the surface have somewhat different structures and therefore melting properties than the crystals nucleating in the bulk of the droplet.

Acknowledgement. The project was supported by the National Research Initiative of the USDA Cooperative State Research, Education and Extension Service, grant number 2003-35503-13852.

A.5. References

1. Awad, T.S. & Sato, K. 2002. Fat crystallization in o/w emulsions controlled by hydrophobic emulsifier additives. *In* Physical properties of lipids, Marangoni, A.G., Narine, S.S. (ed.s), Marcel Dekker, Inc. USA.
2. Kaneko, N., Horie, T., Ueno, S., Yano, J., Katsuragi, T. & Sato, K. 1999. Impurity effects on crystallization rates of *n*-hexadecane in oil-in-water emulsions. *Journal of Crystal Growth*, 197(1-2), 263-270.
3. Mandal, A.B., Gupta, S. & Moulik, S.P. 1985. Characterization of Tween 20 and Tween 80 micelles in aqueous-medium from transport studies. *Indian Journal of Chemistry A*, 24(8), 670-673.
4. McClements, D.J., Dungan, S.R., German, J.B., Simoneau, C. & Kinsella, J.E. 1993. Droplet size and emulsifier type affect crystallization and melting of hydrocarbon-in-water emulsions. *Journal of Food Science*, 58(5), 1148-51, 78.
5. Montenegro, R. & Landfester, K. 2003. Metastable and stable morphologies during crystallization of alkanes in miniemulsion droplets. *Langmuir*, 19(15), 5996-6003.
6. Montenegro, R., Antonietti, M., Mastai, Y. & Landfester, K. 2003. Crystallization in miniemulsion droplets. *Journal of Physical Chemistry B*, 107(21), 5088-94.
7. Povey, M.J.W., Hindle, S.A., Aarflot, A. & Hoiland, H. 2006. Melting point depression of the surface layer in *n*-alkane emulsions and its implications for fat destabilization in ice cream. *Crystal Growth and Design*, 6(1), 297-301.
8. Rosen, M.J. 1989. Surfactants and Interfacial Phenomena. 2nd ed. John Wiley & Sons, USA.
9. Sato, K. & Ueno, S. Molecular interactions and phase behavior of polymorphic fats *In* Crystallization processes in fats and lipids, (ed.s) Garti, N. & Sato, K., 177-210.

10. Skoda, W. & van den Tempel, M. 1963. Crystallization of emulsified triglycerides. *Journal of Colloid Science*, 18(6), 568-584.

11. Sonoda, T., Takata, Y., Ueno, S. & Sato, K. 2006. Effects of emulsifiers on crystallization behavior of lipid crystals in nanometer-size oil-in-water emulsion droplets. *Crystal Growth and Design*, 6(1), 306-312.

12. Ueno, S., Hamada, Y. & Sato, K 2003. Controlling polymorphic crystallization of *n*-alkane crystals in emulsion droplets through interfacial heterogeneous nucleation. *Crystal Growth and Design*, 3(6), 935-939.

13. Vargaftik, N.B. 1975. Tables on the thermophysical properties of liquids and gases: in normal and dissociated states. Hemisphere Publishing Comp, USA.

14. Walstra, P. & van Beresteyn, E.C.H. 1975. Crystallization of milk fat in the emulsified state. *Netherlands Milk and Dairy Journal*, 29(1), 35–65.

VITA

İbrahim Gülseren

EDUCATION

- **Doctor of Philosophy in Food Science**, The Pennsylvania State University, University Park, PA (August 2004-May 2008).
- **Master of Science in Food Science and Technology**, University of Tennessee, Knoxville, TN (January 2003-August 2004).
- **Master of Science in Biotechnology**, İstanbul Technical University, Turkey (October 2001-May 2003).
- **Bachelor of Science in Food Engineering**, İstanbul Technical University, Turkey (October 1997- July 2001).

SELECTED PUBLICATIONS AND PRESENTATIONS

- Gülseren, İ. & Coupland, J.N. 2007. Excess ultrasonic attenuation due to solid-solid and solid-liquid transitions in emulsified octadecane. *Crystal Growth & Design*, 7(5), 912-918.
- Gülseren, İ. & Coupland, J.N. 2007. The effect of emulsifier type and droplet size on phase transitions in emulsified even-numbered *n*-alkanes. *Journal of American Oil Chemists` Society*, 84(7), 621-629.
- Gülseren, İ. & Coupland, J.N. 2006. Ultrasonic velocity measurements in frozen model food solutions. *Journal of Food Engineering*, 79(3), 1071-78.
- Gülseren, İ. & Coupland, J.N. 2007. Extension of scattering theory to predict excess ultrasonic attenuation due to phase transitions in emulsified octadecane. FS & FF 4 - Annual Meeting of the American Oil Chemists' Society, Quebec City, QC, Canada.

STUDENT AWARDS

- 2007 - AOCS Honored Student Award - AOCS Food Structure and Functionality Forum
- 2007 - Finalist for Food Chemistry Poster Competition - IFT Division of Food Chemistry
- 2006 - Alfred P. Schwan Graduate Paper Competition (1st place) - IFT Division of Refrigerated and Frozen Foods